

VOLUME XLII

GEMS & GEMOLOGY

SPRING 2006



*"Paraíba" Tourmaline from
Brazil, Nigeria, and Mozambique
Lead Glass-Filled Rubies
Tortoise Shell*

THE QUARTERLY JOURNAL OF THE GEMOLOGICAL INSTITUTE OF AMERICA



pg. 19



pg. 26

EDITORIAL

- 1 **Symposium 2006: Navigating the Challenges Ahead**
Alice S. Keller
- 2 **The Dr. Edward J. Gübelin Most Valuable Article Award**

FEATURE ARTICLES

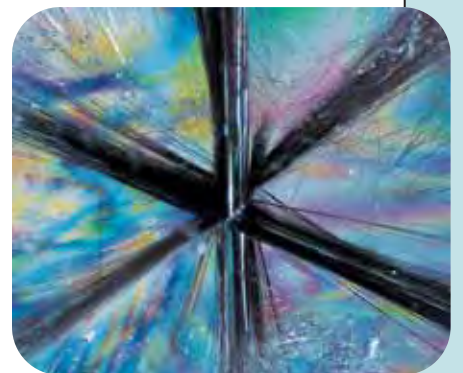
- 4 **“Paraíba”-type Copper-bearing Tourmaline from Brazil, Nigeria, and Mozambique: Chemical Fingerprinting by LA-ICP-MS**
Ahmadjan Abduriyim, Hiroshi Kitawaki, Masashi Furuya, and Dietmar Schwarz
Compares the chemical compositions of bright blue-to-green “Paraíba”-type tourmaline from the three known sources.
- 22 **Identification and Durability of Lead Glass-Filled Rubies**
Shane F. McClure, Christopher P. Smith, Wuyi Wang, and Matthew Hall
Reports on the identifying features of rubies filled with a high-lead-content glass to make them appear more transparent.
- 36 **The Characterization of Tortoise Shell and Its Imitations**
Thomas Hainschwang and Laurence Leggio
Documents the gemological properties of ornamental tortoise shell and its numerous imitations.

REGULAR FEATURES

- 54 **Lab Notes**
Multicolored assembled stone • Diamond with “fingerprint” inclusions
• Pink diamond with etch channels • Two diamonds from the same octahedron
• Translucent brown-orange diamond • Inscriptions inside emerald crystals
• Color-coated star quartz • Variscite, resembling turquoise
- 62 **Gem News International**
2006 Tucson report • Aquamarine from Sri Lanka • Massive haüyne-sodalite from Myanmar • Gem-quality massive pink muscovite from Brazil • Pyrope-spessartine from Tanzania • Transparent faceted sillimanite from India • Sphene from Pakistan
• New spinel from Mahenge, Tanzania • Cuneiform aquamarine inclusion • “Blood trail” in copal • Colored fluid inclusions in quartz • “Platinum quartz” with star
• New Madagascar mining laws • Black diamond with unusual growth structures
• Sapphire with unusual color zoning • Väyrynenite from Pakistan • A convincing moonstone doublet • A rutilated quartz doublet • An unusual triplet • New CRJP Code of Practices • Update on the use of biological remains in gem materials
- 81 **2006 Gems & Gemology Challenge**
- 83 **Book Reviews**
- 85 **Gemological Abstracts**
- 94 **The Last Page: The G&G Twenty-Five Year Index, 1981–2005**



pg. 60



pg. 72

Symposium 2006: Navigating the Challenges Ahead

The essence of navigation is simple: knowing where you are, knowing where you want to be, and charting a course to get there. But navigating today's gem and jewelry industry requires something far beyond the traditional map and compass. It requires knowledge, a strategic perspective on the industry and the world at large, and the willingness to embrace inevitable change.

"Navigating the Challenges Ahead" is a fitting theme for GIA's 4th International Gemological Symposium, Aug. 27–29, 2006, at the Manchester Grand Hyatt Hotel in San Diego, California. Informative sessions will examine the future of diamonds and colored stones, cultured pearls, jewelry design and manufacturing, business perspectives, luxury retailing, e-commerce, and gem identification technology. The speaker lineup includes such visionaries as David Yurman, Nick Paspaley, Nadja Swarovski, François Curiel, and Robert Wan, as well as leading researchers such as Dr. George Rossman and Dr. Alan Collins. Symposium's Debate Centers are fast-paced arenas where provocative industry leaders and audience members will tackle the industry's most controversial issues. State-of-the-art research will be on display at the ever-popular Poster Session, an interactive forum best described as a "Marketplace of New Ideas."

The event's keynote speakers will deliver their perspectives on creativity, leadership, and innovation. This distinguished group features former U.S. Secretary of State Madeleine K. Albright, one of the most influential figures in geopolitics; Frank Abagnale, a former confidence man turned law enforcement consultant whose exploits were the basis of Steven Spielberg's "Catch Me If You Can"; and Deepak Chopra, renowned author and mind/body pioneer. Returning to Symposium for an unprecedented third closing address is Maurice Tempelman, chairman of Lazare Kaplan International Inc. and a senior statesman of the diamond industry.

The academic program will be complemented by unforgettable evening events: GIA's 75th Diamond Anniversary Gala at the Institute's headquarters in Carlsbad; a Sunset Soirée, with the San Diego waterfront as its backdrop; and an Italian Jewelry Evening, where timeless fashion and creativity will come alive.

Another compelling reason to be in San Diego this August is GIA's first-ever Gemological Research Conference (GRC), which is being held immediately before Symposium (Aug. 26–27) at the same site. Many of the brightest minds in gemology and related disciplines will be on hand to discuss the latest research on gem localities, geology of gem deposits, gem characterization techniques, and gem treatment and synthesis. As of this writing, with the event five months away, more than 200 people from some two dozen countries have



For more information on **Symposium**, visit www.symposium.gia.edu or e-mail igs@gia.edu. Visit the **Gemological Research Conference** at www.gia.edu/gemsandgemology or e-mail gemconference@gia.edu.

already registered to attend this scientific forum, one designed for the ardent student of gemology and the avid *G&G* reader.

Rounding out the program are field trips to the world-famous Pala gem pegmatite district in San Diego County. These excursions will give a limited number of participants an opportunity to tour the underground workings of three operating gem mines and join in lively discussions about the formation of tourmaline, morganite, kunzite, and other gems with the mine owners and famous scientists in attendance.

Symposium and the GRC are unique events that offer an experience unlike any other, one that will inform and inspire you in charting your own course for a successful future. All of us at *Gems & Gemology* and GIA look forward to seeing you there.

Alice S. Keller
Editor-in-Chief, *Gems & Gemology*
Co-chair, 4th International Gemological Symposium

The *Dr. Edward J. Gübelin* Most Valuable Article AWARD

Gems & Gemology is pleased to announce the winners of this year's Dr. Edward J. Gübelin Most Valuable Article Award, as voted by the journal's readers. We extend our sincerest thanks to all the subscribers who participated in the voting.

The first-place article was "A Gemological Pioneer: Dr. Edward J. Gübelin" (Winter 2005), which examined the life and career of the eminent Swiss gemologist. Receiving second place was "Characterization and Grading of Natural-Color Yellow Diamonds" (Summer 2005), a study of the gemological and spectroscopic properties of these diamonds. Third place was awarded to "A Review of the Political and Economic Forces Shaping Today's Diamond Industry" (Fall 2005), which chronicled the key developments that have transformed the diamond industry in the past 15 years.

The authors of these three articles will share cash prizes of \$2,000, \$1,000, and \$500, respectively. Following are brief biographies of the winning authors.

Congratulations also to Prateek R. Jhaveri of Arusha, Tanzania, whose ballot was drawn from the many entries to win a five-year subscription to *Gems & Gemology*.



Robert E. Kane



Edward W. Boehm



Stuart D. Overlin



Dona M. Dirlam



John I. Koivula



Christopher P. Smith

FIRST PLACE

A GEMOLOGICAL PIONEER: DR. EDWARD J. GÜBELIN

Robert E. Kane, Edward W. Boehm, Stuart D. Overlin, Dona M. Dirlam, John I. Koivula, and Christopher P. Smith

Robert E. Kane is president and CEO of Fine Gems International in Helena, Montana, and a member of the *G&G* Editorial Review Board since 1981. A former director of the Gübelin Gem Lab in Lucerne, Switzerland, Mr. Kane is well known for his many lectures and articles on diamonds, gemstones, and gem identification. **Edward W. Boehm** is a gem dealer, consultant, and president of JOEB Enterprises in Solana Beach, California. Mr. Boehm holds degrees in geology and German from the University of North Carolina in Chapel Hill. **Stuart D. Overlin** is associate editor of *Gems & Gemology* and has been with the journal since 1997. Mr. Overlin received a bachelor's degree in political science from the U.S. Naval Academy. **Dona M. Dirlam** is director of GIA's Richard T. Liddicoat Gemological Library and Information Center in Carlsbad, California. A longtime contributor to *G&G*, Ms. Dirlam holds a bachelor's degree in earth sciences from the University of Minnesota

at Minneapolis and a master's in geology and geophysics from the University of Wisconsin at Madison. **John I. Koivula** is chief gemologist at the American Gem Trade Association (AGTA) Gemological Testing Center in Carlsbad. A prolific author, Mr. Koivula has spent more than 40 years photographing inclusions in gems. He holds bachelor's degrees in chemistry and mineralogy-geology from Eastern Washington State University.

Christopher P. Smith is director of identification services at the GIA Laboratory in New York and a member of the *G&G* Editorial Review Board. Formerly director of the Gübelin Gem Lab, Mr. Smith has written numerous articles for *G&G* and other publications.

SECOND PLACE

CHARACTERIZATION AND GRADING OF NATURAL-COLOR YELLOW DIAMONDS

John M. King, James E. Shigley, Thomas H. Gelb, Scott S. Guhin, Matthew Hall, and Wuyi Wang

John M. King is technical director of the GIA Laboratory in New York and a frequent writer and lecturer on colored diamonds. Mr. King received his Master of Fine Arts degree from Hunter College, City University of New York. **James E. Shigley** is director of GIA Research in Carlsbad. The editor of *Gems & Gemology in Review: Synthetic Diamonds* (2005) and a contributing editor to the journal, Dr. Shigley received a bachelor's degree in geology from the University of California, Berkeley, and a doctorate in geology from Stanford University. **Thomas H. Gelb** is staff gemologist at the GIA Laboratory in New York. Mr. Gelb is a graduate of the University of Massachusetts and has more than 10 years' experience in diamond grading and gem identification. **Scott S. Guhin** is grading lab manager at the GIA Laboratory in Carlsbad. Mr. Guhin came to GIA in 1990 with an extensive background in retail jewelry. He holds a bachelor's degree in art from San Diego State University. **Matthew Hall** is manager of analytical research at the GIA Laboratory in New York. Mr. Hall has a bachelor's degree in geology from Franklin and Marshall College and a master's in geology and geochemistry from the University of Maryland. **Wuyi Wang** is research scientist at the GIA Laboratory in New York. Dr. Wang holds a Ph.D. in geology from the Tsukuba University in Japan and is an authority on diamond geochemistry.

THIRD PLACE

A REVIEW OF THE POLITICAL AND ECONOMIC FORCES SHAPING TODAY'S DIAMOND INDUSTRY

Russell Shor

Russell Shor is senior industry analyst at GIA in Carlsbad. Well known in the industry for his reporting as diamond editor of *Jewelers Circular Keystone* from 1980 to 1995, he also served as editor of *New York Diamonds* and *GemKey*. Mr. Shor has a degree in journalism from Temple University.



John M. King



James E. Shigley



Thomas H. Gelb



Scott S. Guhin



Matthew Hall



Wuyi Wang



Russell Shor

“PARAÍBA”-TYPE COPPER-BEARING TOURMALINE FROM BRAZIL, NIGERIA, AND MOZAMBIQUE: CHEMICAL FINGERPRINTING BY LA-ICP-MS

Ahmadjan Abduriyim, Hiroshi Kitawaki, Masashi Furuya, and Dietmar Schwarz

Gem-quality bright blue to green “Paraíba”-type Cu-bearing tourmaline is now known from deposits in Africa (Nigeria and Mozambique), in addition to three commercial localities in Brazil (in Paraíba and Rio Grande do Norte States). Stones from these new localities have been mixed into parcels from the original Brazilian Paraíba occurrence. The Nigerian and Mozambique tourmalines that show saturated blue-to-green colors cannot be distinguished from the Brazilian material by standard gemological testing or on the basis of semi-quantitative chemical data (obtained by EDXRF analysis). However, quantitative chemical data obtained by LA-ICP-MS show that tourmalines from the three countries can be differentiated by plotting (Ga+Pb) versus (Cu+Mn), (Cu+Mn) versus the Pb/Be ratio, and Mg-Zn-Pb. In general, the Nigerian tourmalines contained greater amounts of Ga, Ge, and Pb, whereas the Brazilian stones had more Mg, Zn, and Sb. The new Cu-bearing tourmalines from Mozambique showed enriched contents of Be, Sc, Ga, Pb, and Bi, but lacked Mg.

Copper-bearing elbaite with blue-to-green coloration is commonly called “Paraíba” tourmaline in the gem trade. This name refers to the state of Paraíba in Brazil, where such material was first discovered in the late 1980s (figure 1). Similar tourmaline was later found in the adjacent state of Rio Grande do Norte, and Brazil has been supplying limited amounts of this material to the world market for more than two decades. Today, however, Cu-bearing tourmaline is also being sourced from two countries in Africa: Nigeria and Mozambique. Cu-bearing tourmaline is priced in the gem trade according to its appearance as well as its geographic origin. The latter has stimulated the demand for origin information on identification reports issued by some gemological laboratories, and the availability of attractive Cu-bearing tourmaline from several geographic sources has complicated the origin determination of this valuable material.

In this article, we review the gemological proper-

ties and chemical composition of blue-to-green tourmalines from known localities in Brazil, Nigeria, and Mozambique that contain significant amounts of copper. We also present new chemical data determined by laser ablation–inductively coupled plasma–mass spectrometry (LA-ICP-MS) analyses of more than 198 tourmaline specimens from these three countries, and evaluate how these data can be used to determine geographic origin.

BACKGROUND

“Paraíba” tourmaline is by far the most valuable, and perhaps the most popular, of all tourmaline gem varieties. Traditionally, this trade name has been

See end of article for About the Authors and Acknowledgments.

GEMS & GEMOLOGY, Vol. 42, No. 1, pp. 4–21.

© 2006 Gemological Institute of America



Figure 1. Copper-bearing tourmaline is highly prized for its bright blue color. The 4.09 ct oval is from Mina da Batalha, the original locality for “Paraíba” tourmaline, in Paraíba State, northeastern Brazil (top, photo by Masaaki Kobayashi). The 19.90 ct drop-shape tourmaline is from Nigeria (upper right, courtesy of Frank Circelli, Bellagem, Duluth, Georgia; photo © Robert Weldon and GIA). The pear shape is from a new deposit located in the Alto Ligonha region of Mozambique, and weighs more than 40 ct (right, courtesy of August Mayer, Idar-Oberstein; photo © Robert Weldon).

reserved for Cu- and Mn-bearing, bright blue-to-green elbaite from Mina da Batalha, near São José da Batalha in Paraíba State, northeastern Brazil (Fritsch et al., 1990). Originally discovered in 1987, it appeared on the gem market shortly thereafter (Koivula and Kammerling, 1989). Similar but less saturated blue Cu-bearing tourmaline appeared in the gem trade during the 1990s from two mines in Rio Grande do Norte State: Mulungu and Alto dos Quintos (Karfunkel and Wegner, 1996; Shigley et al., 2001). The Mulungu mine is located 5 km north-northeast of the town of Parelhas, and Alto dos Quintos is situated about 10 km south of Parelhas. Although neither of these mines is located in Paraíba state, the tourmalines they produce are commonly referred to as “Paraíba” in the gem trade.

While the “Paraíba” tourmalines from these three Brazilian localities have some similarities, there are notable differences in the production from each mine. Mina da Batalha has been the source of fine blue-green and green tourmalines, with a small per-

centage of the material showing a distinct “neon” blue color. To date, the total production of copper-bearing blue-green and green elbaite from Mina da Batalha has been rather limited, although it is estimated to be at least 600 grams per year, or approximately 10,000 pieces of rough with most crystal fragments weighing less than 5 ct (M. Mizumura, pers. comm., 2005). In recent years, the tourmaline output from Mina da Batalha has dwindled in comparison to its greatest production of the best blue-to-green material, which reached 10,000–15,000 grams during the 1989–1991 period (Shigley et al., 2001). The Mulungu mine has yielded large amounts of good-quality light blue Cu-bearing elbaite (figure 2) and small quantities of blue-green and “emerald” green material. The maximum production is estimated at 1,000 grams of rough fragments per year that typically weigh less than 1 ct each. Most small pieces of rough “Paraíba” tourmaline in the Japanese market are from the Mulungu mine (M. Mizumura, pers. comm., 2005). The Alto dos Quintos mine is another source of



Figure 2. These light blue Cu-bearing tourmalines (0.41–0.50 ct) are from the Mulungu mine in Rio Grande do Norte State, Brazil. Courtesy of Hideki Sakamaki and Yuji Tsukuda; photo by Masaaki Kobayashi.



Figure 3. This ring is set with four Cu-bearing tourmalines (0.13–0.22 ct) from the Alto dos Quintos mine in Rio Grande do Norte State, Brazil. Courtesy of Hideki Sakamaki; photo by Masaaki Kobayashi.

melee-size light blue Cu-bearing elbaite (figure 3), and it also produces some green material. Large pieces weighing several carats are occasionally found. Although the output of “Paraíba” tourmaline from Alto dos Quintos decreased in 2005, the mine still regularly produces small amounts of material. In recent years, the production from all three Brazilian mines has fulfilled most of the Japanese demand for “Paraíba” tourmaline (Kitawaki, 2005).

Elbaite tourmaline from western Nigeria has been known in the gem trade since 2001 (figure 4; Henricus, 2001; Smith et al., 2001; Zang et al., 2001). The material reportedly originated from a mine in the Edeko area, near Ilorin in Ibadan State, southwestern Nigeria. It exhibits a wide range of color, from light blue, violetish blue, “neon” blue, and bluish green to “emerald” green; these colors are mainly due to variations in the copper and manganese contents. The typical inclusions in this tourmaline are similar to those seen in the Brazilian material. The Nigerian production has been sporadic (Shigley et al., 2001; Furuya, 2004), and some reports indicate that most of the Cu-bearing tourmaline from Nigeria has been sold in Germany, Brazil, and Bangkok (Milisenda, 2001).

According to chemical data on Nigerian tourmalines obtained with EDXRF spectroscopy (Smith et al., 2001), electron-microprobe analysis, and LA-ICP-MS (Zang et al., 2001), major amounts of Na, Al, Si, Cu, and Mn—and minor-to-trace contents of Mg, Ca, Ti, Fe, Zn, Pb, and Bi—were reported in violet-blue, bluish green, and green crystals. The highest concentration of copper measured was 2.18 wt.% CuO, and MnO reached 2.59 wt.% in violet-blue

samples (Zang et al., 2001). These studies indicate that there is an overlap in both the chemical composition and gemological properties between Nigerian and Brazilian copper-bearing tourmaline, so that materials from these two countries cannot be identified with these techniques alone. At the 29th International Gemological Conference in Wuhan, China, Furuya (2004) reported that there were two types of Cu-bearing tourmaline from Nigeria. Using qualita-

Figure 4. Cu-bearing elbaite from the Edeko area of western Nigeria are the center stones (3.05–3.56 ct) in these rings. This deposit, discovered in 2001, yields tourmaline with a color range similar to that of the Brazilian material. This high-copper-bearing tourmaline from Edeko is commonly referred to as Nigerian type I tourmaline by Japanese dealers. Courtesy of M. Furuya; photo by Masaaki Kobayashi.



tive EDXRF chemical analysis, he explained that light blue elbaite (which Japanese dealers refer to as *Nigerian type II tourmaline*; figure 5) from the Ofiki region in Ilorin State contained less Cu and more Pb than the high-copper-bearing Edeko material (referred to as *Nigerian type I tourmaline*), which further complicates separation of the Nigerian tourmalines from comparably colored elbaites from Brazil. For the past few years, there has been controversy over whether all of this material from Brazil and Nigeria should be called “Paraíba” tourmaline (Furuya, 2004).

In mid-2005, a new source of attractive Cu-bearing elbaite was discovered in Mozambique (Abduriyim and Kitawaki, 2005). The mining area is reportedly located in the Alto Ligonha region, approximately 100 km southwest of Nampula. A variety of colors have been produced, including blue to green (e.g., figure 6), violet, and pink. Excitement over this new source, and rumors of limited production, caused prices of faceted material to escalate at the September 2005 Hong Kong International Jewelry Fair, where the material first debuted.

Preliminary studies have indicated that the gemological properties and chemical composition of these Mozambique tourmalines resemble similarly colored tourmaline from both Brazil and Nigeria. In some early reports (Wentzell, 2004; Wentzell et al., 2005), color-change (purple in fluorescent light, gray

Figure 5. Tourmalines from the Ofiki area of Nigeria typically have a light blue color, as shown by these stones (0.28–0.43 ct). This material has a low copper concentration, and is commonly referred to as Nigerian type II tourmaline by Japanese dealers. Courtesy of Hideki Sakamaki; photo by A. Abduriyim.



Figure 6. These saturated bright blue (top, 0.70–6.11 ct) and blue-green (bottom, 0.26–5.98 ct) tourmalines are from a new deposit in the Alto Ligonha region of Mozambique. All of these stones were included in this study. Courtesy of Hideki Sakamaki; photos by Masaaki Kobayashi (top); H. Kitawaki (bottom).

to bluish green in incandescent light) tourmalines from the Moiane area in northern Mozambique were shown to contain traces of copper.

MATERIALS AND METHODS

We examined a total of 198 samples of Cu-bearing tourmaline from Brazil, Nigeria, and Mozambique (see table 1). The Brazilian materials included 71 rough and polished samples from Mina da Batalha in colors ranging from “turquoise” blue to “neon” blue, greenish blue to bluish green, and “emerald” green; 14 light blue faceted pieces from the Mulungu mine; and 10 faceted stones from the Alto dos Quintos mine that were light blue and light “neon” blue. All of these samples were either provided by two gem importers (Glorious Gems Co. and YT Stone Co.) or

TABLE 1. Tourmaline specimens used in this study.^a

Sample no. and locality	Quantity	Color	Weight (ct)	Type
Brazil				
B504-T001-007 (Mina da Batalha)	6	"Turquoise" blue	0.60–1.74	Cabochoons
B504-K001-020 (Mina da Batalha)	25	"Neon" blue, intense blue	0.22–0.30	Mixed rough and cut
B504-BG001-040 (Mina da Batalha)	30	Greenish blue to bluish green	0.11–3.21	Mixed rough and cut
B504-G001-015 (Mina da Batalha)	10	"Emerald" green	0.31–3.03	Cabochoons and mixed cuts
B504-M001-014 (Mulungu)	14	Light blue	0.40–0.50	Mixed cuts and fancy cuts
B504-Q001-003 (Alto dos Quintos)	3	Light blue	0.12–0.30	Fancy cuts
B504-Q004-010 (Alto dos Quintos)	7	Light "neon" blue	0.14–0.20	Fancy cuts
Nigeria				
NI001-007	7	Light blue	0.54–2.02	Cabochoons
N249-4-7	4	Violetish blue	0.25–1.12	Cabochoons and mixed cuts
N074-1-4, N249-1-3, NFB001-012, NI-1-6, GP-1-5	30	"Neon" blue to blue	0.34–21.72	Cabochoons and mixed cuts
NFG001-010, TEN-001-020	30	Greenish blue to bluish green	0.23–3.20	Mixed cuts
HVE02-1-15, Nfy001-005	10	"Emerald" green	0.18–2.45	Mixed cuts
Mozambique				
MS001	1	Light blue	0.27	Fancy cut
MA001-007	7	Bright blue	0.70–6.11	Fancy cuts
MVB001-002	2	Violet-blue, pale blue	4.65, 1.65	Polished flat
MBG001-010	10	Bluish green	0.26–5.98	Fancy cuts
MLG001-002	2	Light green	0.46, 0.95	Polished flat
MPP001 (used for heating experiments only)	1	Purplish pink	2.97	Polished flat
MY001 (used for heating experiments only)	1	Yellow	2.15	Polished flat

^a Gemological examination showed that none of the samples were filled with oil or resin.

Figure 7. These light blue and light "neon" blue "Paraíba" tourmalines (0.16–0.24 ct), also part of the study sample, were obtained by one of the authors at the Alto dos Quintos mine in Brazil. Photo by Masaaki Kobayashi.



collected *in situ* from the mines by the authors (see, e.g., figures 2 and 7).

The Nigerian tourmalines consisted of 31 faceted specimens in blue (including "neon" blue), greenish blue to bluish green, and "emerald" green that were

Figure 8. Shown here are some of the tourmalines (0.34–2.45 ct) from Edeko, Nigeria, that were analyzed for this study. Courtesy of Hideki Sakamaki; photo by Masaaki Kobayashi.





Figure 9. The Mozambique study samples included these light green, violet-blue, and pale blue Cu-bearing tourmaline fragments. Photos by Masaaki Kobayashi (left) and A. Abduriyim (right).

obtained by one of the authors (MF) at the October 2003 Bangkok gem fair from a rough stone dealer, Hussain Rezayee, and 50 polished samples in blue (including light blue, violetish blue, and “neon” blue), blue-green, and “emerald” green that were obtained from Nigerian miners by the two gem import companies (figure 8).

We analyzed 18 light blue, bright blue, and bluish green faceted samples of Mozambique tourmaline. We also tested four polished crystal fragments that were light violet-blue, pale blue, and light green (figure 9).

Internal features of all samples were observed with a gemological microscope. Refractive indices of all samples were measured with a standard gemological refractometer (Topcon) using a monochromatic Na-equivalent light source. Specific gravity was determined on all specimens by the hydrostatic method.

Chemical analyses of all samples were obtained by LA-ICP-MS (figure 10; table 2), which is widely used for the determination of major, minor, and trace elements in solids as well as for isotope-ratio

measurements (Jarvis and Williams, 1993; Günther and Hattendorf, 2005). The technique also has been applied to gem materials (see, e.g., Günther and Kane, 1999; Guillong and Günther, 2001). In this technique, a minute amount of the sample is vaporized by a high-energy laser beam, and the vaporized material is ionized into a plasma by a high-frequency power generator. This analytical method is capable of rapidly measuring a wide range of elements from helium to uranium, in very minute amounts (i.e., parts per million [ppm] to parts per billion [ppb] levels). The sample does not need to be placed in a vacuum with this technique, and a localized analysis of a specific area is possible with a narrow laser beam and a charge-coupling device (CCD) camera (to view the specific area). Currently, the spatial resolution (i.e., area of sample analyzed) achievable with laser ablation instruments is in the range of several micrometers, which is comparable to that of most other microbeam techniques (e.g., X-ray, electron, or proton microprobes). The measurement can be performed regardless of the condition of a sample (rough

Figure 10. The LA-ICP-MS system used in this study is shown on the left, with the laser ablation unit in the left foreground and the ICP-MS instrument behind it. The photo on the right is a close-up view of samples in the ablation chamber. Photos by Masaaki Kobayashi (left) and A. Abduriyim (right).



TABLE 2. Physical properties and LA-ICP-MS chemical data for Cu-bearing tourmalines from Brazil, Nigeria, and Mozambique.^a

Property/ chemical composition	Brazil						Nigeria	
	Mina da Batalha			Mulungu	Alto dos Quintos	Edeko		
Color	"Turquoise" blue	"Neon" blue, intense blue	Greenish blue to bluish green	"Emerald" green	Light blue	Light blue, light "neon" blue	Light blue	Violetish blue
No. samples	6	25	30	10	14	10	7	4
Properties								
R.I.								
n_o	1.639–1.642	1.638–1.640	1.638–1.640	1.638–1.640	1.639–1.640	1.638–1.640	1.639–1.640	1.638–1.639
n_e	1.619–1.621	1.618–1.619	1.618–1.620	1.619–1.620	1.619–1.621	1.619–1.620	1.619–1.620	1.618–1.620
Birefringence	0.020–0.021	0.018–0.021	0.018–0.020	0.019–0.020	0.019–0.020	0.019–0.020	0.020	0.018–0.020
S.G.	3.04–3.07	3.04–3.09	3.06–3.08	3.05–3.09	3.08–3.13	3.04–3.09	3.06–3.09	3.08–3.09
Chemical composition								
Major elements (wt.% oxide)								
Al_2O_3	37.85–39.25	37.96–39.02	38.30–39.74	38.17–39.62	37.67–41.85	38.30–41.03	39.14–41.31	39.98–41.09
SiO_2	35.97–36.73	36.36–37.01	36.56–37.11	36.54–37.56	35.96–38.47	36.96–38.11	37.01–38.17	37.51–39.02
B_2O_3	9.42–10.19	9.80–11.34	9.05–11.19	9.57–12.62	8.98–9.96	9.05–11.19	9.81–10.09	10.47–11.49
Minor elements (wt.% oxide)								
Li_2O	1.58–1.71	1.60–1.74	1.65–1.81	1.51–1.85	1.61–1.71	1.34–1.75	1.53–1.84	1.69–1.78
Na_2O	1.98–2.49	2.20–2.35	2.23–2.78	1.70–2.87	1.75–2.47	1.62–2.78	2.14–2.34	2.32–2.78
MnO	0.29–0.34	0.02–2.96	1.25–3.43	0.97–2.52	0.15–0.58	0.13–0.92	1.71–2.49	1.70–2.81
CuO	0.42–0.57	0.69–2.50	0.74–2.17	0.86–2.32	0.40–0.51	0.41–1.33	0.48–0.95	0.60–2.01
Trace elements (ppm)								
Be	7–8	14–176	14–64	7–128	6–9	15–46	5–6	5–58
Mg	0.5–2	2–4470	387–1070	1000–6620	1–3	0.6–97	2–8	2–15
K	100–140	120–150	127–280	96–190	88–140	86–157	120–270	160–240
Ca	1250–1700	1350–7190	3570–8090	1680–6460	980–1770	1610–8880	1160–1630	1480–1540
Sc	0.7–1	1–3	0.8–2	2–4	0.6–1	0.6–1	2–4	2
Ti	18–41	9–410	200–380	280–880	16–42	12–220	17–180	29–110
V	0.5–0.9	0.2–12	0.9–3	2–16	0.6–2	0.2–6	0.3–0.8	0.6–3
Fe	6–41	bdl–350	580–1440	1160–4260	12–130	bdl–590	17–97	38–68
Zn	11–21	10–2490	1510–9400	420–12330	19–92	5–124	12–88	11–93
Ga	160–230	67–160	49–130	44–150	170–250	160–260	140–210	190–270
Ge	3–6	5–43	7–34	4–45	4–10	15–26	10–22	13–57
Sr	bdl	0.1–4	0.4–3	bdl–58	bdl	bdl–2	bdl	bdl–3
Nb	1–3	bdl–3	0.5–4	0.5–0.6	1.2–3	0.8–7	0.1–0.6	0.2–0.5
Sn	bdl–0.5	bdl–2	bdl–2	bdl–4	2–5	3–6	0.5–4	bdl–0.8
Sb	bdl	1–22	16–41	0.2–22	bdl–0.3	3–17	0.2–2	0.3–5
Ta	1–2	1–10	0.2–1	0.4–3	0.9–2	67–23	0.3–3	1–2
Pb	1–5	22–120	37–242	5–180	1–4	31–65	18–36	24–130
Bi	14–56	290–13840	380–4490	290–11730	19–79	78–1130	44–140	150–880

^a The table shows the minimum and maximum values obtained for 95 samples from Brazil, 81 tourmalines from Nigeria, and 22 specimens from Mozambique. Each sample was analyzed in three spots, using a laser repetition rate of 10 Hz and an ablation interval of 15 sec. Data for Ca and K showed poor correlation between each analysis, while the other elements showed little variation. Abbreviation: bdl = below detection limit of the LA-ICP-MS system. Detection limits (ppm) are as follows: Li (1.9), Be (0.1), B (1.5), Na (17), Mg (0.4), Al (0.7), Si (520), K (3.4), Ca (200), Sc

or polished) when using the fourth harmonic (266 nm) and the fifth harmonic (213 nm) of a tunable Nd-YAG laser or using an excimer laser (193 nm). The analysis creates a small surface crater (diameter of ~60–80 μ m and depth of ~5–10 μ m), so on a faceted stone the girdle is the most suitable area for testing. LA-ICP-MS is four orders of magnitude more sensitive than laser-induced breakdown spectroscopy (LIBS; Günther and Hattendorf, 2005).

We used a Merchantek UP-213A/F laser ablation system (New Wave Research) with an Agilent 7500a ICP-MS for this study (again, see figure 10). A 213 nm laser was employed with a power of 2.5 mJ and a spot size of 60 μ m, using a carrier gas mixture of helium (0.50 ml/min) and argon (1.20–1.23 ml/min). The laser repetition rate was 10 Hz, with an energy density of 14.63 J/cm², ablation interval of 15 seconds, elapsed time of 0.01 seconds, and a measure-

Nigeria (cont.)			Mozambique				
Edeko (cont.)			Alto Ligonha				
"Neon" blue to blue	Greenish blue to bluish green	"Emerald" green	Light blue	Bright blue	Violet-blue, pale blue	Bluish green	Light green
30	30	10	1	7	2	10	2
1.638–1.640	1.639–1.641	1.639–1.640	1.639	1.638–1.639	1.639	1.639–1.640	1.639
1.618–1.621	1.620–1.621	1.619–1.620	1.619	1.618–1.620	1.620	1.619–1.620	1.619, 1.620
0.018–0.021	0.019–0.021	0.019–0.020	0.020	0.018–0.019	0.019	0.020–0.021	0.019, 0.020
3.04–3.09	3.06–3.10	3.07–3.09	3.08	3.07–3.09	3.07, 3.08	3.06–3.09	3.09, 3.10
40.60–42.97	39.14–42.31	38.66–41.62	39.53	39.49–41.52	39.20–40.23	37.18–38.69	38.16–38.81
39.43–41.96	36.33–39.74	36.95–39.02	37.64	37.83–39.44	37.10–38.67	36.81–38.26	37.80–38.47
9.80–11.03	10.47–12.31	9.03–11.52	11.84	8.73–9.42	9.11–10.23	9.81–12.22	8.56–9.01
1.80–1.93	1.65–1.99	1.40–2.02	1.68	1.37–2.07	1.33–1.46	1.75–1.88	1.35–1.47
2.32–2.60	2.07–3.03	2.40–2.80	2.21	1.87–2.66	2.15–2.27	1.78–2.89	2.00–2.14
1.71–6.06	1.83–3.96	2.81–5.05	3.55	0.03–0.40	2.62–3.04	3.28–4.81	3.09–3.36
0.60–3.20	0.89–2.15	1.03–2.36	1.19	0.26–0.51	0.33–0.40	2.08–3.21	0.16–0.26
6–52	9–110	5–89	7	71–300	29–33	24–96	38–42
4–38	13–64	61–86	4	bdl–3	bdl–0.4	bdl–7	7–9
130–260	130–290	300–360	230	93–130	140–150	210–240	130–170
1620–5590	1710–6850	2240–5350	1670	1640–9230	4680–5060	1900–6130	1900–2460
2–3	0.8–2	1–2	8	2–6	1–2	9–15	4–11
27–450	280–610	370–870	140	11–46	8–11	19–1190	27–30
0.3–0.6	0.7–2	1–2	1	0.3–0.9	0.4–0.8	0.8–5	1–2
50–660	200–1990	650–3910	150	bdl–490	100–110	36–790	2450–2960
57–270	95–1310	700–1690	110	bdl	4–7	250–980	36–45
130–210	88–290	180–300	300	160–370	210–250	180–260	200–220
9–34	12–47	19–62	22	12–29	6–12	26–65	10–13
bdl–4	0.1–6	0.1–3	0.1	0.1–2	0.5–0.7	0.2–2	0.9–2
0.1–0.4	0.6–2	0.9–1	0.6	0.2–2	3–4	0.4–3	0.4
0.6–1	bdl–0.4	0.4–1	bdl	bdl	5–6	bdl	36–39
0.4–7	8–14	3–14	0.5	14–54	5–6	5–11	11–13
bdl–3	bdl–3	0.9–2	2	0.3–5	2–3	2–8	0.9–1
38–750	56–350	38–420	32	90–210	61–78	250–710	21–23
270–10540	1030–4470	44–2590	92	3340–19480	1300–1460	1090–7910	2080–2800

(0.3), Ti (0.8), V (0.13), Cr (14), Mn (0.3), Fe (7), Cu (0.3), Zn (2.0), Ga (0.2), Ge (0.5), Sr (0.03), Nb (0.02), Sn (0.4), Sb (0.04), Ta (0.01), Pb (0.1), and Bi (0.01). H₂O cannot be measured by LA-ICP-MS, but this value was reported as 3.13 wt.% by Fritsch et al. (1990). Fluorine and chlorine were not measured in this study.

ment time of 40 seconds. Thus, it was possible to detect the signal of all isotope ratios (atomic mass/atomic number of 2–260) and achieve an analytical precision of RSD (relative standard deviation) of less than 10%. However, Mg, Si, K, and Fe occasionally have higher RSDs in tourmaline due to the interference from a material matrix and polyatomic ions such as ²⁴Mg (¹²C¹²C), ²⁸Si (¹²C¹⁶O), ³⁹K (²³Na¹⁶O), ⁵⁶Fe (⁴⁰Ar¹⁶O⁺, ⁴⁰Ca¹⁶O, ²⁸Si²⁸Si).

During laser ablation sampling, matrix-matched calibration is necessary to avoid problems associated with elemental fractionation (i.e., the ablated mass composition is not the same as the actual sample composition). In this study, quantitative analysis was performed by calculating a concentration conversion factor for each element, and a glass reference material (NIST SRM 612; Pearce et al., 1996) was used as an external standard of known isotopic

BOX A: COLOR MODIFICATION WITH HEAT TREATMENT OF SOME MOZAMBIQUE TOURMALINES

It is estimated that 80% of the production of Brazilian Cu-bearing tourmaline does not show bright blue to greenish blue “Paraíba” colors until it has undergone heat treatment. Low to moderate temperatures are used (e.g., 350–550°C in Koivula and Kammerling, 1990; 550°C in Fritsch et al., 1990). Heating is also performed on Nigerian violet and violet-blue tourmaline (Zang et al., 2001). The color can be changed from purplish red to “emerald” green, greenish blue to “neon” blue, and violet blue to “neon” blue (Fritsch et al., 1990; Bernardes, 1999; Shigley et al., 2001). The chromophores Mn and Cu in particular play an important role in the cause of color and the color modification of “Paraíba” tourmaline.

To investigate the effect of heat treatment on the newly discovered Cu-bearing tourmaline from Mozambique, we selected four representative polished fragments (purplish pink, violet-blue, light green, and yellow; see figure A-1). The purplish pink fragment was cut into three sections, with one retained as a control and the other two subjected to progressively higher temperatures. All of the other fragments were cut into two sections, with one of each retained as a color control and the others heat treated. We buried the sections to be

treated in aluminum powder within a crucible. We then heated the crucible in an electric furnace in an oxidizing atmosphere. The temperature was carefully controlled, and heating was performed (and the samples checked) at two-hour intervals at 300, 350, 400, 450, and 500°C. The furnace was then turned off, and the samples cooled to about 60–70°C within one hour.

The purplish pink specimen lightened slightly at 400°C, and its counterpart faded to colorless at 500°C (figure A-1). Pink coloration related to Mn³⁺ absorption at about 515 nm disappeared when the manganese was reduced to Mn²⁺ during heat treatment (figure A-2). Heating of a light violet-blue specimen resulted in “neon” blue coloration at 500°C. This violet-blue sample exhibited a broad band centered at about 690 nm that is related to Cu²⁺; the band remained unchanged after heating, though a broad band related to Mn³⁺ absorption centered at about 515 nm was removed. The color of a light green sample intensified slightly with heating, whereas a yellow specimen remained unchanged by the heating process. No significant changes were seen in the visible-range absorption spectra of the light green and yellow samples after heating to 500°C, but the absorption peaks did shift toward the ultraviolet.

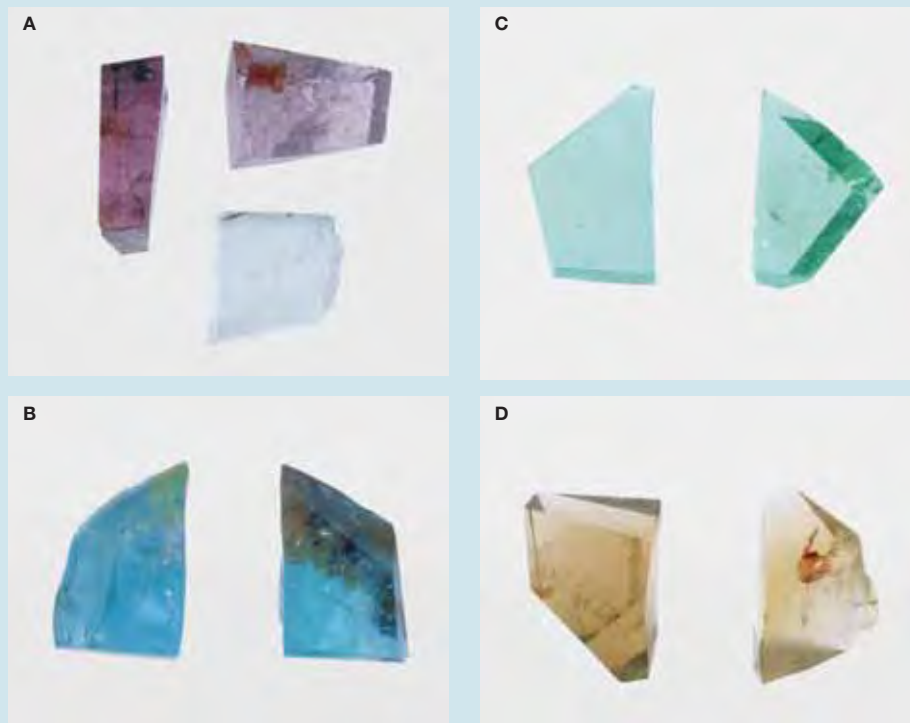
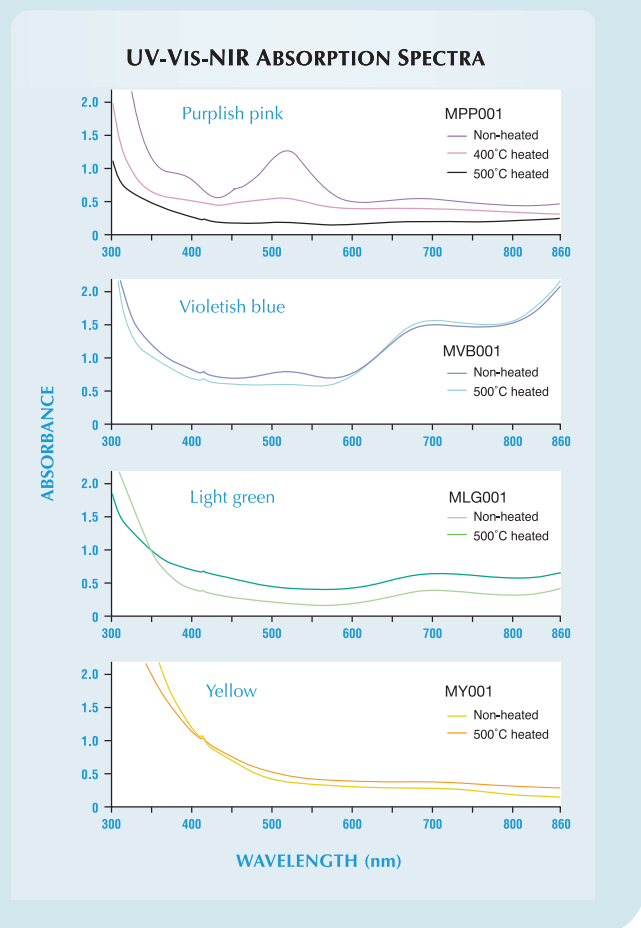


Figure A-1. Four polished fragments of Cu-bearing Mozambique tourmaline were cut into sections, with one section of each retained as the control color and the other(s) subjected to heating experiments. (A) The purplish pink sample started to fade at 400°C (top right), and at 500°C the material was colorless (bottom right). (B) The light violet-blue specimen became “neon” blue (right) after heating to 500°C. (C) The green fragment became only slightly more intense (right) with heating to 500°C. (D) The yellow sample was not improved by heating. Before they were sliced for the heating experiments, the samples weighed 2.97 ct, 4.65 ct, 0.95 ct, and 2.15 ct, respectively. Photos by Masaaki Kobayashi.

From these preliminary experiments, it appears that not all color varieties of Mozambique Cu-bearing tourmaline can be improved by heat treatment at these conditions. However, if the proper starting materials are selected, heating may yield favorable color modification. Because exposure to heat can damage some stones, especially those with liquid inclusions and pre-existing fractures, it is critical that the starting material is carefully selected and the temperature controlled precisely.

Figure A-2. These UV-Vis-NIR spectra of Cu-bearing Mozambique tourmalines of various colors show absorption characteristics before and after the samples were heated in an oxidizing atmosphere. The purplish pink sample (MPP001) exhibits a decrease in Mn^{3+} absorption at about 515 nm, when this element was reduced to Mn^{2+} as the temperature increased from 400°C to 500°C. The violetish blue sample (MVB001) exhibits a broad band centered at about 690 nm that is related to Cu^{2+} ; the band remained unchanged after heating, although the sample turned “neon” blue when heated to 500°C. No significant changes are seen in the absorption spectra of the light green (MLG001) and yellow (MY001) samples after heating to 500°C.



composition to calculate the mass of measured isotopic ratios in the tourmaline samples. The contents of major and minor elements were calculated in weight percent (wt.%) oxides, while the trace elements are reported in parts per million by weight. Three analytical runs were performed on separate locations on each sample (on the girdle of the faceted stones), and average data are reported for each sample in table 2. Detection limits of 3σ (standard deviations) were calculated for 26 selected elements that were analyzed 10 times in empty runs, and are reported in the footnote to table 2.

To investigate the effects of heat treatment on the new Mozambique Cu-bearing tourmaline, we conducted experiments on four representative crystal fragments (purplish pink, violet-blue, light green, and yellow, as described in table 1) using an Advantec model FUH712PA electric furnace. UV-visible spectroscopic analyses were conducted with a Shimadzu UV-2450 spectrophotometer on both heated and unheated sections of each crystal fragment (see box A).

RESULTS AND DISCUSSION

Gemological Properties. The physical properties of our Cu-bearing tourmaline samples are reported in table 2 and summarized below. The refractive indices of 95 samples from Brazil were $n_o=1.638-1.642$ and $n_e=1.618-1.621$, birefringence was 0.018–0.021, and S.G. values varied from 3.04 to 3.13. The R.I. values mostly fell within the ranges reported for Cu-bearing elbaite tourmalines from Brazil (e.g., Mina da Batalha—Fritsch et al., 1990; Mulungu—Shigley et al., 2001; and Alto dos Quintos—Milisenda, 2005), but our range of S.G. values was slightly higher.

The gemological properties of the 81 tourmaline samples from Edeko, Nigeria, were: R.I.— $n_o=1.638-1.641$ and $n_e=1.619-1.620$; birefringence—0.018–0.021; S.G.—3.04–3.10. These values are consistent with data reported for similar Nigerian material by Smith et al. (2001). All specimens exhibited typical tourmaline inclusions, such as two-phase liquid-gas inclusions, healed fractures, “feathers,” and crystals (e.g., mica, figure 11). Fritsch et al. (1990), Koivula et al. (1992), Cassedanne (1996), and Shigley et al. (2001) reported that similar features were common in “Paraíba” tourmalines from Brazil.

It is notable, however, that most of the Nigerian tourmalines (all of which were faceted) displayed thin yellowish brown needle-like growth tubes oriented parallel to the optic axis (figure 12).

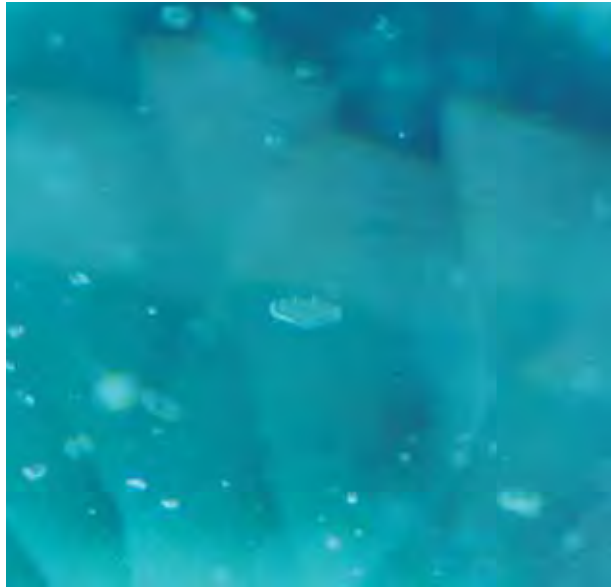


Figure 11. The mica inclusions seen in this Nigerian tourmaline formed transparent hexagonal platelets. Photomicrograph by Makoto Okano; magnified 50 \times .

We observed these growth tubes most frequently in the blue tourmalines, but they also were seen in a few of the green samples. The Brazilian and Mozambique faceted samples showed few of these yellowish brown growth tubes, but some were distributed near the surface of crystal fragments from both countries; their coloration is possibly due to iron-oxide staining. In faceted stones, these tubes may be indicative of tourmalines from Nigeria. Interestingly, four of our Nigerian specimens also contained inclusions of native copper (identified by LA-ICP-MS) that appeared brownish yellow with magnification (figure 13). A distinct yellow reflectance in the apparent metallic luster was visible when the stones were viewed with a fiber-optic light source. Thin platelets and scattered grains of the native copper, ranging from 10 to 150 μm long in varying thicknesses, were observed in orientations parallel to the *c*-axis. Koivula et al. (1992) and Brandstätter and Niedermayr (1994) reported seeing platelet-like native copper inclusions in some tourmalines from Mina da Batalha, Paraíba, but only one of our samples from this locality contained these inclusions.

Gemological properties obtained for our 22 Mozambique tourmaline samples were: R.I.— $n_o=1.638\text{--}1.640$ and $n_e=1.618\text{--}1.620$; birefringence— $0.018\text{--}0.021$; and S.G.— $3.06\text{--}3.10$. These properties fell within the ranges listed for elbaite tourmaline from Brazil and Nigeria (table 2; see also Fritsch et al., 1990). The internal features consisted of the liq-

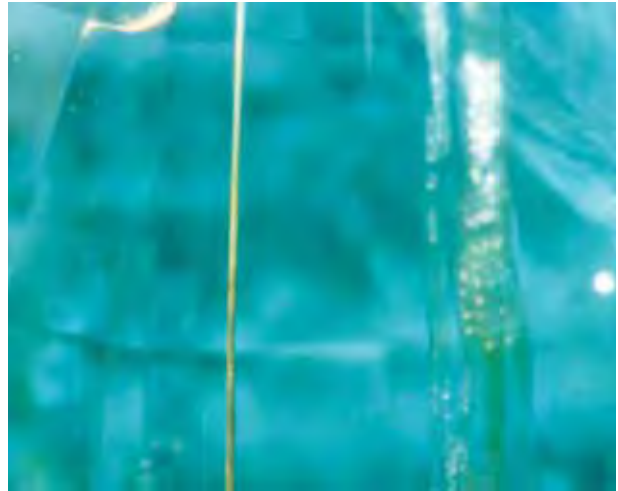


Figure 12. Most of the Nigerian tourmalines contained yellowish brown growth tubes. Photomicrograph by A. Abduriyim; magnified 40 \times .

uid inclusions, two-phase liquid-gas inclusions, and healed fractures that are commonly seen in tourmaline; no particles of native copper were observed.

Chemical Analysis. The chemical data for the Cu-bearing tourmalines from Brazil, Nigeria, and Mozambique are summarized in table 2. For the purposes of this article, these results are described below for each of three color groups: “Paraíba” blue, blue-green, and “emerald” green.

Figure 13. These brownish yellow-appearing metallic inclusions in Nigerian tourmaline were identified as native copper by LA-ICP-MS. The copper platelets are oriented parallel to the *c*-axis of the tourmaline. Photomicrograph by A. Abduriyim; magnified 60 \times .



“Paraíba” Blue. Included in this color group are light blue, violetish blue, “turquoise” blue, “neon” blue, and blue tourmalines. The 31 Mina da Batalha tourmalines in this color range were “turquoise” blue, “neon” blue, and intense blue. These samples consistently contained 18 minor and trace elements (Li, B, Be, Na, Mg, K, Ca, Sc, Ti, V, Mn, Fe, Cu, Zn, Ga, Ge, Pb, Bi). Other trace elements such as Sr, Nb, Sn, and Sb were above the detection limits in some specimens. Generally, our Mina da Batalha “turquoise” blue specimens had lower Cu and Mn contents than in the other colors (i.e., up to 0.57 wt.% CuO and 0.34 wt.% MnO). Our “neon” blue and intense blue specimens contained more Cu and Mn than previously has been reported for blue elbaite tourmaline from Mina da Batalha (up to 2.50 wt.% CuO and 2.96 wt.% MnO; see table 3)

By comparison, our Nigerian “Paraíba” blue tourmaline showed more Cu and Mn than these specimens from Mina da Batalha. The latter samples contained limited amounts of the trace elements Ga, Ge, and Pb, while Be and Zn were relatively abundant.

The 14 specimens of Brazilian Mulungu tourmaline analyzed for this study were all light blue, and they contained relatively low levels of Cu and Mn (mostly below 0.51 wt.% CuO and 0.58 wt.% MnO). The Cu contents of our samples were a little higher than the level reported for a blue sample by Shigley et al. (2001): 0.44 wt.% CuO (table 3). The trace elements Sc, Ga, Ge, Nb, Sn, and Pb were consistently detectable, but contents of K, Ti, Ge, and Pb were low compared to our samples of light blue tourmaline from Nigeria.

Three light blue specimens from Alto dos

Quintos, Brazil, were quite similar in color to Mulungu tourmaline, with seven specimens of lighter “neon” blue color. Most analyzed elements for these Alto dos Quintos stones were in good agreement with those of the Mulungu specimens, except that Ca, Bi, Sb, Ta, and Pb showed higher values.

The Nigerian specimens analyzed in this color group were violetish blue, “neon” blue, and light blue; they contained 0.48–3.20 wt.% CuO and 1.70–6.06 wt.% MnO. The light blue tourmalines revealed the lowest Cu and Mn contents (<0.95 wt.% CuO, <2.49 wt.% MnO), and four violetish blue specimens showed almost the same range of Cu (0.60–2.01 wt.% CuO) as reported in violet-blue Nigerian tourmalines by Zang et al. (2001; table 3). The transition-metal elements Ti, V, and Fe were at trace levels, but Cr was characteristically below the detection limits of our instrument (<13.7 ppm). Other trace elements (Mg, Ti, Fe, Ca, K, Zn, Ga, Ge, Pb, and Bi) were usually present in significant concentrations in all the “Paraíba” blue Nigerian tourmalines, in agreement with Zang et al. (2001). Of the light elements, Li₂O was between 1.53 and 1.93 wt.%, while B₂O₃ had a wider range (9.80–11.49 wt.%), and Be was detected only in trace amounts.

The bright blue specimens of Mozambique tourmaline showed amounts of Al and Si comparable to those of Cu-bearing elbaite from Nigeria and Brazil. However, the Cu and Mn contents of most Mozambique samples were lower than in samples from Nigeria and Brazil. They ranged from 0.26 to 0.51 wt.% CuO and 0.03 to 0.40 wt.% MnO. The trace amounts of Be, Ca, Sr, Sb, Pb, and Bi were higher than those found in “Paraíba” blue tourmalines

TABLE 3. Contents of Cu and Mn in “Paraíba” blue, blue-green, and “emerald” green tourmaline from Brazil and Nigeria, as reported in the literature.

Samples and Cu/Mn content	Brazil						Nigeria	
	Mina da Batalha (Fritsch et al., 1990)			Mulungu (Shigley et al., 2001)		Alto dos Quintos (Milisenda, 2005)		Edeko (Zang, 2001)
Color	“Paraíba” blue (blue)	Blue-green	“Emerald” green	“Paraíba” blue (light blue)	Blue-green	“Paraíba” blue (light blue, blue)	Blue-green	“Paraíba” blue (violetish blue)
No. samples	1	3	1	1	5	10	2	3
Oxides (wt.%)								
CuO	0.72	1.08–2.37	2.38	0.44	0.41–0.69	0.32–1.52	1.28, 1.48	0.51–2.18
MnO	2.30	0.85–1.48	2.16	0.42	0.79–3.15	0.11–2.53	2.44	2.13–2.59

from other localities, and Mg, Zn, and Sn were below the detection limits of our LA-ICP-MS system in most of the Mozambique samples. One specimen (MS001) of light blue color had significantly higher Cu and Mn contents than our light blue tourmalines from Nigeria and Rio Grande do Norte. Subsequent analyses of two polished crystal fragments (MVB001-002, violetish blue and pale blue) revealed the highest concentration of Cu measured in Mozambique tourmalines of similar color (up to 0.40 wt.% CuO), as well as enriched Mn (up to 3.04 wt.% MnO). Notably high amounts of Ca and Bi—and low levels of Ti, Zn, and Ge—were detected in these two specimens, while Mg was below or near the detection limit (<0.40 ppm).

Blue-Green. This color series consists of greenish blue to bluish green samples. We measured slightly higher contents of Al and Si in the Nigerian tourmalines compared to those from the other localities. The transition-metal elements Mn, Fe, and Ti strongly correlated to blue-green color, especially in

Nigerian tourmaline with the stronger coloration. Most of the Brazilian tourmalines were notably enriched in Mg, Zn, and Sb, and depleted in Ga, Ge, and Pb, while the highest Bi content was found in blue-green samples from both Brazil and Nigeria.

The Cu and Mn contents were especially noteworthy in the bluish green to greenish blue tourmalines from Mozambique, which contained much more of these elements (up to 3.21 wt.% CuO and 4.81 wt.% MnO) than did the samples from the other two countries. Although the trace elements Sc, Ga, and Pb in most of the specimens from Mozambique were higher than in equivalently colored tourmaline from Nigeria and Brazil, only minute amounts of Mg were detected in a few of the Mozambique stones.

“Emerald” Green. In the “emerald” green Nigerian tourmalines analyzed, most compositions overlapped those of the blue-green series from this area. However, the amounts of Ti, Mn, Fe, Cu, and Bi dif-

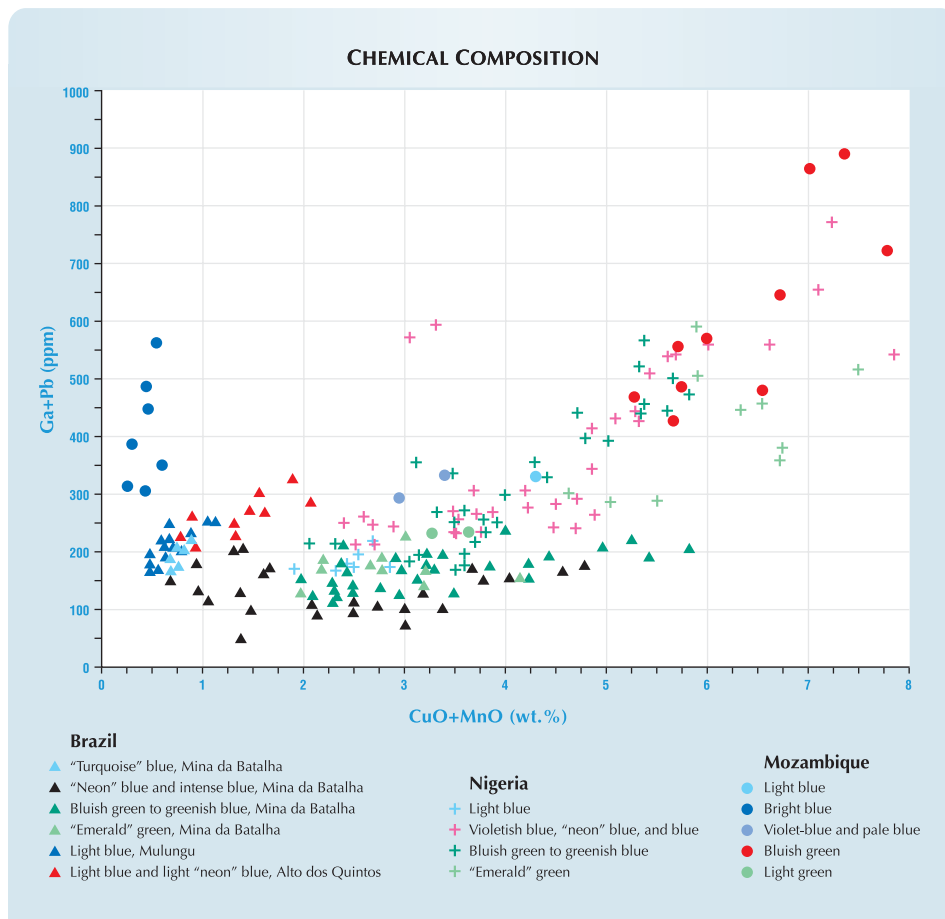


Figure 14. Chemical data obtained by LA-ICP-MS on all 198 samples are plotted according to CuO+MnO versus Ga+Pb in this diagram. The Nigerian tourmalines commonly had higher CuO+MnO and Ga+Pb values. The Brazilian samples showed some discrete populations compared to the Nigerian tourmalines, with lower Cu, Mn, and Pb contents overall. The bright blue Mozambique tourmalines had some of the lowest Cu and Mn contents, but these elements (together with Pb) were enriched in the blue-green tourmalines from this locality. Relatively high levels of Ga+Pb also were typical of the Mozambique samples.

ferred between the two color groups. As expected, the contents of the chromophores Ti, Mn, and Fe were highest in our “emerald” green specimens and lowest in the light blue samples. Notably, the “emerald” green specimens from Mina da Batalha typically contained much more Mg and Zn than those from Nigeria. None of our Mozambique samples displayed a distinct “emerald” green color; rather, they were light green. Our two light green specimens (MLG001-002) revealed much lower Cu than was detected in “Paraíba” blue material from the same locality, as well as in Nigerian and Brazilian samples from all three color series. These light green samples also contained low amounts of Mg, Ti, Zn, and Pb, and enriched Sn.

Chemical Fingerprinting. To evaluate the usefulness of chemical data for separating the tourmalines from the various localities, we plotted two different combinations of minor and trace elements (figures 14 and 15) in light of the chemical trends noted above.

The tourmalines from Nigeria and from all three localities in Brazil are relatively distinct in the diagrams. As seen in figure 14, by plotting Ga+Pb versus CuO+MnO it is possible to separate the tourmalines according to the three color series: “Paraíba” blue, blue-green, and “emerald” green. The light blue Nigerian samples show some overlap with blue-green and “emerald” green Mina da Batalha specimens. However, the tourmalines of similar light blue color from Mulungu and Alto dos Quintos, as well as “turquoise” blue samples from Mina da Batalha, define an area of lower Cu and Mn contents.

The Mozambique tourmalines show distinct variations in their composition according to color. The seven bright blue stones fall into a very limited field that is characterized by low concentrations of CuO+MnO (<1 wt.%) and enriched Ga+Pb (>300 ppm; figure 14). These tourmalines can be clearly differentiated from the Nigerian and Brazilian stones on this basis. The Mozambique light blue and bluish

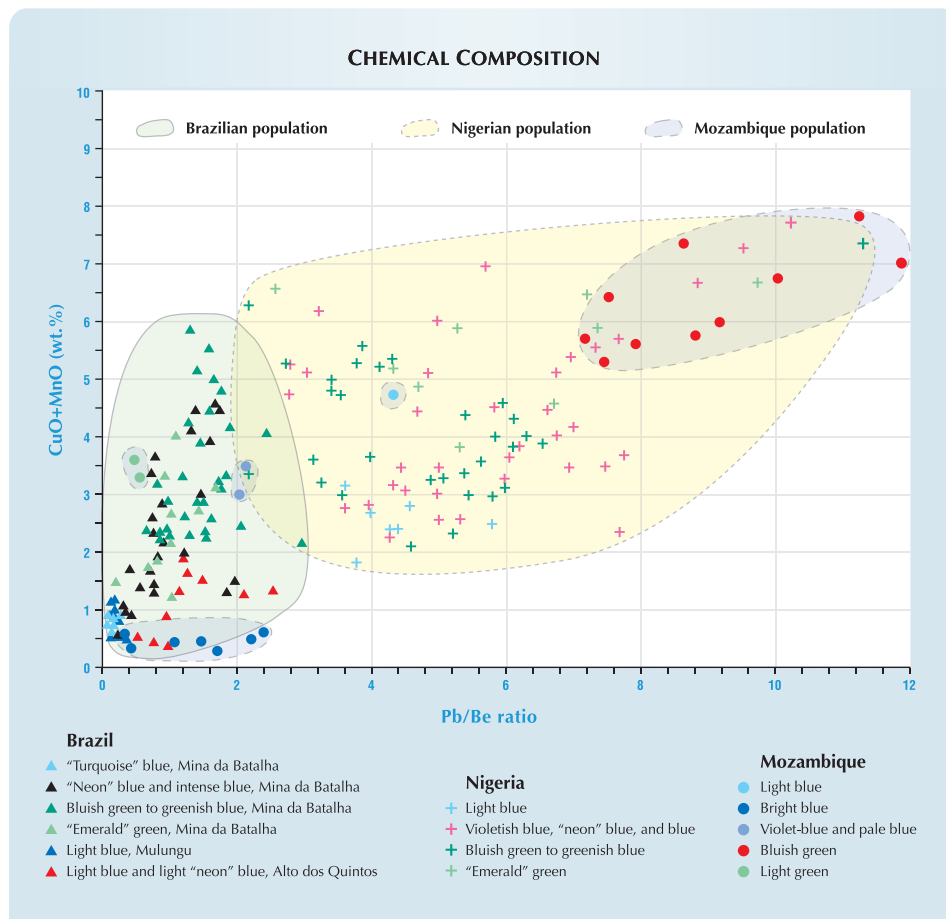


Figure 15. In this plot of CuO+MnO versus the ratio Pb/Be, there is clear separation of most Nigerian and Brazilian specimens, but a few blue-green from these localities show minor overlap. The Mozambique samples overlap the Nigerian and Brazilian fields in various places according to color.

green tourmalines are characterized by higher concentrations of CuO+MnO (>4 wt.%) and a similar concentration of Ga+Pb (>300 ppm), which is distinctly higher than Brazilian stones but overlaps the Nigerian samples. The data for the four crystal fragments of Mozambique tourmaline (light green, violetish blue, and pale blue) show lower concentrations of CuO+MnO (<4 wt.%). The violetish blue sample is distinct from “Paraíba” blue material from the Brazilian localities, but it overlaps samples of the same color from Nigeria. Although the composition of the two light green fragments overlap the Brazilian and Nigerian blue-green and “emerald” green samples in figure 14, they are chemically distinct in their very low CuO contents.

The CuO+MnO versus Pb/Be diagram (figure 15) is more effective at separating the Nigerian and Brazilian tourmalines. The Pb/Be ratio for the Brazilian tourmalines is usually less than 3, whereas this ratio for Nigerian tourmalines is typically much higher (3 to 11). A few blue-green specimens from Nigeria show a very small overlap with similarly colored Mina da Batalha tourmaline.

The blue-green tourmalines from Mozambique had the highest values of Cu, Mn, Ga, and Pb in this

study. However, the points representing these 10 samples lie in fields that almost completely overlap the Nigerian blue-green and “emerald” green stones. The lowest ratios of Pb/Be in the Mozambique tourmalines were found in the low Cu- and high Mn-bearing violetish blue and light green fragments, as well as in the lowest Cu- and Mn-bearing bright blue samples; they overlap the Brazilian population in figure 15.

According to the data from this study, the chemical fingerprinting methods used in figures 14 and 15 are not very effective at separating the Mozambique blue-green elbaite from the Nigerian tourmalines, but they are effective in separating tourmalines from the two African localities from those found in Brazil. In addition, our samples from the three Brazilian mines fell into discrete or partially overlapping fields. The chemical data also showed that, in general, the more intense blue-green and “emerald” green colors correlated to higher Cu and Mn contents.

However, a number of trace elements such as Mg, Ga, Pb, and Bi were present at different levels in the Mozambique blue-green elbaite compared to what was detected in blue-green stones from Nigeria. A ternary diagram of Mg-Zn-Pb (figure 16)

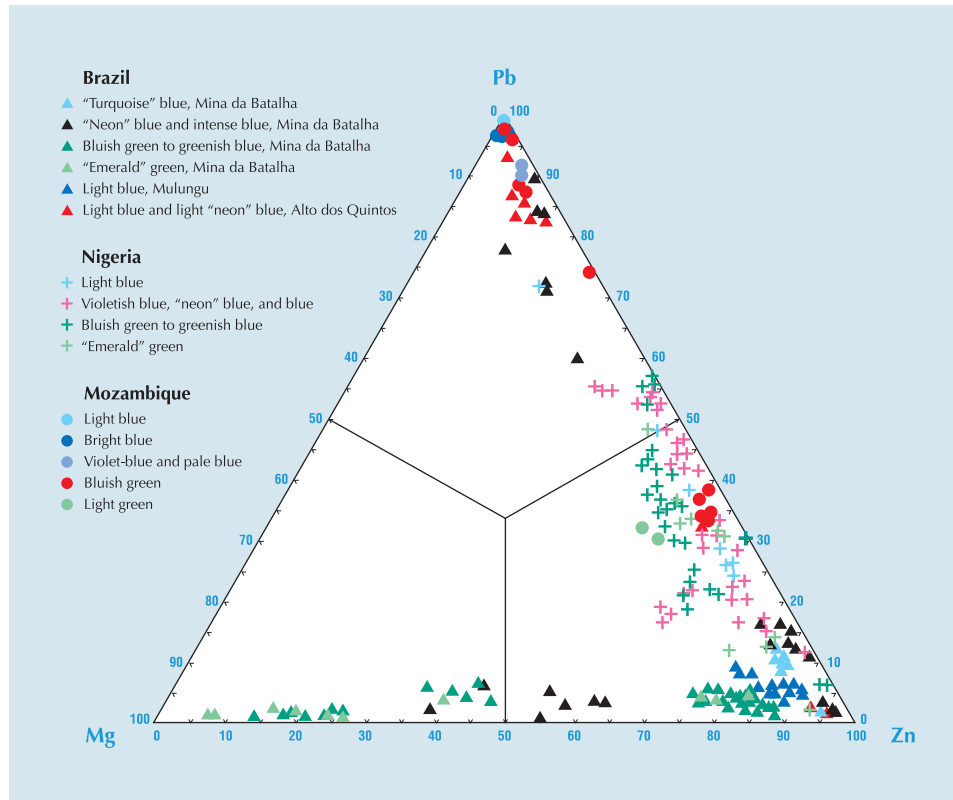


Figure 16. This Mg-Zn-Pb ternary diagram indicates that the Nigerian specimens are typically Pb-Zn dominant, the Brazilian samples are Mg-Zn dominant, and the Mozambique tourmalines are Pb dominant with some transitional Pb-Zn compositions.

provides a convenient way to help differentiate some Cu-bearing tourmaline from these three countries. The Nigerian specimens occupy the Pb-Zn-dominant fields, while most of the Brazilian tourmalines fall into the Mg-Zn region, and most of the Mozambique samples are Pb dominant (with some intermediate Pb-Zn compositions). There is a clear separation in the tourmaline samples from two of the Brazilian mining areas (Mina da Batalha and Mulungu), and in the samples from Nigeria, and Mozambique. However, some Alto dos Quintos specimens overlap the Nigerian and other Brazilian stones. Most importantly, whereas the low Cu- and high Mn-bearing (violet-blue, pale blue, and light green) Mozambique samples cannot be separated conclusively from the Brazilian materials with figures 14 and 15, this ternary diagram clearly distinguishes these localities.

NOMENCLATURE OF "PARAÍBA" TOURMALINE

The Association of Gemmological Laboratories (AGL) in Japan currently specifies that a blue-to-green tourmaline showing the characteristic "neon" color due to copper can only be called "Paraíba" as a trade name on an identification report when the stone is confirmed to be from Brazil. AGL allows the "Paraíba" name to be used for tourmalines from Rio Grande do Norte (Mulungu and Alto dos Quintos), since separating them from Mina da Batalha stones is difficult, and material imported into Japan is a mixture of tourmalines from both states. This policy is consistent with that advocated by most gem dealers who are handling the Brazilian "Paraíba" tourmaline. However, as supported by the research reported in this article, Cu-bearing tourmalines from Brazil, Nigeria, and Mozambique are difficult to distinguish from one another by standard gemological testing methods. Therefore, AGL and the Laboratory Manual Harmonization Committee (LMHC) decided to reconsider the nomenclature for "Paraíba" tourmaline. The LMHC consists of representatives from the AGTA-Gemmological Testing Center (U.S.), CIS-GEM (Italy), GAAJ Laboratory (Japan), GIA Laboratory (USA), GIT-Gem Testing Laboratory (Thailand), Gübelin Gem Lab (Switzerland), and SSEF Swiss Gemmological Institute (Switzerland). At the LMHC's October 2005 meeting in Lucerne, and at the February 2006 Gemstone Industry & Laboratory Conference in Tucson, the LMHC group agreed to define "Paraíba" tourmaline as a blue ("neon" blue,



Figure 17. Surrounded by diamonds, the center stone in this ring is a 10.91 ct oval-cut Paraíba tourmaline that was faceted in 2003 from a crystal found during the original discovery of this tourmaline in the late 1980s at Mina da Batalha. The intense "neon" blue color of this unheated stone is representative of the finest tourmaline from this mine. Courtesy of a private collector, in collaboration with Brian Cook and Butch Vallee (*The Crystal Image*, Laguna Beach, California) and Mona Lee Nesseth, *Custom and Estate Jewels*, Laguna Beach; photo © Harold & Erica Van Pelt.

or violet), bluish green to greenish blue, or green elbaite tourmaline containing Cu and Mn, similar to the material that was originally mined in Paraíba, Brazil; any "Paraíba" tourmaline, regardless of its geographic origin, shall be described with the following wording on a gem identification report:

- Species: Elbaite
- Variety: Paraíba tourmaline
- Comment: The name "Paraíba tourmaline" is derived from the locality where it was first mined in Brazil.
- Origin: Origin determination is optional

This policy is consistent with current CIBJO practice, which defines "Paraíba" tourmaline as having a "green to blue color caused by copper," but no definition is made according to locality. Thus, CIBJO also considers "Paraíba" tourmaline to be a general variety or trade name.

At present, AGL will fall into step with the recommendation of the LMHC group, and will disclose a new nomenclature for "Paraíba" tourmaline later this year.

CONCLUSION

Since the initial discovery of magnificent brightly colored tourmaline at Mina da Batalha in Brazil's Paraíba State (figure 17), Cu-bearing elbaite has also been mined from Brazil's Rio Grande do Norte State (Mulungu and Alto dos Quintos), as well as in Nigeria and Mozambique. Overlap in the gemological properties and chemical compositions of tourmaline from these localities makes it difficult to distinguish their geographic origins with the testing techniques available in most gemological laboratories.

The common presence of yellowish brown needle-like growth tubes in the Nigerian tourmalines is suggestive of their origin. Also, native copper was most commonly seen in the Nigerian and a few Brazilian tourmalines, but thus far it has not been documented in stones from Mozambique.

This study has shown that chemical fingerprinting by the LA-ICP-MS technique is useful for distinguishing Cu-bearing tourmaline from the various localities.

Geochemical plots of CuO+MnO versus Ga+Pb, CuO+MnO versus Pb/Be, and Mg-Zn-Pb reveal that quantitative data for these elements may permit a reliable distinction of Brazilian stones from their counterparts mined in Nigeria and Mozambique. The Nigerian tourmalines contained larger amounts of the trace elements Ga, Ge, and Pb, whereas Brazilian tourmalines were enriched in Mg, Zn, and Sb. The Mozambique samples showed high contents of Be, Sc, Ga, and Pb, and Bi, but a lack of Mg.

Although the major laboratories have agreed to use *Paraíba tourmaline* as a trade name for blue ("neon" blue, or violet), bluish green to greenish blue, or green Cu- and Mn-bearing elbaite, some labs may wish to provide the additional service of establishing the precise country of origin. On the basis of the research completed to date, such a distinction usually requires quantitative chemical analysis. As further discoveries are made in other parts of the world, additional research will be needed to reconfirm the criteria or establish new ones.

ABOUT THE AUTHORS

Dr. Abduriyim (ahmadjan@gaaj-zenhokyo.co.jp) is manager, and Mr. Kitawaki is director, of the research laboratory at the Gemmological Association of All Japan in Tokyo. Mr. Furuya is president of the Japan Germany Gemmological Laboratory, Kofu, Japan. Dr. Schwarz is research manager of the Gübelin Gem Lab, Lucerne, Switzerland.

ACKNOWLEDGMENTS


The authors gratefully thank Hideki Sakamaki (Glorious Gems Co., Tokyo), Yuji Tsukuda (YT Stone Co., Tokyo), and Masaru Mizumura (Kofu, Japan, a representative of the Japan Jewellery Association), for information and samples that made this study possible. We are also grateful to Dr. Ichiro Sunagawa for critically reading and improving the manuscript.

REFERENCES

- Abduriyim A., Kitawaki H. (2005) Gem News International: Cu- and Mn-bearing tourmaline—More production from Mozambique. *Gems & Gemology*, Vol. 41, No. 4, pp. 360–361.
- Bernardes M.O. (1999) The mystic of Paraíba tourmaline. Unpublished report delivered at the International Colored Gemstone Association (ICA) Congress, Abano Terme, Italy, May 16–19.
- Brandstätter F., Niedermayr G. (1994) Copper and tenorite inclusions in cuprian-elbaite tourmaline from Paraíba, Brazil. *Gems & Gemology*, Vol. 30, No. 3, pp. 178–183.
- Cassedanne J. (1996) Le gîte de tourmaline de São José da Batalha (Paraíba-Brésil). *Revue de Gemmologie a.f.g.*, No. 127, pp. 6–11.
- Fritsch E., Shigley J.E., Rossman G.R., Mercer M.E., Muhlmeister S.M., Moon M. (1990) Gem-quality cuprian-elbaite tourmalines from São José da Batalha, Paraíba, Brazil. *Gems & Gemology*, Vol. 26, No. 3, pp. 189–205.
- Furuya M. (2004) Electric blue tourmaline from Nigeria: Paraíba tourmaline or new name? *Proceedings of the 29th International Gemmological Conference 2004*, Wuhan, China, September 13–17, China University of Geosciences (Wuhan) and Hong Kong Institute of Gemmology, pp. 111–112.
- Guillong M., Günther D. (2001) Quasi 'non-destructive' laser ablation-inductively coupled plasma-mass spectrometry fingerprinting of sapphires. *Spectrochimica Acta Part B*, Vol. 56, pp. 1219–1231.
- Günther D., Hattendorf B. (2005) Solid sample analysis using laser ablation inductively coupled plasma mass spectrometry. *Trends in Analytical Chemistry*, Vol. 24, No. 3, pp. 255–265.
- Günther D., Kane R.E. (1999) Laser ablation-inductively coupled plasma-mass spectrometry: A new way of analyzing gemstones. *Gems & Gemology*, Vol. 35, No. 3, pp. 160–161.
- Henricus J. (2001) New Nigeria tourmaline find excites trade interest. *Jewellery News Asia*, No. 207, pp. 77–78, 87.
- Jarvis K.E., Williams J.G. (1993) Laser ablation inductively coupled plasma mass spectrometry (LA-ICP-MS): A rapid technique for the direct, quantitative determination of major, trace, and rare-earth elements in geological samples. *Chemical Geology*, Vol. 106, No. 3–4, pp. 251–262.
- Karfunkel J., Wegner R.R. (1996) Paraíba tourmalines: Distribution, mode of occurrence, and geologic environment. *Canadian Gemmologist*, Vol. 17, No. 4, pp. 99–106.
- Kitawaki H. (2005) Journey through Brazil mines: Hometown of "Paraíba" tourmaline. *Gemmology*, Vol. 36, No. 435, pp. 19–23.

- Koivula J.I., Kammerling R.C., Eds. (1989) Gem News: Paraíba tourmaline update. *Gems & Gemology*, Vol. 25, No. 4, pp. 248–249.
- Koivula J.I., Kammerling R.C., Eds. (1990) Gem News: Treated Paraíba tourmaline. *Gems & Gemology*, Vol. 26, No. 1, pp. 103–104.
- Koivula J.I., Kammerling R.C., Fritsch E., Eds. (1992) Gem News: Tourmaline with distinctive inclusions. *Gems & Gemology*, Vol. 28, No. 3, pp. 204–205.
- Milisenda C.C. (2001) Gemmologie Aktuell: Cuprian tourmaline from Nigeria. *Gemmologie: Zeitschrift der Deutschen Gemmologischen Gesellschaft*, Vol. 50, No. 3, pp. 121–122.
- Milisenda C.C. (2005) "Paraíba-Tourmaline" aus Quintos de Baixo, Rio Grande do Norte, Brasilien. *Gemmologie: Zeitschrift der Deutschen Gemmologischen Gesellschaft*, Vol. 54, No. 2–3, pp. 73–84.
- Pearce N.J.G., Perkins W.T., Westgate J.A., Gorton M.P., Jackson S.E., Neal C.R., Chenery S.P. (1996) Application of new and published major and trace elements data for NIST SRM 610 and NIST SRM 612 glass reference materials. *Geostandards Newsletter*, Vol. 20, No. 2, pp. 115–144.
- Shigley J.E., Cook B.C., Laurs B.M., Oliveira Bernardes M. (2001) An update on "Paraíba" tourmaline from Brazil. *Gems & Gemology*, Vol. 37, No. 4, pp. 260–276.
- Smith C.P., Bosshart G., Schwarz D. (2001) Gem News International: Nigeria as a new source of copper-manganese-bearing tourmaline. *Gems & Gemology*, Vol. 37, No. 3, pp. 239–240.
- Wentzell C.Y. (2004) Lab Notes: Copper-bearing color-change tourmaline from Mozambique. *Gems & Gemology*, Vol. 40, No. 3, pp. 250–251.
- Wentzell C.Y., Fritz E., Muhlmeister S. (2005) Lab Notes: More on copper-bearing color-change tourmaline from Mozambique. *Gems & Gemology*, Vol. 41, No. 2, pp. 173–175.
- Zang J.W., da Fonseca-Zang W.A., Fliss F., Höfer H.E., Lahaya Y. (2001) Cu-haltige Elbaite aus Nigeria. *Berichte der Deutschen Mineralogischen Gesellschaft, Beihefte zum European Journal of Mineralogy*, Vol. 13, p. 202.

NOW AVAILABLE!



GEMS & GEMOLOGY[®] IN REVIEW SYNTHETIC DIAMONDS


**The best of *Gems & Gemology* on the subject of synthetic diamonds:
now available in one comprehensive research volume.**

- More than 30 years of cutting-edge synthetic diamond research by leading gemological researchers and producers
- Editorial commentary by Dr. James Shigley of GIA Research
- Insights on the past, present, and future of synthetic diamonds, and their effects on the gem and jewelry industry
- 50 separate entries comprising more than 300 pages of material
- Includes two wall charts in a sturdy bound-in pouch: the Separation of Synthetic and Natural Diamonds (1995), and Characteristics of HPHT-Grown Synthetic Diamonds (2004)
- Softbound in an attractive slipcase

\$49.95

(plus shipping and handling)

To order your copy today, visit
GIA Gem Instruments & Books at
www.gia.edu



Some of the material in *SYNTHETIC DIAMONDS* is from *Gems & Gemology* issues that are long out of print. That means you won't find this information anywhere else.

IDENTIFICATION AND DURABILITY OF LEAD GLASS–FILLED RUBIES

Shane F. McClure, Christopher P. Smith, Wuyi Wang, and Matthew Hall

In early 2004, the GAAJ laboratory in Japan issued a lab alert about rubies they had seen that had large numbers of fractures filled with high-lead-content glass, which made them appear very transparent. Since then, large quantities of this material have reached international markets. This dramatic treatment is not difficult to identify with a standard gemological microscope, since it has characteristics similar to clarity-enhanced diamonds (flash effect, gas bubbles, etc.). However, locating filled cavities in reflected light is more challenging, as the surface luster of the filler is close to that of ruby. The filling material appears to be very effective in reducing the appearance of fractures. Durability testing of a few samples by highly skilled jewelers indicated that the filler was fairly resistant to heat exposure during jewelry repair procedures, but it reacted readily with solvents.

Gem corundum has been a mainstay of the jewelry industry for centuries. The demand for rubies and sapphires has usually outdistanced supplies, and for much of history only the very wealthy could afford them. With the discovery of additional deposits during the 20th century, the supply of these gems increased dramatically. However, there continued to be more demand for these beautiful stones than Mother Nature could provide.

Thus enters the art of treatment. We use the term *art* here because many if not most of the treatments were not developed by scientists but rather by experimenters who relied largely on luck or trial and error. Many of those who developed these techniques never fully understood the science or the “why” of what they were doing, but they understood the “what” and the “how” very well.

Corundum, as a very durable material, lends itself to many treatments. And ruby, being the most prized color of corundum, is often a prime focus of these treatments. Over the years, ruby has been subjected to heat treatment to change its color and/or improve its clarity; fracture healing to improve clarity and get a higher yield from naturally fractured

rough; glass filling of cavities to improve appearance and add weight; and diffusion, dyeing, coating, and synthetic overgrowth, among others.

The latest venture into ruby treatments involves an improvement in clarity enhancement. In the past, the fractures in rubies have been filled with oils, which do little to improve apparent clarity, and glasses, mostly silica based, which are better than oils but, in our opinion, still not very effective because of their relatively low refractive index.

This newest treatment is based on the same principle that has been applied to emerald and diamond: use of a filling material that closely matches the refractive index of the host material to minimize the appearance of the fractures. In the case of this new treatment, the results are remarkable (figure 1). This article looks at the introduction of this technique, its identification in ruby, and its response to various durability tests.

See end of article for About the Authors and Acknowledgments.
GEMS & GEMOLOGY, Vol. 42, No. 1, pp. 22–34.
© 2006 Gemological Institute of America



Figure 1. These stones (2.15–7.42 ct) are typical of the final result achieved with the filling of fractures in rubies with high-lead-content glass. Photo by Elizabeth Schrader.

BACKGROUND

Silica glass has been used extensively to fill cavities and fractures in rubies since the 1980s. Cavity filling was noted first, and it was described as early as 1984 (Kane, 1984). This filling did improve the stones' face-up appearance and could add weight, but it could also readily be detected with magnification.

The early 1990s witnessed the marketing of huge quantities of ruby from Mong Hsu, Myanmar, with multiple cavities and fractures that were filled with, or partially healed by, glassy substances added during high-temperature heat treatment (Peretti et al., 1995; McClure and Smith, 2000). The term *residue* began to be applied to this kind of material, in reference to the glass that was a side effect of the real intent, which was to heal the fractures. The R.I. of this silica glass is significantly lower than that of the host corundum, so even a fracture entirely filled with it can still be easily seen (figure 2). Therefore, even though the appearance of the fractures is improved, silica glass is not the most efficient material for enhancing the clarity of rubies.

The first report of a new type of ruby clarity treatment came in an Internet alert issued by the Gemological Association of All Japan in early 2004 (GAAJ Research Laboratory, 2004). They described rubies with inordinate amounts of very low-relief fractures that had been filled with a high-lead-content glass. Since the GAAJ report, a large number of these stones have been examined by gemological laboratories around the world, and they have been offered for sale at trade shows in Bangkok, Hong

Kong, Switzerland, the United States, and elsewhere. Rubies below 1 ct to over 100 ct have been identified as lead-glass filled (see, e.g., figure 3), with a large number between 5 and 10 ct. In addition to the GAAJ lab alert, several articles have provided observations on this material (see, e.g., AGTA, 2004, 2005, 2006; Rockwell and Breeding, 2004; Li-Jian et al., 2005; Milisenda et al., 2005; Pardieu, 2005; Smith et al., 2005; SSEF, 2005; Sturman, 2005; Themelis, 2005).

Lead-Glass Filling of Rubies. The actual treatment process was described by Vincent Pardieu of the

Figure 2. Silica glass (in the older method) has a significantly lower R.I. than corundum. When it is used to fill fractures in ruby, it improves their appearance, but the fractures are still very visible. Photomicrograph by S. F. McClure; magnified 30 \times .

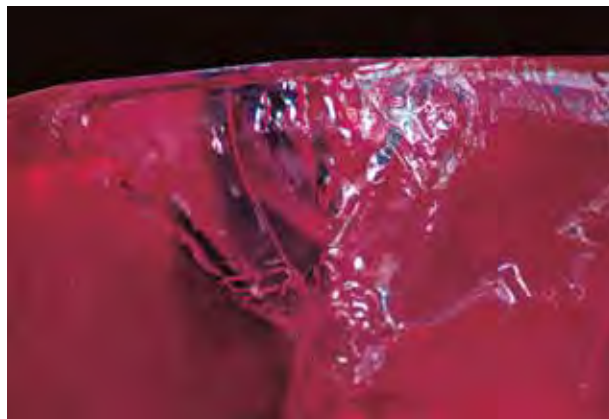




Figure 3. Many extremely large lead glass-filled rubies (here, 52.60 and 26.07 ct) have been seen in the market. Rubies courtesy of Golden Stone USA Inc., Los Angeles; photo © Robert Weldon and GIA.

Asian Institute of Gemological Sciences (AIGS; Pardieu, 2005). The following description is summarized from that article. Mr. Pardieu cited as the source of this information the person purported to be doing the treatment at the time, Mahiton Thondisuk of Chantaburi, Thailand.

The first step involves preforming the material to remove any matrix or obvious impurities. The second step is referred to as "warming," that is, heating the stone to moderate temperatures (reportedly 900–1,400°C). Often used as a first step in standard heat treatment, "warming" removes potential impurities from the fractures and may improve the color.

The third step involves mixing the stone with powders that are composed primarily of lead and silica but may also contain sodium, calcium, potassium, and metal oxides such as copper or bismuth. This mixture is then heated again, reportedly to approximately 900°C, fusing the powders into a glass that penetrates the fractures in the stone.

Unlike the process that produces the silica-glass fillings seen previously, the filling of corundum with lead glass initially did not involve the partial healing of fractures. In fact, there was significant evidence to show that these stones had not been exposed to the high temperatures necessary to heal fractures.

According to Pardieu, the original starting material for lead-glass filling was very low grade pink, red, or purplish red corundum from Andilamena in Madagascar that was typically translucent to opaque. For the most part, it is unusable as a gem in its natural state (figure 4). Of course, this treatment can be applied to fractured ruby from any locality. We have now seen lead glass-filled stones that appeared to be from Tanzania and Myanmar. The effectiveness of

the treatment is amazing, in that it transforms corundum that is opaque and nearly worthless into material that is transparent enough for use in jewelry.

The Present Study. To characterize this treated material as well as determine its identifying features, we examined dozens of samples by standard gemological methods and other analytical techniques. We also tested the durability of the treatment by subjecting samples to routine jewelry manufacturing and repair procedures, as well as to conditions of standard wear and care. The results of this testing, and procedures for identification, are described here.

Readers should bear in mind that the properties we report below are restricted to those observed in the samples we obtained for this study. Although a broad range of samples were selected from several different vendors over more than 14 months, stones treated in a similar fashion but with glass of a different composition may be in the market, and these may have different properties and different reactions to the durability tests.

MATERIALS AND METHODS

We collected the samples of lead glass-filled rubies and pink sapphires used for this study from late 2004, when large quantities of this treated material first became available on the market, until February 2006. We obtained them in Bangkok and New York City in late 2004, at the June 2005 JCK and AGTA Las Vegas gem shows, and at the 2005 and 2006 Tucson gem shows, all from different sources. We examined a total of 50 faceted samples, ranging from 0.43 to 9.19 ct.

Standard gemological equipment was used to characterize the basic properties of 10 selected samples including: a refractometer, a desk-model spectroscope, long- and short-wave ultraviolet lamps, and a polariscope. All samples were examined with a binocular microscope and fiber-optic illumination.

Qualitative (30 samples) and semiquantitative (2 samples) chemical analyses were performed by energy-dispersive X-ray fluorescence (EDXRF) spectroscopy using a Kevex Omicron spectrometer operated at a voltage of 25kV with no filter, a 50 micron collimator, and a 500 second livetime.

Observations and chemical analyses were also performed on four samples using a JEOL-JXA8800 scanning electron microscope with a wavelength-dispersive spectrometer (SEM-WDS) at the Geophysical Laboratory of the Carnegie Institution of

Washington, in Washington, DC. Operating conditions for both electronic imaging and wavelength-dispersive analyses were 10 μ A beam current and 15 kV accelerating potential. The presence of any element with a concentration above 100 ppm (from B to U in the periodic table) will be detected. Even though we used a focused electron beam, which was about 1–2 μ m in diameter, due to the limited surface area of the filling material and the poor quality of the polish on most of the samples tested, chemical analysis was performed without calibration against standard materials.

X-radiography was performed on five samples using a Hewlett-Packard Faxitron series X-ray cabinet.

The samples were also tested for their durability in standard conditions of manufacture, wear, and repair. Heating experiments were performed on a total of 10 samples using a Lindberg/Blue box furnace in an ambient atmospheric environment. The temperature of the furnace was raised to the target values first and then the sample (held in an Al_2O_3 ceramic disk) was placed inside. The temperatures were 100, 200, 600, 700, 800, and 1,000°C. Selected samples were exposed to each of these temperatures for periods of 5, 10, and 60 minutes each. In addition, one sample was held at 200°C for an extended period of 16 hours. After a specific heating period, the samples were taken out, cooled in air, and reexamined.

We also exposed eight rubies filled with high-lead-content glass to a series of jewelry repair procedures. These included steam cleaning, ultrasonic cleaning, setting (including mounting, filing and polishing), and retipping of prongs. Details on these tests are given in the section on durability testing below.

A total of eight reagents were used to assess the Pb-glass filler's resistance to chemical attack. Three reagents consisted of caustic soda, aqua regia (nitrohydrochloric acid), and a standard jeweler's pickling solution (sodium bisulphate). The latter two are frequently used in jewelry manufacturing or repair; caustic soda is a more reactive base than standard pickling solution. We also tested the treatment for its durability to a range of household products: concentrated lemon juice, a typical aerosol oven cleaner, ammonia, a standard drain cleaner, and bleach. For each chemical (with the exception of the pickling solution, for which three samples were used), one ruby with Pb-glass filler was placed in a beaker and covered with the reagent (typically 10–20 ml). In addition to using a fume hood for all experiments, we covered toxic solutions (aqua regia and ammonia) with a baking soda filter over the beaker top to min-

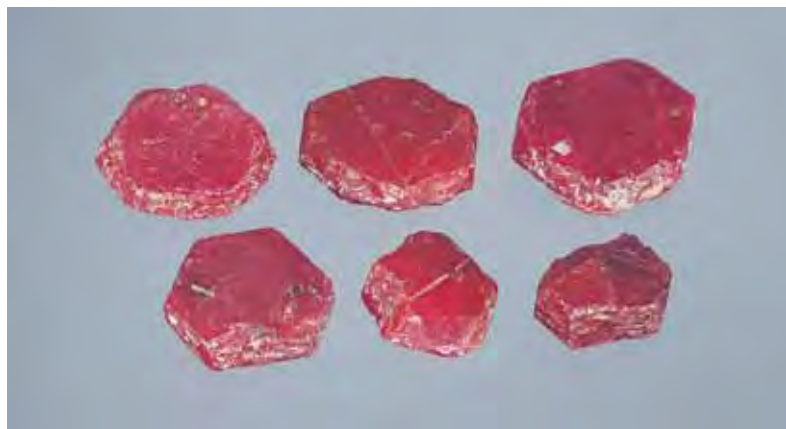


Figure 4. The starting material for this ruby treatment is very low quality and until now was only useful as mineral specimens. The crystals shown here range from 7.28 to 22.08 ct. Photo by Maha Calderon.

imize noxious fumes. Each experiment run was conducted at or just below the boiling point to accelerate any reaction; a small laboratory hot plate with variable temperature control was constantly adjusted to keep the reagents at this temperature. Experiment run time was four hours (except for aqua regia, which was one hour long), to mimic the cumulative effect of multiple exposures for shorter periods of time. The beaker was then removed from heat and allowed to cool. Once cooled, the stones were cleaned and examined for alterations to the Pb-glass filler.

RESULTS

Visual Appearance. All the samples collected for this study were transparent to semitransparent and could be considered jewelry quality. The color of many of the specimens was slightly brownish and often of lower saturation—so that some of them would be considered pink sapphire. However, several of the authors saw large parcels of lead glass-filled corundum in early 2006 that could easily be categorized as medium-quality ruby. Two of these rubies were acquired for this study (one is shown in figure 5).

Standard Gemological Properties. The long- and short-wave UV fluorescence, visible-range absorption spectrum, pleochroism, birefringence, optic character, and specific gravity were consistent with ruby/pink sapphire in general. It is interesting to note, however, that the specific gravity of one 1.34 ct stone was slightly higher (4.03) than usual for corundum. This stone had several large, deep, filled cavities. We do not have data on the S.G. of the glass filler, but it is well



Figure 5. Some of the specimens we acquired for this study, such as this 2.85 ct stone, would be considered medium-quality ruby. Photo by C. D. Mengason.

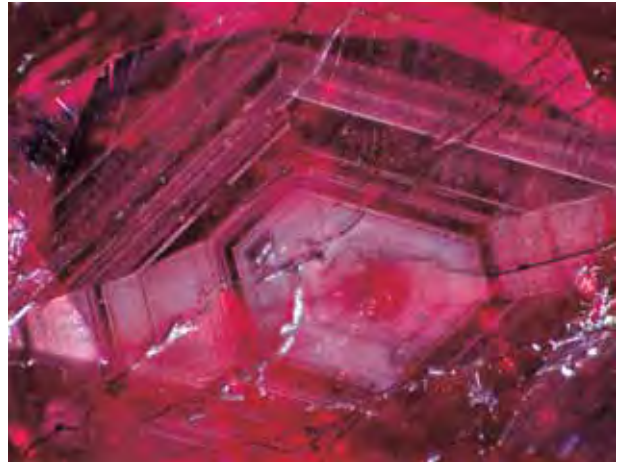


Figure 6. Dense clouds of fine, unaltered rutile needles following the growth structure prove that this lead glass-filled ruby has not been exposed to extremely high temperatures. Photomicrograph by S. F. McClure; magnified 20 \times .

known that high-lead-content glass has a high specific gravity, so it is not surprising that it could affect the overall S.G. of the stone. Standard R.I. readings and birefringence were recorded for all of the samples. In addition, we obtained a single approximate R.I. reading of 1.75–1.76 for the lead-glass filler on areas where it filled larger cavities.

Internal Features. All the samples we examined revealed naturally occurring internal features that ranged from extensive twinning and parting planes to various mineral inclusions. Some mineral inclusions

showed evidence of thermal alteration, whereas others did not. Most significantly, many of these stones revealed dense clouds of fine, unaltered rutile needles following the hexagonal structure of the ruby (figure 6). This is clear evidence that these stones had not been exposed to temperatures high enough to damage rutile (greater than 1,500°C; Emmett et al., 2003).

When examined with a microscope or a standard jeweler's loupe, virtually all the samples were dominated by numerous large fractures of very low relief. In addition, blue flashes were readily noted as the

Figure 7. One of the most important identification features of this treatment is a blue flash effect similar to that seen in filled diamonds and emeralds. The strength of the flash varied considerably, sometimes being relatively weak, as can be seen in this example. Photomicrograph by S. F. McClure; magnified 15 \times .

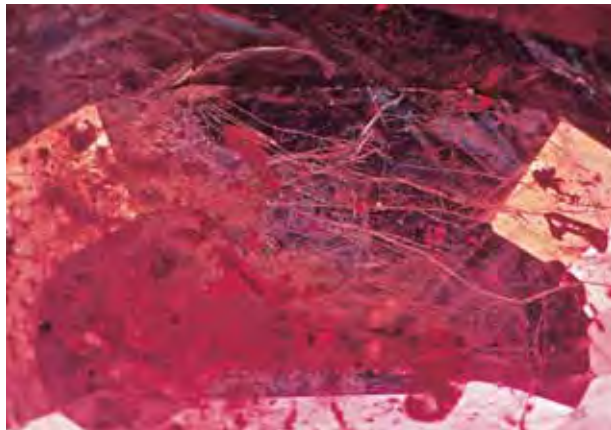


Figure 8. In some of the samples, the flash effect was very strong and an orange flash could also be seen. Here, the blue is quite strong in brightfield illumination, and the orange flash is easily seen in darkfield. Photomicrograph by S. F. McClure; magnified 10 \times .



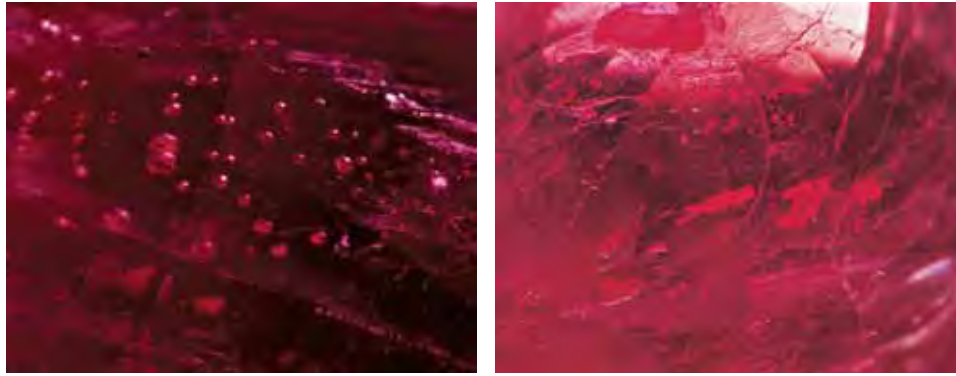


Figure 9. Numerous flattened and rounded gas bubbles were present in almost all the corundum with filled fractures that we examined. Photomicrographs by C. P. Smith (left, 28×) and S. F. McClure (right, 20×).

stones were rotated and repositioned for a complete view of the interior. The strength of the flash effect varied from relatively subtle (figure 7) to quite strong, although usually with the same intensity in samples obtained from the same source. In some stones, an orange flash was visible as well (figure 8). Also seen with magnification in all the samples were numerous flattened and rounded gas bubbles and voids within the glass fillings (figure 9). Where filled cavities were large enough, spherical gas bubbles were sometimes visible. This was reminiscent of the features we first noted in clarity-enhanced diamonds 18 years ago (Koivula et al., 1989). Although the filling material in rubies might be different, the effect of the treatment—to minimize the visibility of fractures and cavities—was almost identical to that achieved with fracture filling in diamonds.

In the majority of the samples, the glass filling did not appear to be colored. However, we did note that along thick seams or cavities of the glass there was a distinct yellow hue in a few samples and a more subtle pink coloration in others. In several of the lower-

quality samples we acquired at the Tucson shows in 2006, we observed large filled cavities where the yellow color of the filler was readily apparent, even through the body of the stone (figure 10).

Surface Characteristics. Previously, examining the surface of some heated rubies in reflected light would reveal the presence of cavities or depressions that had become a reservoir for the flux typically used to induce the healing of fractures. These agents often would form a silicon-rich glass that had a significantly lower refractive index than the ruby host, resulting in a lower surface luster. We were somewhat surprised to see how effective this new treatment was at reducing the surface visibility of large cavities and wide fractures, which in some cases extended across the width or length of the sample. In many of the study samples, we noted that lead glass-filled cavities, even very large ones, were difficult to detect. Cavities filled with silica glass or heating residues are typically very visible—even with darkfield illumination (figure 11). Use of the higher-R.I. lead glass, how-

Figure 10. The yellow color of the lead-glass filler is visible here in a very large internal cavity. Photomicrograph by S. F. McClure; magnified 30×.

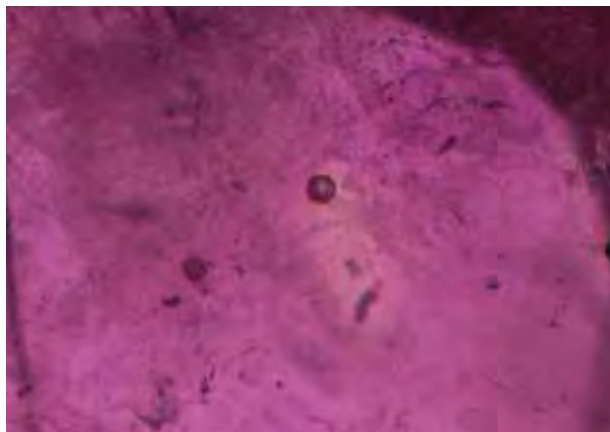
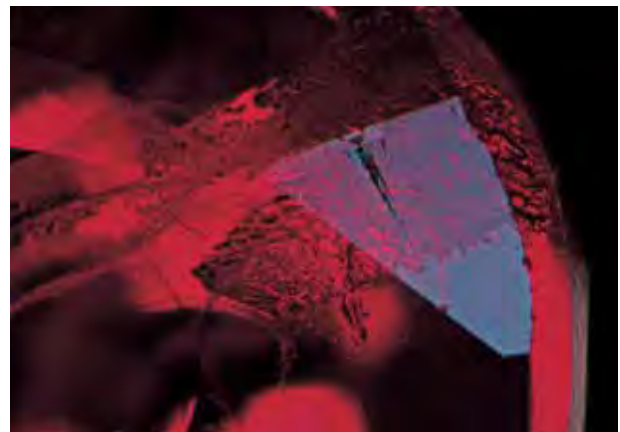


Figure 11. Cavities filled with silica glass typically remain very visible in the microscope. Photomicrograph by S. F. McClure; magnified 37×.



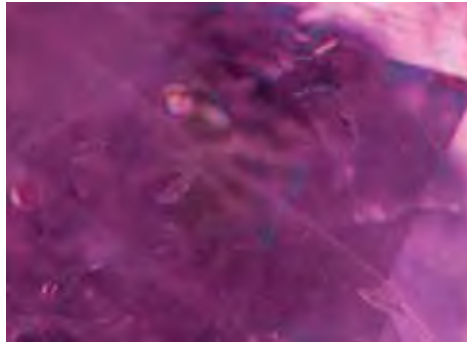
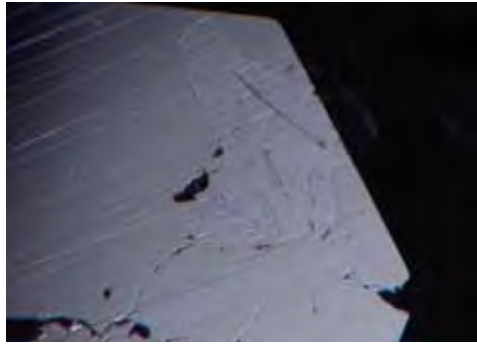
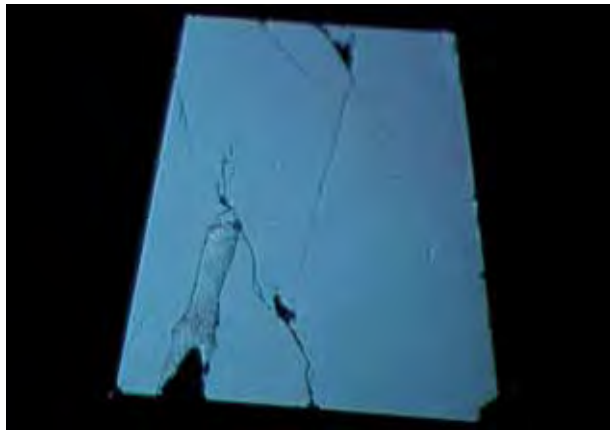


Figure 12. Cavities filled with high-lead glass can be challenging to see. In the image on the left (reflected light), the surface luster of the filler is very close to that of the corundum. On the right, the same filled cavity is not visible at all in darkfield; only the outline of blue flash suggests its presence. Photomicrographs by S. F. McClure; magnified 30 \times .

ever, makes the cavities virtually disappear (figure 12). Even the traditional reflected-light technique was less reliable, as careful positioning of the stone in figure 12 was necessary to make the subtle difference in surface luster visible. Many examples were seen where the surface luster of the glass was comparable to the luster of the ruby, and only careful examination revealed that the luster was lower than, equal to, or higher than (figure 13) that of the ruby. Many times the only noticeable difference was in the quality of the polish: Glass, particularly high-lead-content glass, is significantly softer than corundum, which makes the polish noticeably inferior to the host (figure 14). In a few samples, we also noted that shrinkage had occurred in the Pb-glass that was filling cavities (figure 15).

It is interesting to note that one lead glass-filled ruby that was submitted to the GIA Laboratory showed evidence of oxidation of the filler at the surface, undoubtedly a consequence of the extreme lead content (figure 16).

Figure 13. Sometimes the surface luster of the lead-glass filling is noticeably higher than the surrounding corundum. Photomicrograph by S. F. McClure; magnified 36 \times .



Chemical Composition. All 30 of the samples that were analyzed qualitatively with EDXRF showed a significant lead content, as did the two measured semiquantitatively. To obtain a more precise evaluation of the composition of the glass filler alone, we analyzed fillings in four stones by SEM-WDS.

SEM is a very useful technique for analyzing lead glass-filled ruby, because the glass and surrounding ruby show a large difference in brightness in back-scattered-electron (BSE) images (figure 17). The filling process is so efficient that the glass can successfully penetrate fractures as thin as 5 μm . BSE images taken at high magnification illustrate that the boundary between the glass and the host ruby is sharp. No precipitation of secondary corundum was observed in any of the samples analyzed. In contrast, in some Si-rich glass-filled rubies we have examined in the lab, we observed that the deposition of secondary corundum formed a zigzag boundary between the glass and the host ruby (figure 18).

SEM-WDS chemical analysis of glass in fractures

Figure 14. Glass, particularly high-lead-content glass, is significantly softer than corundum, so sometimes the best way to notice a glass-filled cavity in reflected light is by the poor polish on its surface. Photomicrograph by C. P. Smith; magnified 45 \times .



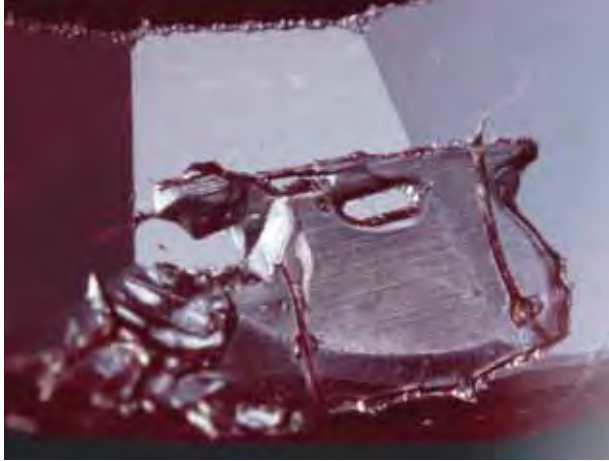


Figure 15. Shrinkage of the glass in this large cavity (over 1.0 mm in longest dimension) appears to have taken place subsequent to polishing, causing the polished surface of the glass to be lower than that of the surrounding ruby. Photomicrograph by C. P. Smith; magnified 45 \times .

less than 10 μm wide is problematic due to beam overlap with the surrounding ruby. However, consistent results were obtained for glass-filled areas with relatively large surfaces: major components—PbO (71–76 wt.%), Al_2O_3 (12–15 wt.%), and SiO_2 (11–13 wt.%); minor components (<1 wt.%)— Na_2O , K_2O , CaO, FeO; and trace amounts of MgO, P_2O_5 , and TiO_2 . These results are similar to those that have been described by others (e.g., Li-jian et al., 2005).

Figure 17. This back-scattered-electron image (taken with a scanning electron microscope) shows lead glass-filled fractures of varying widths. Because of the higher average mass of elements in the glass, it is much brighter than the host ruby. Width of the image is about 1.6 mm.

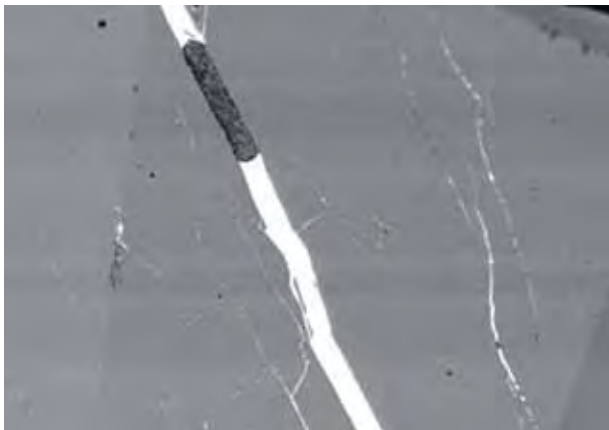


Figure 16. One example recently submitted to the GIA Laboratory showed an obvious oxidation of the glass at the surface. Photomicrograph by S. F. McClure; magnified 40 \times .

It is interesting to note that semiquantitative EDXRF analyses of the lead glass in two samples acquired in 2006 showed very similar composition to that of rubies acquired in 2004, which suggests that the composition is fairly consistent over time.

X-radiography. This test was shown to be successful in detecting the high-lead-content glass used for filling fractures in diamonds many years ago (Koivula et al., 1989), working on the basis that lead glass strongly absorbs X-rays. As expected, the lead glass-filled fractures in our samples were easily visible in the X-radiograph (figure 19). Others have also reported using this test effectively (Befi and Dutoit, 2005; Kitawaki et al., 2005).

DURABILITY TESTING

Once a method of detection for any given treatment is established, invariably the next question that arises is “Is it durable?” To test this, we set up a series of experiments, focusing mainly on the conditions these stones might encounter in normal situations of wear, care, and manufacture or repair. We first reported the results of some of these tests at the 2005 ICA Congress in Bangkok, Thailand.

Controlled Heating. The first question we wanted to answer was how much heat this lead-glass filler could survive. The melting point of the material is very important, as it determines how well the filler can stand up to jewelry manufacturing techniques. We suspected that the glass might not withstand

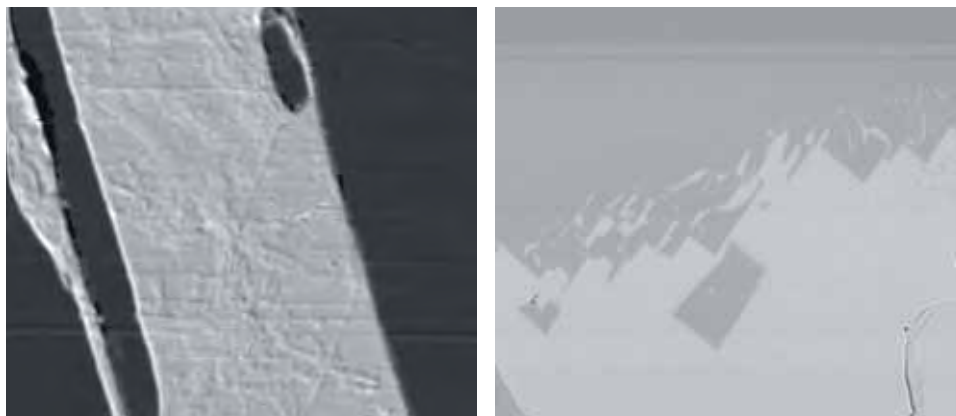
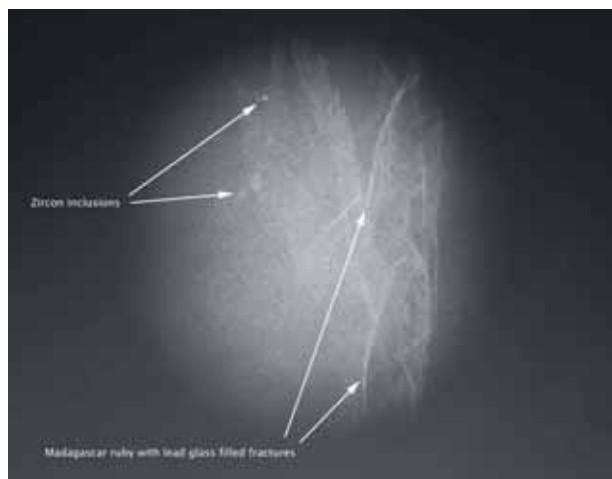


Figure 18. No chemical reaction between the lead glass and the host ruby was detected with the SEM (left, BSE image width ~100 μm); the boundary between the two phases is sharp. In contrast, in the silicon glass-filled ruby (right, BSE image width ~390 μm), deposition of secondary corundum formed a zigzag boundary between the glass and the ruby.

normal jewelry repair techniques such as the retipping of prongs, primarily because of our experiences with the lead glasses used to fill fractures in diamonds (e.g., Koivula et al., 1989).

No change was observed in the samples held at 100°C, at 200°C for 16 hours, or at 600°C. At 700°C, we observed the first sign of a change to the glass: Almost immediately, minor amounts of glass started sweating out of filled fractures and beading on the surface (figure 20). After only a few minutes at this temperature, the glass in larger filled cavities started to melt and flow (figure 21). At 800°C, the glass started bubbling at the surface of the fractures (figure 22). These tests clearly show that the melting point of the lead glass in these samples is between 600° and 700°C. Of course, changes in the composition of the glass from one treater to another or from one time frame to another could result in a change to the melting point.

Figure 19. The lead-glass filler is readily seen in an X-radiograph because lead glass strongly absorbs X-rays. Some scattered zircon crystals are also visible in this image.



Jewelry Repair Procedures. No damage to the lead-glass fillings was observed with standard steam cleaning, ultrasonic cleaning, setting, and even retipping of prongs, when these procedures were performed carefully on the limited number of stones tested, as described below. Some damage was seen with immersion in a pickling solution (figure 23) and exposure to other reagents. The specific tests and results are described below.

Steam Cleaning. Two rubies were selected for steam cleaning. A standard steam cleaner was used, maintaining an approximate pressure of 40–50 psi. Each stone was held in a pair of tweezers in the steam at a distance of approximately one inch for 30 seconds, allowed to cool, and examined in the microscope for damage. This procedure was repeated 15 times for each stone. No damage to the filler was detected in either stone.

Figure 20. At 700°C, minor amounts of the lead-glass filler began sweating out of the fractures and beading on the surface. Photomicrograph by C. P. Smith; magnified 50 \times .

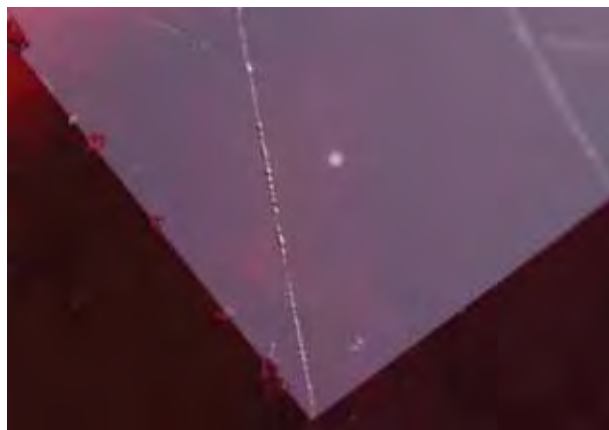




Figure 21. Heating at 700°C for only a few minutes caused the lead-based glass in larger cavities to start to flow. Photomicrograph by C. P. Smith; magnified 24×.

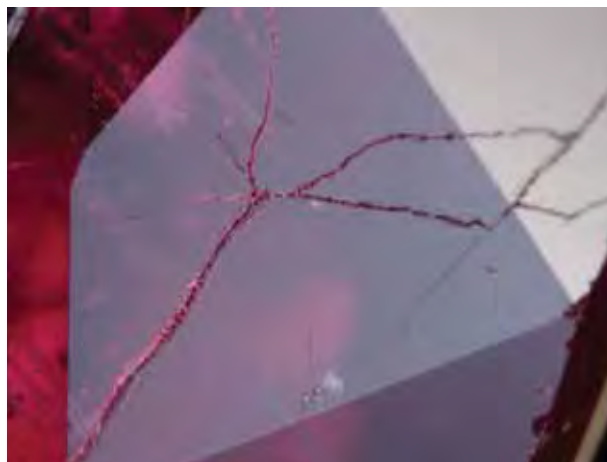


Figure 22. At 800°C, the lead-glass filler actually started to bubble where fractures reached the surface. Photomicrograph by C. P. Smith; magnified 22×.

Ultrasonic Cleaning. Two different rubies were selected for ultrasonic cleaning. The ultrasonic bath was filled with a standard soap solution that was warmed slightly. Both stones were placed in a wire basket and suspended in the solution with the cleaner turned on. The stones were removed after 15 minutes and checked for damage; then they were returned to the ultrasonic for another 15 minutes and checked again. Subsequent additional runs (and rechecks) of 30 minutes, 60 minutes, and another 60 minutes were performed for a cumulative total of three hours in the cleaner. No damage to the filler was observed in either stone.

Setting. Four different rubies were set in standard 14K yellow gold mountings, the process consisting of mounting the stone, filing the prongs, and polishing the setting. Since lead glasses tend to be relatively soft, we examined the stones carefully after these seemingly benign procedures. No damage to the filler was observed in any stone.

Retipping of Prongs. Although jewelers' guidelines typically advise against exposing any ruby or sapphire to the direct heat of a torch during the retipping of prongs, many jewelers routinely perform this procedure with the stone in place. To test the resistance of the filler to standard retipping procedures, we enlisted the aid of two of GIA's Jewelry Manufacturing Arts instructors, Mark Maxwell and Adam Kelley, and began with one of the previously mounted stones. We started with retipping because the temperatures the stones are exposed to during this process are much higher than those for other repair procedures such as sizing. If the filler did not survive the higher-temperature procedure, we would move to one that required lower temperatures to determine the lowest point at which the filler would be damaged.

After some discussion with the instructors, it was decided that they would first perform a retipping procedure that exposed the stone to the lowest temperature possible, assuming the procedure was done correctly. If there was no damage with that

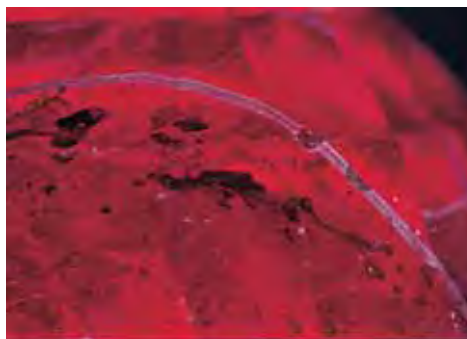
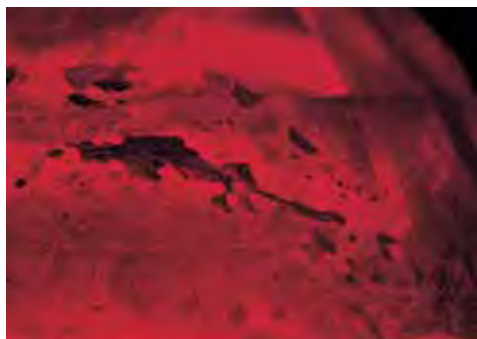


Figure 23. The large fracture in this lead glass-filled ruby is hard to see (left), except for the straight edges on the two flattened gas bubbles in the top center. After immersion in a standard pickling solution for 20 minutes (right), etching of the filler made the edges of the fracture clearly visible. Photomicrographs by S. F. McClure; magnified 30×.



Figure 24. Caustic soda was used to see how much damage a stronger base solution would inflict on the glass. The image on the left shows the 2.08 ct lead glass-filled ruby before the test began; after one hour of exposure (right), the damage to the filler was significant. Photomicrographs by C. P. Smith.

method, we would move to a procedure (on a different stone) that would require the maximum temperature to retip a prong.

The first method involved soldering a piece of 14K wire to the prong to be repaired with a “soft” solder, which would then be filed down to rebuild the prong. After the soldering procedure, the mounted stone was immersed in a warm standard pickling solution for one minute. The stone, which had been carefully examined before heating, was examined again. It now showed thin white lines where the fractures reached the surface.

The thought occurred to us that this near-surface damage of the lead-glass filler could be from the heat or the pickling solution, so we repeated the experiment on a second stone and examined it with the microscope immediately after the soldering procedure without placing it in the pickling solution. This time there was no visible damage to the filler. This indicated that the earlier damage was related to the pickling solution, the testing of which will be outlined below.

Next, a higher-temperature procedure was performed on another sample. This retipping process involved soldering a ball of 14K gold to the prong. This requires heating of the prong, and therefore the ruby, to a much higher temperature than the earlier procedure. Again the stone was examined (without putting it in pickling solution) and was found to have suffered no damage.

Immersion in Pickling Solution. The second lead glass-filled stone that was subjected to the lower-temperature retipping procedure was placed in the warm pickling solution for one minute to duplicate the first incident. Again, on reexamination we noted a thin ribbon-like area of damage at the point where the filled fractures reached the surface.

This result established a connection between the pickling solution and the damaged filler. Two new unmounted stones with lead-glass filler were chosen

and then placed in the pickling solution for 5 and 20 minutes respectively. On reinspection, both stones showed near-surface damage (see, e.g., figure 23), with the depth corresponding directly to the duration of immersion. It was now clear that the caustic pickling solution was etching the lead-glass filler, which made the fractures far more visible.

Exposure to Other Corrosive Solutions. The relatively aggressive solutions, caustic soda and aqua regia, had an immediate reaction with the glasses, etching them readily. In fact, the glass was etched/removed from all the cavities and to a relatively shallow depth in all the fractures after only a few minutes of exposure. However, extending this exposure to 4 hours had little further impact on the removal of the filler. After these tests were performed, the stones looked dramatically different from their appearance prior to testing (see, e.g., figure 24). Nevertheless, because the glass was removed only to a limited depth, their overall appearance was still better than what it would have been if the stone was in its untreated state.

Exposure to Household Products. We also decided to test various products that the stones might encounter once they were purchased by an end-consumer. We were very surprised to find that the aerosol oven cleaner had a similar, very aggressive reaction with the glass, readily etching it. In addition, the ammonia, bleach, and even concentrated lemon juice also had an effect, if less dramatic. In these instances, typically the glass was etched at the very surface of the stones, with the traverses of the fractures newly visible as criss-crossing lines (figure 25).

DISCUSSION AND CONCLUSION

The significance of any new treatment typically revolves around two points: (1) how effective it is, and (2) whether it can be detected—especially using routine gem testing equipment. As with any treat-

ment, clarity enhancement by lead-glass filling must be disclosed at all levels of sale to protect consumer confidence.

In the case of lead-glass filling in rubies, the intent is clearly to enhance the apparent clarity of the stone. The treatment is very effective in this regard. Stones that are almost opaque can be improved to the point of being semitransparent to transparent. This makes it possible to market a great deal of previously unusable material.

Fortunately, this treatment is easily detected with magnification. The identifying characteristics are similar to those for diamonds that have been clarity enhanced with a glass filling: very low-relief fractures, gas bubbles and voids (unfilled areas) in fractures, and a blue and orange flash effect. There is also the possibility of a light pink or yellow color to the filler in areas where it is very thick, such as large cavities. However, cavities filled with lead glass are more difficult to detect than those filled with silica glass, so careful observation is required in all cases.

A third concern of consumers and the industry alike is the durability of the treatment to jewelry manufacturing and repair procedures, as well as under normal conditions of wear and care. The lead based-glass filler in the stones we tested turned out to be fairly durable to heat exposure during jewelry repair procedures. However, only three stones were tested and the instructors who performed these procedures for us were highly skilled jewelers. As the controlled heating experiments indicated, too much heat with a torch could still damage this filler, so it would be prudent to unmount stones treated in this manner to be safe.

The filler reacted readily with solvents, particularly with a common jeweler's pickling solution, so these stones should not be exposed to such solutions under any circumstances. Not only does this make it more important to remove such stones from their settings before repair procedures, but it also means that consumers should be informed that damage could occur if the stone is exposed to some common household chemicals.

An interesting debate took place among laboratories as a result of this treatment. The type of starting material used frequently will not display conclusive evidence of heating. The inevitable question then arose: Is the presence of lead-glass filler in fractures sufficient proof that the stone has been subjected to enough heat to say it is heat treated? Our experiments showed that, at least in the samples we obtained, temperatures of at least 700°C were neces-



Figure 25. Ammonia, bleach, and even concentrated lemon juice damaged the lead-glass filler at the very surface, producing the whitish areas shown here. Photomicrograph by C. P. Smith; magnified 32×.

sary to soften the glass. For it to flow into fractures, the temperature would obviously have to be much higher—800° or 900°C at least. We know that these temperatures are high enough to facilitate changes in corundum, particularly in relation to color (Nassau, 1994). It has been hypothesized that formulations of lead glasses could be developed that would have much lower melting points, but as we have not yet observed such glasses ourselves, we maintain that the presence of this glass in fractures is sufficient proof to say the stone also has been heat treated.

What is perhaps most remarkable about this treatment is the type of material it brings to the market. High-temperature heat treatment and healing of fractures brought Mong Hsu ruby to the market years ago for what was at the time a very low price. Clarity enhancement with high-lead-content glass has brought ruby and pink sapphire to the market for even lower prices. Of course, the color of the low end of this material is not ideal, but some of the samples acquired for this study were only \$2.00 per carat—stones over 1 ct in size that were mostly transparent face up and ranged from purplish red to purplish pink. Inexpensive synthetics cost more than this. We purchased the 2.31 lead glass-filled ruby in figure 5 at the 2006 Tucson shows for \$20 per carat. Certainly, better-quality stones—also represented as lead-glass filled, as these were—are being sold for significantly higher prices, but we believe the low end is a new low for treated natural ruby.

From the moment we saw this treatment, we believed it would eventually be used for much higher-quality goods. The efficiency of the treatment is such

that a single large fracture in an otherwise clean ruby could be made to “disappear” to the unaided eye, exactly as filled fractures can be made to “disappear” in emeralds and diamonds. In fact, we have already seen several stones that fall into this category.

With glass being such a versatile material, other formulations may be possible, which could change the properties of the filler, including its melting point. The properties we reported here are only those we observed in our study samples. Last year, two laboratories (AGTA and GAAJ) reported seeing a lead-glass filler in star rubies that did not exhibit a flash effect (Befi and DuToit, 2005; Kitawaki et al., 2005). While

no quantitative chemical data was given in either report, it is clear from the lower surface luster of the filler in the images provided that the R.I.—and therefore the composition—of the filler discussed in those reports must be different from the lead-glass fillers we studied. Thus, it is probable there are stones on the market that have been treated in a similar fashion with a glass of different composition. It is imperative that laboratories worldwide continue to monitor the material reaching the market, so that if and when a change occurs that might alter the identifying characteristics of the stones, the greater gemological community can be made aware of it as soon as possible.

ABOUT THE AUTHORS

Mr. McClure is director of identification services at the GIA Laboratory in Carlsbad. Mr. Smith is director of identification services, Dr. Wang is research scientist, and Mr. Hall is manager of analytical research, at the GIA Laboratory in New York.

ACKNOWLEDGMENTS: The authors thank Paul Wild, Colorline, and Harpaz Gem & Pearl Inc. for graciously providing samples. They are grateful to Dr. Yingwei Fei of the Carnegie Institute of Washington for arranging the SEM-

WDS analysis. Mark Maxwell and Adam Kelley, Jewelry Manufacturing Arts instructors in the GIA Education department, provided advice and assistance by retipping the prongs of some of the sample rubies. The authors acknowledge with appreciation David Kondo, Kyaw Soe Moe, Paul Johnson, Wendi Mayerson, and Carolyn van der Bogert (all of the GIA Laboratory New York Identification Department), as well as Mike Breeding, Andy Shen, and Sam Muhlmeister (of the GIA Laboratory Carlsbad Research Department) and Ken Scarratt (of the GIA Research Laboratory Bangkok) for analyses of the samples and many fruitful discussions.

REFERENCES

- AGTA Gemological Testing Center (2004) New ruby treatment arrives in the United States. www.agta-gtc.org/2004-07-02_rubytreatment.htm, July 2.
- AGTA Gemological Testing Center (2005) Lead glass fracture filling in ruby. www.agta-gtc.org/2005-01-06_glassfilledruby.htm, Jan. 6.
- Befi R., Dutoit G. (2005) Glass-filled star ruby. www.agta-gtc.org/2005-09-20_glass-filled_star_ruby.htm, Sept. 20.
- Emmett J.L., Scarratt K., McClure S.F., Moses T., Douthit T.R., Hughes R., Novak S., Shigley J.E., Wang W., Bordelon O., Kane R.E. (2003) Beryllium diffusion of ruby and sapphire. *Gems & Gemology*, Vol. 39, No. 2, pp. 84–135.
- GAAJ Research Laboratory (2004) Lead-glass impregnated ruby. www.gaaj-zenhokyo.co.jp/researchroom/kanbetu/2004/gaaj_alert-040315en.html, Mar. 15.
- Kane R.E. (1984) Natural rubies with glass-filled cavities. *Gems & Gemology*, Vol. 20, No. 4, pp. 187–199.
- Kitawaki H., Abduriyim A., Okano M. (2005) Lead glass-permeated ruby—Update. *Gemmology*, Vol. 36, No. 425, pp. 14–15.
- Koivula J.I., Kammerling R.C., Fritsch E., Fryer C., Hargett D., Kane R.E. (1989) The characteristics and identification of filled diamonds. *Gems & Gemology*, Vol. 25, No. 2, pp. 68–83.
- Li-jian Q., Zeng C.G., Xin-qiang Y. (2005) Lead-rich glass substance in filled treated rubies. *Journal of Gems and Gemology*, Vol. 7, No. 2, pp. 1–6.
- McClure S.F., Smith C.P. (2000) Gemstone enhancement and detection in the 1990s. *Gems & Gemology*, Vol. 36, No. 4, pp. 336–359.
- Milisen da C.C., Horikawa Y., Henn U. (2005) Rubine Mit Bleihaltigen Glasern Gefullt. *Gemmologie: Zeitschrift der Deutschen Gemmologischen Gesellschaft*, Vol. 54, No. 1, pp. 35–42.
- Nassau K. (1994) *Gemstone Enhancement: History, Science and the State of the Art*, 2nd ed. Butterworth/Heinemann Ltd., Oxford, UK, 127 pp.
- Pardieu V. (2005) Lead glass filled/repared rubies. www.aigslaboratory.com/Filearticle/55.pdf, Jan. 17.
- Peretti A., Schmetzer K., Bernhardt H.-J. (1995) Rubies from Mong Hsu. *Gems & Gemology*, Vol. 31, No. 1, pp. 2–27.
- Rockwell K.M., Breeding C.M. (2004) Gem Trade Lab Notes: Rubies, clarity enhanced with a lead glass filler. *Gems & Gemology*, Vol. 40, No. 3, pp. 247–249.
- Smith C.P., McClure S.F., Wang W., Hall M. (2005) Some characteristics of lead-glass filled corundum. *Jewellery News Asia*, No. 255, pp. 79, 82–84.
- SSEF Swiss Gemmological Institute (2005) Lead glass filled fractures in rubies. *Facette*, No. 12, p. 10, www.ssef.ch/facette12.pdf.
- Sturman N. (2005) Gem News: Lead glass-filled rubies appear in the Middle East. *Gems & Gemology*, Vol. 41, No. 2, pp. 184–185.
- Themelis T. (2005) Glass-filled rubies. *Australian Gemmologist*, Vol. 22, No. 8, pp. 360–365.

THE CHARACTERIZATION OF TORTOISE SHELL AND ITS IMITATIONS

Thomas Hainschwang and Laurence Leggio

Tortoise shell has long been used as an ornamental gem material for art objects, jewelry, and personal items such as combs and eyeglass frames. Though humans have used tortoise shell for thousands of years, the material reached the height of its popularity during the 18th, 19th, and early 20th centuries. The advent of plastic imitations, as well as the passage of laws protecting sea turtles beginning in the 1970s, have led to a drastic reduction in the amount of tortoise shell in the market. Nevertheless, because older material can still be traded, especially in antique pieces, and because numerous imitations exist, proper identification is still important. This study summarizes the gemological properties of tortoise shell and its imitations. In addition to standard gemological data, the results of several spectroscopic techniques are presented; transmission and specular reflectance infrared spectroscopy were found to be of particular value.

The term “tortoise shell” generally refers to the carapacial (dorsal shell) and plastron (belly) plates of the hawksbill sea turtle (*Eretmochelys imbricata*). The use of tortoise shell dates at least to pre-dynastic Egypt (3500–3100 BC), from which period dishes, combs, bracelets, and the like are known (“Animal products...,” 2005). Tortoise shell objects were popular with both the ancient Greeks and wealthy citizens of ancient Rome (Bariand and Poirot, 1998). The commercial exploitation of this material in Europe began as early as the 15th century in Spain (“Natural plastics,” 2005), and many types of tortoise shell objects have been produced since then. These include furniture inlays, eyeglass frames, decorative boxes, rings, bracelets, and earrings (see, e.g., figure 1). In Japan, tortoise shell crafting, or *bekko*, has been an important industry since at least the 17th century, most of it centered in Nagasaki (Pedersen, 2004). *Bekko* objects such as hair ornaments are still being created today from stockpiled material.

The vast majority of worked tortoise shell material comes from the shells of two species of sea turtles: the hawksbill and, more rarely, the green turtle (see box A). The shells of these turtles exhibit attractive patterns that normally consist of light to dark brown

patches, though a homogeneous “cream”-colored variety called *blond tortoise shell* also exists. The popularity of tortoise shell during the 18th through early 20th centuries caused these animals to be hunted almost to extinction, leading to a near-worldwide ban on collection in the 1970s, as well as a ban on international trade in tortoise shell products (Spotila, 2004; box B). For the modern gemologist, tortoise shell has become a rather exotic material, for which a thorough gemological study is lacking.

BACKGROUND ON TORTOISE SHELL AND PLASTICS

Tortoise shell is composed of β -keratin, an insoluble protein (Voet et al., 2005), and is almost identical in composition to hair and nail. The structure of tortoise shell defines this material as a natural polymer: It consists of long chains of organic molecules and thus has a high molecular weight. Each of these organic molecules is called a *monomer* (from the Greek meaning

See end of article for About the Authors and Acknowledgments.
GEMS & GEMOLOGY, Vol. 42, No. 1, pp. 36–52.
© 2006 Gemological Institute of America



Figure 1. A popular and often-seen gem material during the 18th and 19th centuries, tortoise shell has since become a rare oddity for most gemologists. Shown here are a pair of Egyptian revival earrings, approximately 6.5 cm long. From Mona Lee Nesseseth, *Custom and Estate Jewels*, Los Angeles; courtesy of Tricia and Michael Berns. Photo © Harold & Erica Van Pelt.

“single part”); they combine to form a *polymer* (from the Greek meaning “many parts”). *Polymer* is a generic term for a long molecule with repeating parts; a molecule is considered a polymer when it exceeds about 1,000 atoms in length (Bloomfeld, 2000). There are many types of polymers, both organic and inorganic, with a wide variety of properties. All the materials described in this study are organic polymers; other natural organic polymers include horn, tree resins and fossilized tree resins (amber), natural rubber, bitumen, and waxes (Langenheim, 2003).

The term *plastic* refers to a broad class of materials of various chemical combinations, mainly of the organic elements carbon, oxygen, nitrogen, and hydrogen (and sometimes including inorganic elements such as chlorine). Plastics are covalently bonded polymers with various added components

(Bloomfeld, 2000; Van der Vegt, 2002) and can be classified as *natural*, *semisynthetic*, and *synthetic*. Natural plastics include shellac, rubber, asphalt, cellulose, and tortoise shell. Semisynthetics (so-called because they are natural materials that have been chemically modified) include cellulose nitrate (e.g., Celluloid, Xylonite, Parkesine), cellulose acetate (e.g., Safety Celluloid, Bexoid, Clarifoil, Tenite), and casein formaldehyde (e.g., Lactoid, Erinoid, Galalith; Van der Vegt, 2002). Most plastics used today are fully synthetic; these include phenol formaldehyde resin (Bakelite) and polyester resins (e.g., PET and polyurethane), among many others.

Plastics can also be divided into *thermosetting* and *thermoplastic* materials. Thermosetting plastics can be liquefied and hardened only once, similar to concrete. Once such a material has been hardened (poly-

BOX A: SEA TURTLE CLASSIFICATION AND BIOLOGY

As explained in Perrine (2003) and Spotila (2004), turtles are reptiles belonging to the order of the Chelonians, a very ancient group that originated in the late Triassic, about 230 million years ago. Marine turtles appeared about 80 million years ago and represent reptiles that had adapted to life in the sea. There are only two families of contemporary marine turtles: the Cheloniidae and the Dermochelyidae. The first corresponds to the sea turtles that have a shell, and today this family consists of six species:

- Hawksbill turtle, *Eretmochelys imbricata* (Linnaeus, 1766)
- Green turtle, *Chelonia mydas* (Linnaeus, 1758)
- Loggerhead turtle, *Caretta caretta* (Linnaeus, 1758)
- Kemp's Ridley turtle, *Lepidochelys kempii* (Garman, 1880)
- Olive Ridley turtle, *Lepidochelys olivacea* (Eschscholtz, 1829)
- Flatback turtle, *Natator depressa* (Garman, 1880)

The black turtle (*Chelonia agassizii*; Bocourt, 1868) was at one time regarded as a separate species,

Figure A-1. The shell of a hawksbill turtle is the traditional source for the tortoise shell used as a gem and ornamental material. Commercial harvesting of hawksbill turtles is now prohibited by international treaties. Photo by Johan Chevalier.



but recent research using mitochondrial DNA testing has shown that it is in fact a variety of green turtle (Karl and Bowen, 1999).

Of these six species, only the shell of the hawksbill turtle (figure A-1) and, more rarely, the green turtle (figure A-2) is typically used for ornamental objects and jewelry. The shells of these two species often cannot be easily distinguished, especially after being worked into objects, except by analysis of the ratio of the two amino acids lysine and histidine (Hendrickson et al., 1976).

The second family corresponds to turtles that have a body covered only by a leathery skin. Today, this family consists of only one species: the Leatherback turtle, *Dermochelys coriacea* (Vandelli, 1761). Marine turtles are migrating species with worldwide distribution.

The Hawksbill Turtle. The name originates from the turtle's bill, which has a shape reminiscent of a hawk's. The 13 plates of its carapace overlap another like the tiles of a roof, which is the source of the scientific name *Eretmochelys imbricata* (*imbricatus* being Latin for "covered with tiles"). The plates have a maximum thickness of 9–12 mm (Bariand and Poirot, 1998). The relief of the carapace diminishes with age, as the plates become thicker and lose the typical imbrications. The carapace can be brown-red to brownish orangy yellow, with dark brown to black marbling or yellow to brownish yellow striations; the plastron scutes (horny plates; figure A-3) that cover the "belly" of the animal are white to yellow, sometimes with a little dark pigmentation. This turtle, which represents the only species that has been commercially exploited for ornamental tortoise shell, has a maximum length of about 95 cm (a little over 3 ft.) and an average weight of 62 kg (137 lbs.).

The Green Turtle. The name *green turtle* originates from the color of its flesh; the carapace of adult animals is olive or brown, patchy or marbled. The coloration varies considerably from one individual to another. In young adults, the carapace typically is mahogany brown with light striations; later, the green-yellow color becomes predominant. *Chelonia mydas* is a large species (80–130 cm long) with an average weight of 160 kg (a maximum of 400 kg has been reported).

Only rarely has the carapace of the green turtle



Figure A-2. Though it superficially resembles that of a hawksbill turtle, the shell of the green turtle (shown here) has only rarely seen use as a gem material because its thinner shell plates are much more difficult to work. Photo by Erich Frederico Betz.

been used as an ornamental material, since it is usually not as attractive as the shell of the hawksbill turtle, and since the scutes are much thinner and thus more difficult to work. Nevertheless, it can occasionally be seen, especially as inlay in "Boulle" furniture from the 17th and 18th centuries. The species is considered to be in danger of extinction because of over-harvesting and unsustainable exploitation.

Figure A-3. The plastron (belly) plates of the hawksbill turtle have also been worked into objects; the resulting material is often referred to as blond tortoise shell. Photo © Smaro Touliatou/ARCHELON.



merized), generally it cannot easily be melted. Thermoplastic materials have properties similar to those of wax, as they can be melted and shaped multiple times. The reason for these differences is that the polymer chains in thermoplastic materials remain linear (i.e., they do not undergo a chemical change during molding) and thus can be separated easily by heat. In contrast, the polymer chains in a thermosetting plastic are chemically altered during molding and form a three-dimensional network by "cross-linking." Cross-linked plastics tend to have superior properties compared to linear plastics, such as greater resistance to heat and chemicals (Bloomfeld, 2000).

Tortoise shell is a natural thermoplastic material, and behaves very much like certain synthetic or semisynthetic plastics. Using heat and pressure (molding), the artisan can fuse several thin pieces into one thick piece and then, to a certain degree, form it into desired shapes (Bariand and Poirot, 1998).

Imitations of tortoise shell (see, e.g., figure 2) first appeared after the development of artificial plastics in the 19th century. Possibilities for using natural plastics were identified in the 17th century by the Englishman John Osbourne ("Natural plastics," 2005), who produced moldings from horn. The first semi-synthetic plastic, and the first material used to imitate tortoise shell, was cellulose nitrate, also known as *Celluloid*, which was invented in 1862 by Alexander Parkes (Sears, 1977; Buist, 1986). The problem with this material, however, was its high flammability. In 1892, cellulose acetate was developed by Cross, Bevan, and Beadle (Sears, 1977); this material, which is much less flammable than celluloid, was marketed as *Safety Celluloid*. Around the same time, in 1897, casein formaldehyde was invented by Adolf Spitteler (Gibbs, 1977); it is produced by the interaction of the milk protein casein with formaldehyde. Bakelite, invented and patented around 1907 by Leo Baekeland (Farrar, 1968; Buist, 1986), was the first fully synthetic plastic, produced by the condensation of phenol and formaldehyde. Many of the other plastics commonly used for imitating tortoise shell, such as polyester, were developed between 1930 and 1950 (Buist, 1986).

Typically, tortoise shell can be readily identified by microscopy and luminescence techniques. In some cases, however, it may be difficult to separate tortoise shell from other organic materials in polished objects unless spectroscopic methods are used.

Although tortoise shell is a natural plastic, the term *plastic* alone in this article refers to semisynthetic or synthetic imitations.

BOX B: LEGAL ASPECTS OF TRADE IN TORTOISE SHELL

A number of international treaties and conventions govern trade in tortoise shell. The most comprehensive and important is the Convention on International Trade in Endangered Species (CITES), which was first agreed upon in 1973. The primary aims of CITES are surveillance of the international trade in wild animals and plants, and assurance that this commercial exploitation does not endanger the survival of protected species. There are currently more than 160 CITES member countries, including the United States, Canada, Japan, Australia, and all members of the European Union. Since this convention became effective, no protected species has become extinct.

CITES governs all trade (export, re-export, and import from international waters) of the species listed in its three Annexes, depending on the degree of protection necessary. Annex I, which includes sea turtles, covers species in danger of extinction. Trade in these species or in products derived from them is authorized only in exceptional conditions, such as for purely scientific research. (Annexes II and III provide lesser degrees of protection for species not in danger of extinction.) Only older tortoise shell material, dating prior to 1975, can be traded under CITES; all other trade is prohibited. For more information on the legal aspects of tortoise shell, see "Special issue..." (2002), Perrine (2003), and Spotila (2004).

MATERIALS AND METHODS

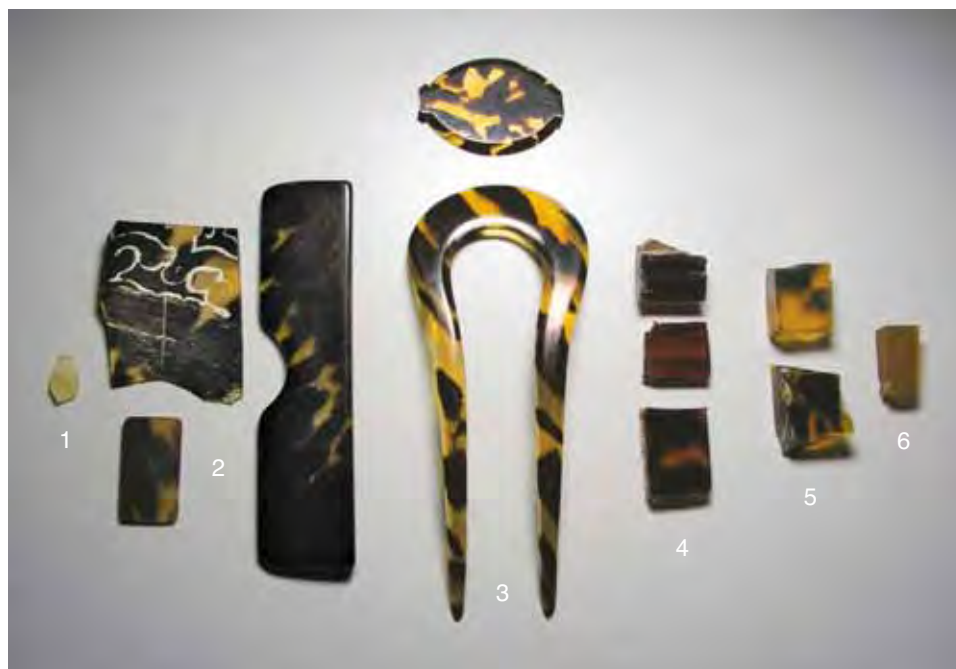
Several samples of tortoise shell and its imitations were analyzed for this study (see, e.g., figure 3). The tortoise shell materials included five unworked pieces (one from a green turtle from French Guyana and four samples from hawksbill turtles, two from Cameroon and two of unknown origin), 10 polished samples of unknown origin, and one object (a small box) made of blond tortoise shell; one polished sample stabilized with artificial resin was analyzed prior to this study,

and its properties will be mentioned only briefly in the Discussion section. During the examination of a large collection of jewelry by one of the authors (TH), 15 objects made of tortoise shell were analyzed, all of which had been worked in part by heat and pressure. The observations made on these objects are also included in this study. The synthetic and semisynthetic plastic imitations included the following (number of samples in parentheses): cellulose nitrate (3), cellulose acetate in various colors (10), polyester (3),

Figure 2. Because of the expense of the genuine material and legal restrictions on its collection, tortoise shell has frequently been imitated by various plastics. Inexpensive imitations such as these are very common in the consumer market. Photo by D. Mengason.



Figure 3. A wide variety of materials have been used to imitate tortoise shell, and their appearances are often superficially similar. Shown here are some of the materials examined in this study. From left: horn (1), tortoise shell (2), cellulose nitrate (3), cellulose acetate (4), polyester (5), and casein formaldehyde (6). Photo by T. Hainschwang.



casein formaldehyde (1), and phenol formaldehyde (1). The plastics were obtained from two manufacturers of polymer materials in the Rhône-Alpes region (France) and from various collections. A piece of horn (similar in appearance to blond tortoise shell) and a sample of human nail also were included to investigate their similarities to tortoise shell.

The samples were analyzed by standard gemological methods including microscopy, fluorescence to long- and short-wave UV radiation (all samples), specific gravity (hydrostatic method; one sample of each type of material, except nail), and refractive index testing (on all polished samples, representing all substances, except nail) using a GIA Instruments refractometer.

Characteristic odors were noted by hot point and hot water testing on one randomly selected sample of each material. For the hot point testing, the material was touched with a needle that had been heated by a simple flame; the hot water testing was performed by immersing the sample for 30 seconds in water with a temperature of approximately 60°C (140°F).

Infrared (IR), visible–near infrared (Vis-NIR), and photoluminescence (PL) spectral analyses were performed for selected samples of all materials included in this study. Samples were chosen based on their color, transparency, and thickness. IR transmission spectra were recorded at room temperature with a PerkinElmer Spectrum BXII Fourier-transfer infrared (FTIR) spectrometer (4 cm⁻¹ resolution) using a deuterium triglycine sulfate (DTGS) detector. The spec-

tra were recorded from samples of ~5 mm thickness and thin films. The “thick” spectra (recorded for five samples of tortoise shell and one or two samples each of the other materials) were taken because most samples of tortoise shell and imitation tortoise shell may not be damaged or destroyed for analysis, and these will commonly have a thickness of ~5 mm. These spectra, taken in the range of 7800–3700 cm⁻¹, are representative of what can generally be obtained from finished objects by nondestructive transmission FTIR spectroscopy. Since pieces of this thickness show too much absorption below ~5000 cm⁻¹, thin films were prepared from randomly selected samples of all materials included in this study, to obtain spectra of the entire range between 7800 and 400 cm⁻¹. A total of 11 thin films were tested: one for each of the plastics and one for each of the natural materials, except for the tortoise shell, for which four samples were polished into a thin film. To collect such complete spectra without the use of the KBr powder method, we had the thin samples polished down to a thickness of <0.01 mm.

Specular reflectance IR spectra were recorded for four samples of tortoise shell and one or two samples each of the other materials (except nail) with the same FTIR system using a PerkinElmer specular reflectance accessory, with 4 cm⁻¹ resolution. This method is commonly employed to observe the mid-infrared spectra of polished minerals without using the destructive KBr pellet technique; the infrared beam is not transmitted through a sample, but rather is reflected off the polished surface. This

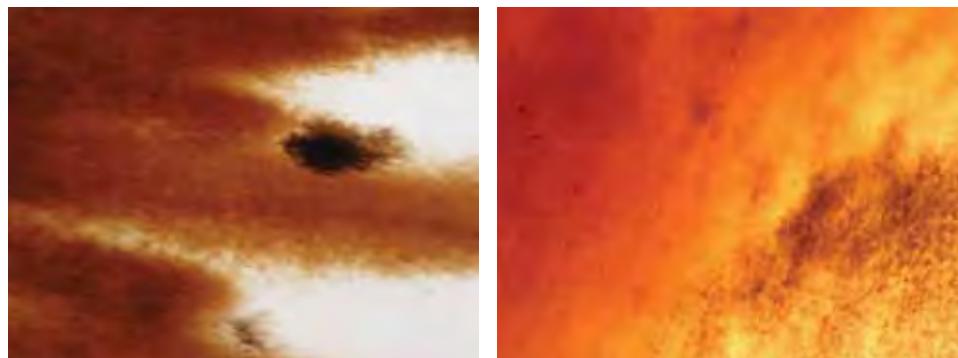


Figure 4. When examined with magnification, tortoise shell typically has a distinctive appearance consisting of tiny spots that make up the large brown patches. Photomicrographs by T. Hainschwang; magnified 25× (left), 60× (right).

produces data similar to KBr powder absorption spectra but with some differences, such as shifted and asymmetric peaks, depending on the materials analyzed. In the authors' experience, organic materials such as tortoise shell show significantly different spectra in reflectance versus transmission modes, whereas other gem materials such as garnet produce very similar spectra in both modes. Specular reflectance spectra can be transformed into true absorption spectra by the Kramers-Kronig transform (White, 1974).

Vis-NIR transmission spectra in the range of 400–1000 nm were recorded for two samples of tortoise shell, three samples of cellulose acetate, and one sample of each of the other materials with a custom SAS 2000 system equipped with an Ocean Optics SD2000 dual-channel spectrometer (optical

resolution 1.5 nm) using a 2048-element linear silicon charged-coupling device (CCD)-array detector; samples were analyzed in an integration sphere. The spectra are shown in transmission mode to enhance the visibility of the broad bands useful for distinguishing these materials.

PL spectra were recorded for one sample of each material using a 532 nm semiconductor laser, with the same spectrometer and CCD detector that were used for the Vis-NIR spectra, at a resolution of 1.5 nm. All spectra were recorded at room temperature.

RESULTS

Visual Appearance and Gemological Properties. The tortoise shell samples varied in color, the most common being a light brownish yellow with darker

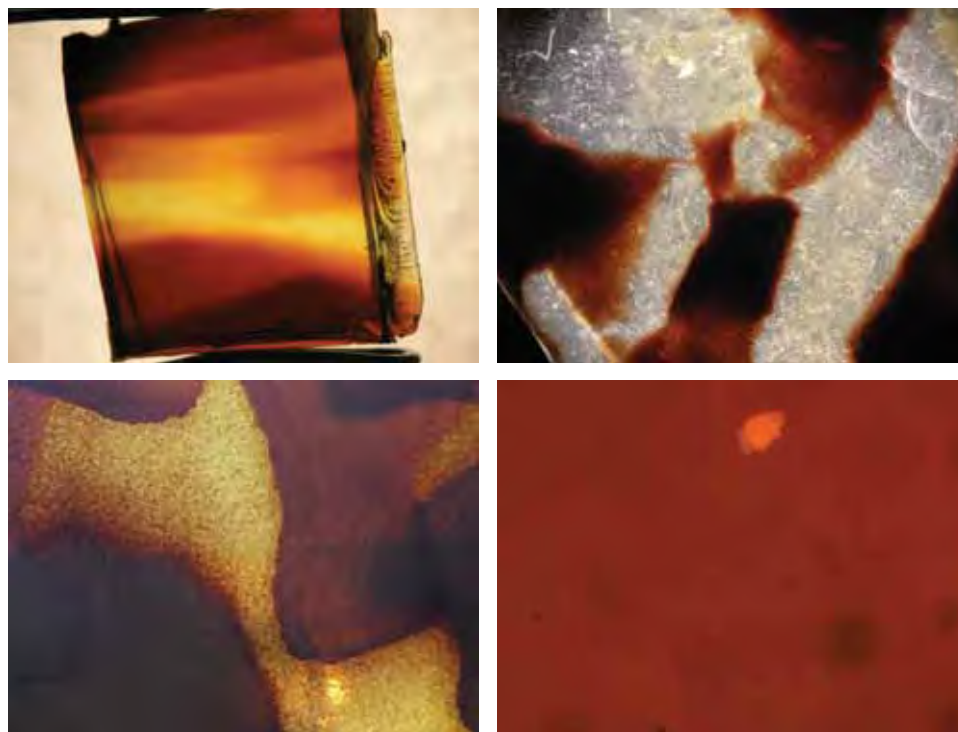


Figure 5. In contrast to tortoise shell, imitations such as cellulose acetate (top left) and cellulose nitrate (top right) show a homogenous appearance lacking the tiny spots of pigment typical of tortoise shell. In some polyester imitations (bottom), the color is distributed as small spots, though these do not resemble the pigment spots in natural tortoise shell. These inclusions are typically small white to black flakes, likely unmelted source material. Photomicrographs by T. Hainschwang, magnified 15× (top left), 10× (top right), 13× (bottom left), 80× (bottom right).

brown patches. The small box made of blond tortoise shell was a largely homogenous “cream” color. One unworked sample was almost entirely dark brown to nearly black. Microscopic observation revealed that the dark patches were made up of tiny spots (figure 4).

The plastic imitations covered a range of colors from “blond” to patchy to nearly black. Their color appearance was commonly very different from that of tortoise shell. Even if they were macroscopically similar, magnification revealed an absence of the “spotty” micropattern; instead, the brown patches were quite homogenous and unlikely to be confused with true tortoise shell. In some polyester imitations, the color was distributed in small spots (figure 5), but these were still very different from the pigment spots seen in tortoise shell.

Three samples of tortoise shell that had been worked by the use of heat and pressure into desired shapes and thickness lacked the typical spotty appearance. Thus, these somewhat resembled the plastic samples under the microscope. Interestingly, none of the plastic samples contained the trapped gas bubbles that are frequently seen in plastics and could help

identify such materials. However, all the plastic samples contained small flaky particles of unknown nature (again, see figure 5), which were most likely unmelted remnants of the source materials.

Standard gemological properties for tortoise shell and its plastic imitations are given in table 1. Often these properties will be sufficient to identify the material; however, there is overlap in some properties, especially specific gravity and refractive index. Unfortunately, the most useful gemological test for the identification of these substances, the hot point, is a destructive one: Tortoise shell smells like burned hair (as does horn), while plastics have very different odors. An alternative to the hot point is the hot water test, which involves rinsing the materials under hot tap water. It was noted in this study that this test will provoke the characteristic odor of most plastics without damaging them. Cellulose nitrate, cellulose acetate, casein formaldehyde, and phenol formaldehyde may be identified in this fashion. Tortoise shell does not have a discernable odor when tested by this method, and as long as the water temperature does not exceed ~80°C, the material will not be damaged.

TABLE 1. The standard gemological properties of tortoise shell and its imitations.

Material	R.I. ^a	S.G. ^a	Long-wave UV ^b	Hot point odor ^c	Crossed polarizers
Tortoise shell	1.54	1.26–1.35	Chalky blue-white (light areas), dark patches appear brown with super-imposed chalkiness. Intensity: medium	Burnt hair	Light appearance (aggregate-like); cross-hatched interference colors in worked/bent samples
Horn (pale yellow, to imitate blond tortoise shell)	1.54	1.26–1.35	Chalky blue-white. Intensity: medium-strong	Burnt hair	Light appearance (aggregate-like)
Cellulose nitrate (<i>Celluloid</i>)	1.50–1.51	1.36–1.42 (rarely up to 1.80)	Chalky bluish yellow (light areas). Intensity: medium. Dark patches fluoresce orange brown. Intensity: weak	Camphor	Dark appearance
Cellulose acetate (<i>Safety Celluloid</i>)	1.49–1.51	1.29–1.40 (rarely up to 1.80)	Variable: chalky bluish green to chalky bluish white. Intensity: very weak to weak. Sometimes brown patches fluoresce orange. Intensity: medium	Vinegar	ADR (4 times dark in 360° rotation), in some samples very weak ADR only
Polyester	1.56	1.23	Chalky yellowish green. Intensity: weak	Acrylic	ADR (4 times dark in 360° rotation)
Casein formaldehyde (<i>Galalith</i>)	1.55–1.56	1.32–1.34	Chalky yellow. Intensity: medium	Burned milk	ADR (cross-hatched extinction)
Phenol formaldehyde (<i>Bakelite</i>)	1.61–1.66	1.25–1.30	Inert to chalky yellowish blue. Intensity: very weak	Formaldehyde, acrylic	ADR (cross-hatched appearance)

^aR.I. and S.G. ranges are from Webster, 1994 (except for polyester, the values of which were determined by the authors); values of samples included in this study were determined to be within the given ranges.

^b Short-wave UV radiation excited the same luminescence, but the intensity was considerably weaker in all materials

^cThe odor, even if weaker, can be readily provoked in most plastics by immersion in hot water (~60°C).



Figure 6. When exposed to long-wave UV radiation, the fluorescence reactions of the materials in figure 3 are quite distinct despite their similarities in normal light. As seen here, tortoise shell's chalky blue-white reaction usually can allow easy separation from imitations. From left: horn (1), tortoise shell (2), cellulose nitrate (3), cellulose acetate (4), polyester (5), and casein formaldehyde (6). Photo by T. Hainschwang.

Fluorescence to both long- and short-wave UV radiation was chalky blue-white for the light areas of tortoise shell, while the dark patches appeared brown with a superimposed chalkiness (figure 6). The plastics showed variable luminescence, which depended on the dyes used to color the materials. The plastics themselves generally luminesced chalky blue with a yellow modifier (and thus sometimes appeared green) to chalky yellow (again, see figure 6). Dyes may induce a different luminescence: The cellulose nitrate samples showed a very slight

orange-brown luminescence in the brown areas, while the brown patches in certain samples of cellulose acetate exhibited an orange luminescence of medium intensity. For all samples, the only noticeable difference between long- and short-wave UV was the strength of the emission excited by the two sources; the luminescence color was the same.

When rotated between crossed polarizers, the tortoise shell samples appeared light in all positions (i.e., an aggregate reaction similar to, for example, chalcedony and jadeite). The same was true for the

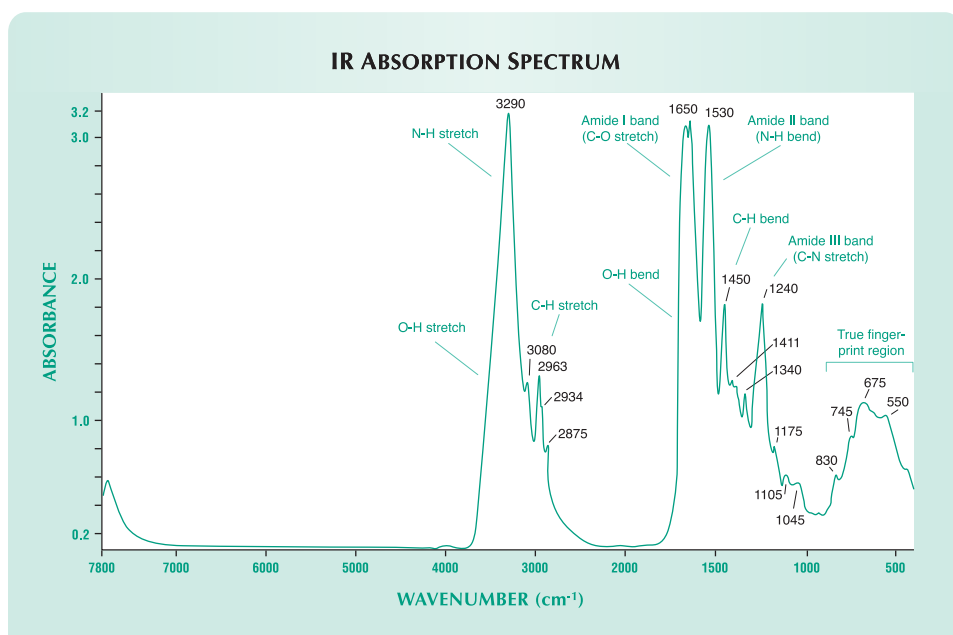


Figure 7. The IR spectrum of a thin film (<0.01 mm thick) of tortoise shell shows several distinctive absorption peaks. It is almost identical to that of the protein keratin, and thus shows characteristic absorptions due to organic functional groups such as CH, NH, and OH. The region below 2000 cm^{-1} is expanded for clarity.

samples of horn and nail. This appearance in tortoise shell was seen as long as the material had not been forced into a curved shape; in curved objects such as bangles, a weak cross-hatched pattern of interference colors could be observed, but no extinction. The reactions of all the plastic imitations were distinctly different from that of tortoise shell, with none of those samples exhibiting tortoise shell's aggregate-like reaction. The cellulose nitrate samples stayed dark when rotated between crossed polarizers; this was the only truly isotropic material seen in this study. All the other plastics showed anomalous double refraction (ADR) either as cross-hatched extinction patterns or as four sequential extinctions per full rotation. Such ADR reactions indicate the presence of strain.

Transmission IR Spectroscopy. The thin-film IR spectrum of the tortoise shell was mainly characterized by strong absorptions around 3290, 1500, and 600 cm^{-1} (figure 7). The strong band at 3290 cm^{-1} corresponds to the N-H stretch (Coates, 2000; Naumann, 2000). OH-related absorption found in the same region was superimposed by the strong NH absorption and therefore was not visible. The absorptions around 2900 cm^{-1} correspond to the C-H stretch. The CH bend was visible as a distinct band at 1450 cm^{-1} . (*Stretch* and *bend* are terms used in IR spectroscopy to

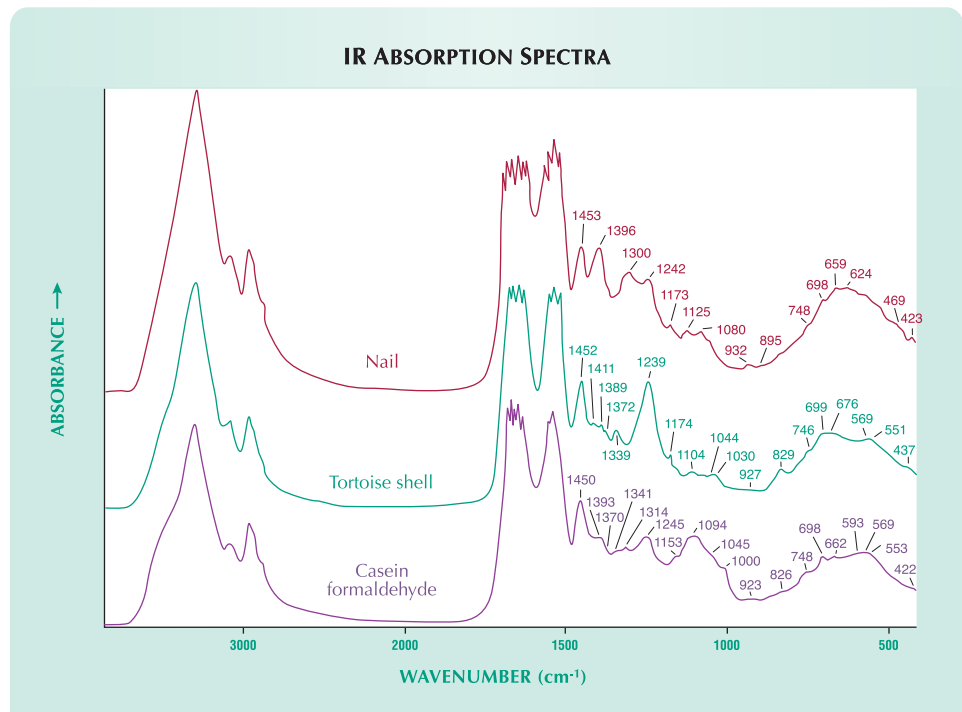
describe absorptions due to the stretching and bending motions of molecules; *overtone* and *combination* describe additional smaller absorptions produced by transitions to higher energy levels. These are found at multiple and combined [sum and difference] frequencies of the stretching and the bending vibration [Coates, 2000]).

The strong bands at 1650, 1530, and 1240 cm^{-1} are called *amide bands* (amide I, II, and III; Naumann, 2000) and correlate to the C-O stretch, N-H bend, and C-N stretch, respectively. The broad, complex band between 900 and 400 cm^{-1} has been called the "true fingerprint region" of proteins by Naumann (2000), because it is more characteristic of protein-based substances than the region ~2000 to 400 cm^{-1} , which is commonly used as the "fingerprint region" to identify substances such as gem materials.

The IR spectra of tortoise shell, horn (not shown), and human nail were nearly identical (figure 8); this confirms that horn-like materials and tortoise shell are chemically very similar and mainly composed of proteins, in these specific cases keratin.

The thin-film IR spectra of the plastic imitations were distinctly different from the spectrum of tortoise shell. Most of the plastics were characterized by distinct CH- and often OH-related bands at 3200–2900 and at 3600–3400 cm^{-1} , respectively (figure 9), and by complex bands that are due to other structural groups

Figure 8. The thin-film IR spectra of human nail, tortoise shell, and casein formaldehyde plastic are very similar due to their similar chemical compositions. The inset shows the distinctive features that are found in the region between 1500 and 400 cm^{-1} . The region below 2000 cm^{-1} is expanded for clarity.



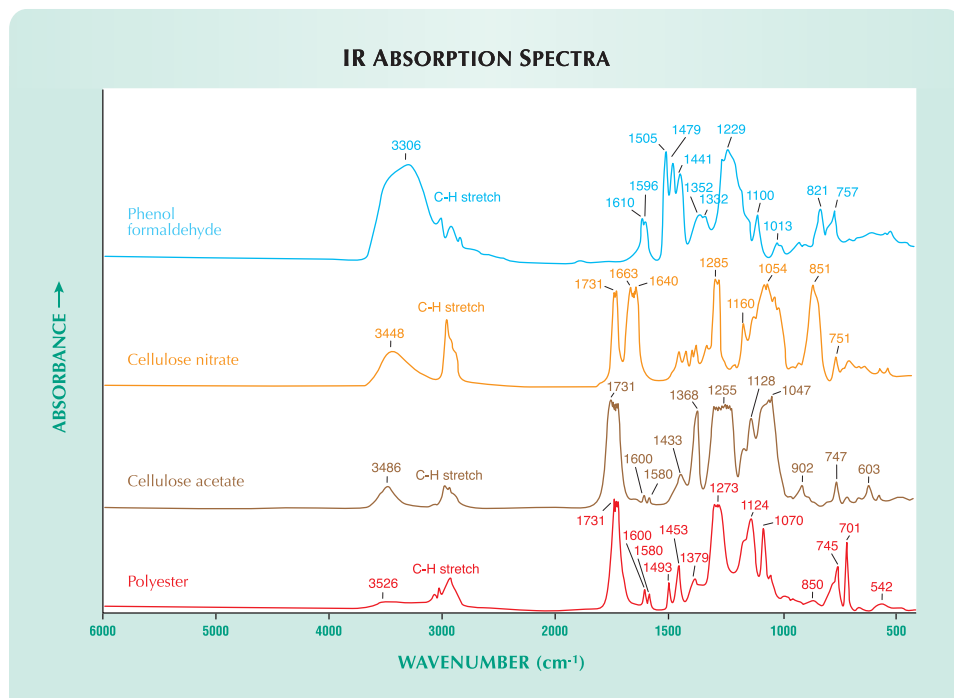
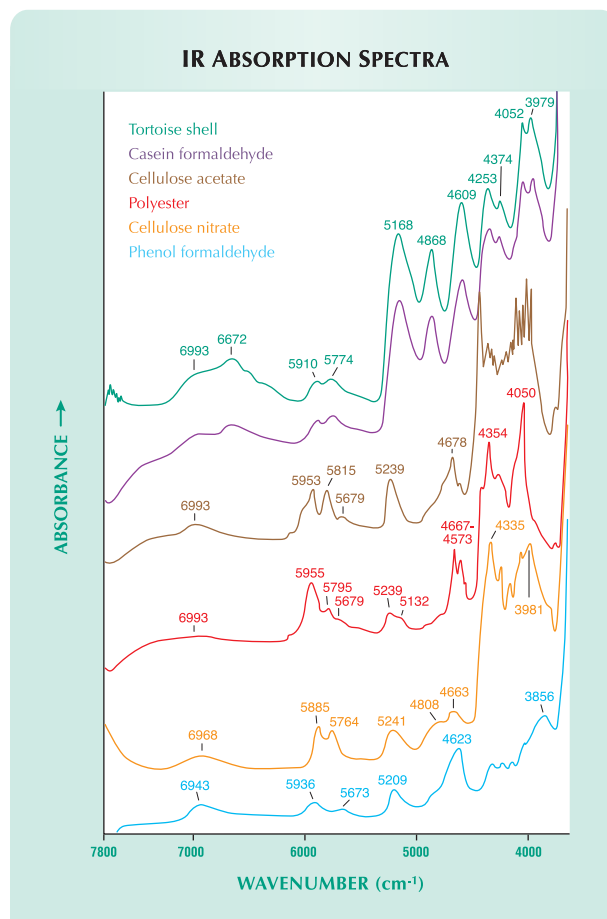


Figure 9. The IR spectra of thin films of the other plastic imitations are distinctly different from the spectrum of tortoise shell seen in figures 7 and 8. The CO-, NH-, and CN-related bands are missing in these materials. The region below 2000 cm⁻¹ is expanded for clarity.

and the “backbone” (C-C) structure. It would be far too complex for the purposes of this article to discuss all structural groups present in each of the plastic imitations and even more so to assign specific bands visible in the FTIR spectrum to a particular group. The combination of functional group absorptions and backbone-related absorptions is characteristic of all polymers and allows their identification as such (Coates, 2000). Most of the plastics analyzed lacked the CO-, NH-, and CN-related absorption features that are typical of tortoise shell and other protein-based substances. The only exception, casein formaldehyde, had an IR spectrum very similar to that of tortoise shell (figures 8 and 10). Differences that distinguish these materials in the infrared can be found in the limited region of 1500 to 400 cm⁻¹ (again, see

Figure 10. The IR spectra of thicker (~5 mm) samples of tortoise shell and its imitations also show distinct differences. These spectra are closer to what can be obtained nondestructively from large objects fashioned from tortoise shell or one of its imitations. The bands in the NIR will be distinct, while the absorptions below 4000 cm⁻¹ will not be visible because of their intensity and the limitations of the detector. Most of the materials tested could be distinguished based on this limited region, except the samples of tortoise shell and casein formaldehyde, which were identical.



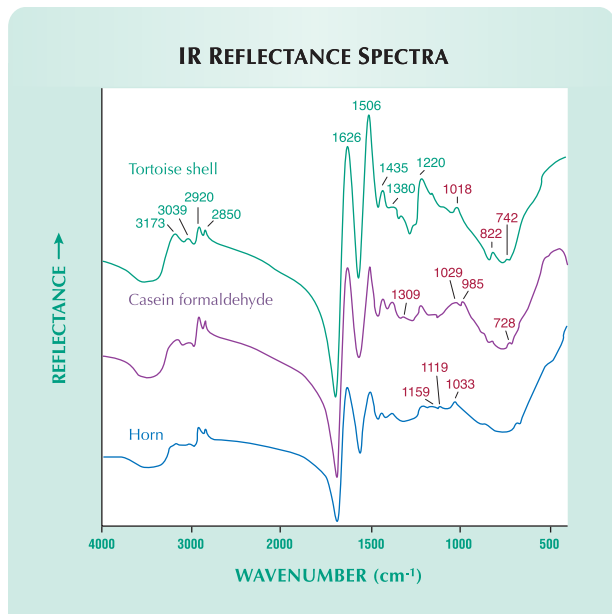


Figure 11. Although the specular reflectance IR spectra of tortoise shell, horn, and casein formaldehyde are similar, they can be distinguished by the minor features indicated in red. The spectrum of the nail is not included, because the sample was too small and irregular for acceptable specular reflectance FTIR analysis. The region below 2000 cm^{-1} is expanded for clarity.

figure 8): The spectrum of casein formaldehyde exhibited a rather strong, complex, broad band centered at 1094 cm^{-1} , which was absent from the spectrum of tortoise shell. In addition, many of the bands were shifted and their general shape varied, especially the very broad, complex band extending from 900 to 400 cm^{-1} . Additionally, the absorption at $\sim 1240 \text{ cm}^{-1}$ was much more intense in the spectrum of tortoise shell than in that of casein formaldehyde.

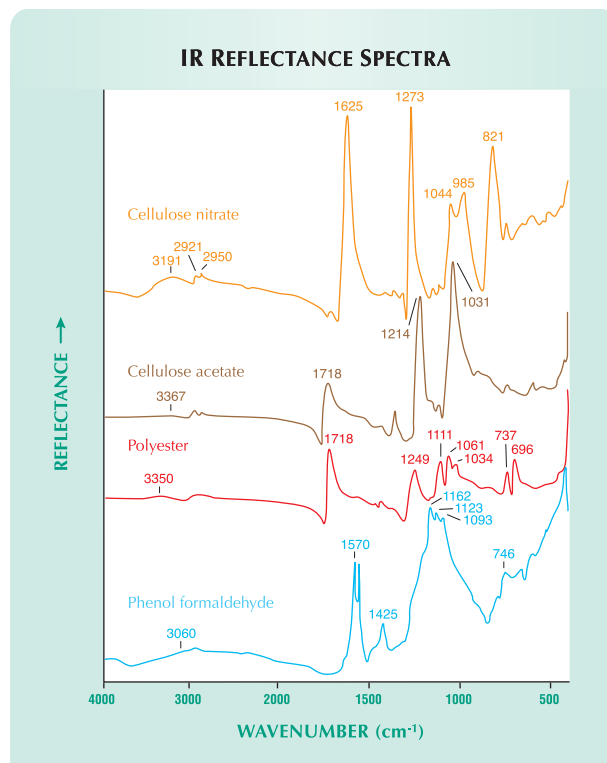
The IR spectra of the same materials in 5-mm-thick samples showed strong absorptions in the near-IR region between 7800 and 3700 cm^{-1} . All absorptions from 3700 to 400 cm^{-1} were too intense and thus not resolvable. In all but one case, the NIR region of the spectra of the plastics was distinctly different from that of tortoise shell; the exception was casein formaldehyde, which could not be distinguished from tortoise shell based on the limited NIR region of its spectrum (again, see figure 10).

Specular Reflectance IR Spectroscopy. All the samples tested, natural and artificial, exhibited relatively weak reflectance. In the experience of the authors, this is typical for such organic materials (including plastics). The reflectance spectra again showed a close similarity between tortoise shell and

casein formaldehyde (figure 11), and distinct differences between these two substances and all the other imitation materials (figure 12). However, we did note minor differences between casein formaldehyde and tortoise shell: Weak bands at 1018, 822, and 742 cm^{-1} were characteristic for tortoise shell, while features at 1309, 1029, 985, and 728 cm^{-1} were only seen in casein formaldehyde (again, see figure 11). The spectrum of horn, shown here for comparison, again illustrates the similarity between the two organic materials.

Vis-NIR Spectroscopy. The Vis-NIR transmission spectra of the tortoise shell samples and all of the plastic imitations revealed differences, even though these were sometimes subtle. The spectra of the light and dark parts of the tortoise shell samples (figure 13A) were characterized by a smooth rise in transmittance toward the NIR region without distinct absorption bands. The darker spots showed total absorption below 530 nm. The spectra of the imita-

Figure 12. Again, the specular reflectance IR spectra of the non-protein-based plastic imitations are very different from the tortoise shell spectrum seen in figure 11. The region below 2000 cm^{-1} is expanded for clarity.



VIS-NIR TRANSMISSION SPECTRA

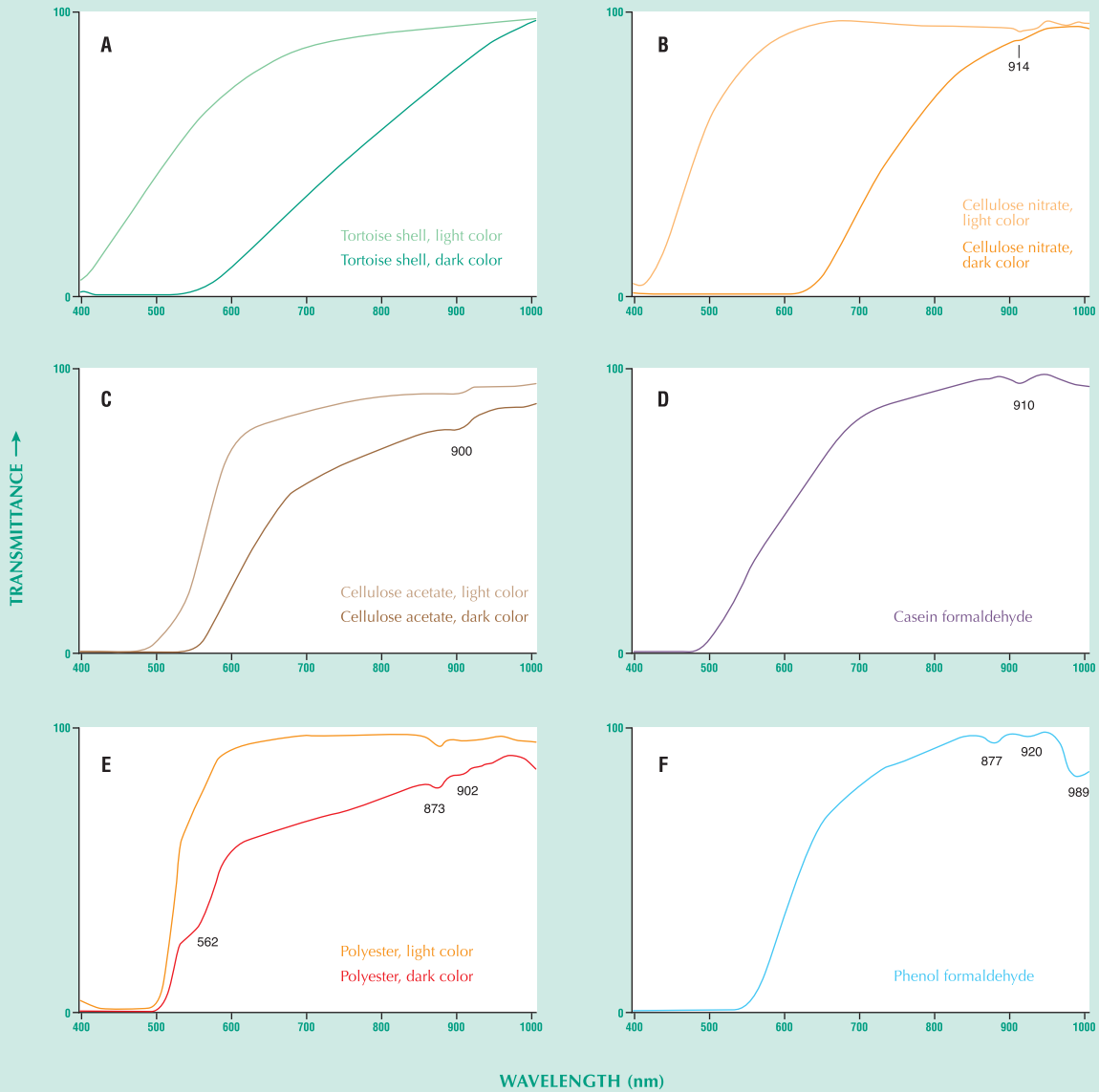


Figure 13. The Vis-NIR transmission spectra of tortoise shell show few if any notable features compared to the plastic imitations, exhibiting a lack of distinct absorption bands and a smooth rise in transmittance. More-irregular transmission curves, including absorption bands mainly in the NIR, are typical for the plastic imitations. Horn and nail show spectra (not shown) that are similar to those of tortoise shell.

tions were not as smooth and exhibited a different curvature. Broad bands, mainly in the NIR, could be seen in the spectra of all the imitations: at 914 nm for cellulose nitrate (figure 13B); at 900 nm for cellulose acetate (figure 13C); at 910 nm for casein formaldehyde (figure 13D); at 562, 873, and 902 nm for polyester (figure 13E); and at 877, 920, and 989 nm for phenol formaldehyde (figure 13F). Most of the imitations showed total absorption below around 500 nm.

Photoluminescence Spectroscopy. The PL spectra of the materials analyzed (figure 14) showed differences in their general shape. Tortoise shell, horn, and casein formaldehyde exhibited nearly identical emissions that consisted of one broad band that was most intense at 578 nm. Cellulose nitrate and cellulose acetate showed a broad band at 603 nm, while polyester showed two broad bands, one at 578 nm and one at 628 nm. Despite these general

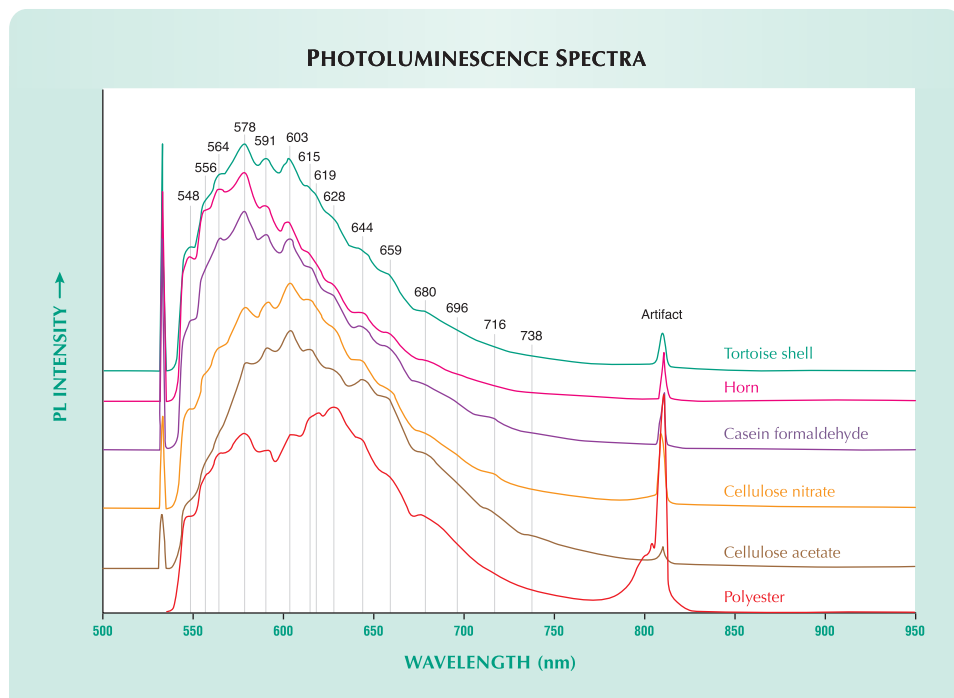


Figure 14. The photoluminescence spectra of tortoise shell and its plastic imitations show differences in curve shape, but, surprisingly, the same individual peaks are present in all spectra.

differences, the same individual PL peaks were present in the spectra of all samples.

DISCUSSION

The separation of tortoise shell and its imitations is not difficult with standard gemological testing, provided all the necessary tests can be performed. The combination of microscopy, R.I., S.G., UV fluorescence, and appearance between crossed polarizers is sufficient to determine whether a sample is tortoise shell or an imitation. Even though horn can be very similar in overall appearance to blond tortoise shell, its structure is distinctly different, since it is rather fibrous. As seen in figure 6, UV fluorescence alone may be sufficient to separate tortoise shell from visually similar material. Any orange and green luminescent plastic is quickly identified, as are samples with the characteristic “brown and cream” tortoise pattern that have homogeneous luminescence, since the patches in tortoise shell show a very different reaction from that seen in the cream-colored parts.

That said, the identification is not always straightforward, for several reasons:

1. Plastics and horn can imitate blond tortoise shell effectively, and the differences in luminescence are far less obvious.
2. Tortoise shell and its imitations are normally

worked into objects, and thus standard gemological tests beyond UV luminescence and a “hot point” may not be feasible (e.g., the S.G. of a tortoise shell box inlaid over gold will not be useful for identification). In addition, the relatively poor polish of tortoise shell and plastics, especially antiques, often does not allow the precise determination of a refractive index.

3. Mixtures of resins and tortoise shell and resin-stabilized tortoise shell exist. This material, at least one sample of which has been analyzed by the authors, shows properties intermediate between tortoise shell and plastic.
4. Plastics are materials with properties that can be drastically altered by slight compositional variations, changes in polymerization or cross-linking, or the use of dyes. Thus, there is always the possibility that new materials that imitate tortoise shell much more effectively will enter the marketplace.
5. In some cases, the exact identity of the plastic is important to the owner of an imitation, since some collectors are looking for specific plastics such as Bakelite.

These factors indicate that in some cases there may be a need for testing beyond that done with standard gemological tools.



Figure 15. Though new production of tortoise shell objects has nearly ceased as a result of legal restrictions, gemologists must still be prepared to identify older material that is still on the market. Shown here is an archeological revival necklace; the carved urn pendant is approximately 4 × 8 cm. From Mona Lee Nesseth, *Custom and Estate Jewels*, Los Angeles; courtesy of Tricia and Michael Berns. Photo © Harold & Erica Van Pelt.

Transmission IR spectroscopy can reliably identify all materials based on their intrinsic and material-specific absorptions between 2000 and 400 cm^{-1} ; however, complete spectra can be obtained only if a small amount of the substance is polished into a thin section or powdered and prepared into KBr pellets. Because these preparation techniques are destructive, they are of only limited usefulness for the gemologist. Nevertheless, transmission IR spectra of thicker samples commonly supply enough information to distinguish tortoise shell

from its imitations and to identify the plastics. The absorptions in the near-infrared region are generally quite specific for the analyzed material, but the fact that not all features are observable may prevent a conclusive identification, as can be seen in the case of casein formaldehyde plastic. The complex IR spectra are not easily interpreted; simplified, it can be stated that the spectra of organic substances are a combination of absorptions due to functional groups such as C-H or N-H and those due to the skeletal vibrations associated with the “backbone,” commonly the C-C linkages of a substance. The slightest differences in structure, molecule length, and composition will change the IR spectra. Such differences are present in all organic materials even if very similar, as with horn and tortoise shell; thus, they can all be distinguished by transmission IR spectroscopy, given proper sample preparation (Coates, 2000).

Vis-NIR spectra can supply useful information, but the presence of different dyes may change the spectra considerably. Some of the bands seen in the region around 900 nm may be interpreted as combination bands and/or overtones of OH-related vibrations (Adamo et al., 2005). This proposal is supported by the fact that the intensity of the OH-related band at $\sim 3500 \text{ cm}^{-1}$ correlates well with the intensity of the bands in the 900 nm region. It is apparent that tortoise shell contains very little OH compared to artificial plastics. Such near-infrared OH-related bands are known from water-containing minerals such as beryl, topaz, and euclase (see, e.g., Adamo et al., 2006), although in the experience of the authors the bands in these materials are much sharper. This is probably due to the crystallinity of such minerals as compared to the amorphous structure of the plastics. While some plastics can be mostly crystalline (with minor amorphous domains), such materials are translucent or opaque (Bloomfeld, 2000). The main drawback of transmission IR spectroscopy and Vis-NIR spectroscopy is their very limited use for large or irregular objects. In many cases, an analysis by these methods is impossible without breaking off a piece of the material in question.

Kiefert et al. (1999) showed that resins can be easily identified by Raman spectroscopy. This result is applicable to tortoise shell and its plastic imitations, but it needs further research to be confirmed. The method found most suitable during the course of this study was specular reflectance IR

spectroscopy, which allows the analysis of large objects with a simple accessory. In the experience of the authors, this method is highly effective in the identification of mineral species, and this study has shown that it is also useful for the separation of these various natural and synthetic organic materials.

Photoluminescence spectroscopy may also be used, but the substances in this study showed very similar emissions and in at least one case, that of casein formaldehyde, the spectrum was identical to that of tortoise shell. The reason for the presence of the same 15 emissions in all these materials is not known to the authors.

CONCLUSIONS

Although trade in contemporary tortoise shell has been largely banned internationally since the early 1970s, jewelry (figure 15) and other objects (figure 16) fashioned during the more than two centuries when it was a popular ornamental material can still be seen in the marketplace. This study has shown that, typically, tortoise shell can be easily distinguished from all materials used to imitate it, and that only protein-based plastics such as casein formaldehyde may pose a potential problem if not analyzed properly.

The application of standard gemological testing methods allows the unambiguous distinction of most tortoise shell from its imitations, which

Figure 16. During several centuries of popularity, a wide variety of objects were crafted from tortoise shell. The carved box at the bottom is approximately $10.5 \times 6.5 \times 2.5$ cm; the book is approximately $12 \times 8.5 \times 1.5$ cm. The book and carved box are from Mona Lee Nesseth, Custom and Estate Jewels, Los Angeles; courtesy of Tricia and Michael Berns. The chain is courtesy of Elise Misiorowski. Photo © Harold & Erica Van Pelt.



include semisynthetic and synthetic plastics. However, the identification of objects made of blond tortoise shell and the precise determination of a particular plastic require the use of more sophisticated laboratory techniques. Of the meth-

ods tested, the technique determined to be most versatile and useful for this purpose is specular reflectance IR spectroscopy. The results of this study can also be applied to plastics used to imitate other gem materials.

ABOUT THE AUTHORS

Mr. Hainschwang (thomas.hainschwang@gia.edu) is a research gemologist at GIA GemTechLab in Geneva, Switzerland. Miss Leggio is working on her Diplôme d'Université de Gemmologie on sea turtles, tortoise shell, and imitations of tortoise shell at the University of Nantes, France.

ACKNOWLEDGMENTS: The authors thank Christian Bonnet (eyeglasses manufacturer, Sens, France) and Jacques Fretey

(International Union for the Conservation of Nature and Natural Resources [IUCN], Paris) for their advice, loans, and donations of tortoise shell samples; and Jean Lescure (Laboratoire de Zoologie [Reptiles et Amphibiens], Muséum National d'Histoire Naturelle, Paris) and George Balazs (Pacific Islands Fisheries Science Center, Honolulu, Hawaii) for fruitful discussions. The authors also thank Jacques Meynier, Meynier et Fils S.A., Lavans Les St. Claude, France, and Gérard Piassale, Plastimod S.a.r.l., Yonnax, France, for supplying plastic imitations for this study.

REFERENCES

- Adamo I., Pavese A., Prospero L., Diella V., Merlini M., Gemmi M., Ajo D. (2005) Characterization of the New Malossi Hydrothermal Synthetic Emerald. *Gems & Gemology*, Vol. 41, No. 4, pp. 328–338.
- Animal products in ancient Egypt (2005) http://nefertiti.iwebland.com/animal_products/ [accessed Feb. 9, 2006].
- Bariand P., Poirot J.-P. (1998) *Larousse des Pierres Précieuses*. Larousse Bordas, Paris, 284 pp.
- Bloomfield A. (2000) *How Things Work: The Physics of Everyday Life*, 2nd ed. John Wiley & Sons, Chichester, UK.
- Buist J.M. (1986) Resume—the origins of polymers and their cellular derivatives. *Progress in Rubber and Plastics Technology*, Vol. 2, No. 3, pp. 17–30.
- Coates J. (2000) Interpretation of infrared spectra, a practical approach. In R.A. Meyers, Ed., *Encyclopedia of Analytical Chemistry*, John Wiley & Sons, Chichester, UK, pp. 10815–10837.
- Daley R.E., Daley S.J. (1996) *Organic Chemistry*. WCB, Boston, pp. 1186–1238.
- Farrar W.V. (1968) Formaldehyde: The centenary of a simple molecule. *Chemistry in Britain*, Vol. 4, No. 11, pp. 500–502.
- Gibbs S. (1977) People and polymers. A brief history of the accidental progression of the plastics industry. *Plastics and Rubber International*, Vol. 2, No. 5, pp. 221–224.
- Hendrickson J.R., Wood J.R., Young R.S. (1977) Lysine:histidine ratios in marine turtle shells. *Comparative Biochemistry and Physiology, Part B: Biochemistry & Molecular Biology*, Vol. 57, No. 4, pp. 285–286.
- International Instruments and Marine Turtle Conservation (2002) Special issue of the *Journal of International Wildlife Law and Policy*. Vol. 5, No. 1–2.
- Karl S.A., Bowen B.W. (1999) Evolutionary significant units versus geopolitical taxonomy: Molecular systematics of an endangered sea turtle (genus *Chelonia*). *Conservation Biology*, Vol. 13, No. 5, pp. 990–999.
- Kiefert L., Hänni H.A., Chalain J.-P., Weber W. (1999) Identification of filler substances in emeralds by infrared and Raman spectroscopy. *Journal of Gemmology*, Vol. 26, No. 8, pp. 501–520.
- Langenheim J.H. (2003) *Plant Resins: Chemistry, Evolution, Ecology, Ethnobotany*. Timber Press, Portland, OR.
- Natural plastics (2005) <http://www.plastiquarian.com/naturals.htm> [date accessed: 10/19/05].
- Naumann D. (2000) Infrared Spectroscopy in Microbiology. In R.A. Meyers, Ed., *Encyclopedia of Analytical Chemistry*, John Wiley & Sons, Chichester, UK, pp. 102–131.
- Pedersen M.C. (2004) *Gem and Ornamental Materials of Organic Origin*. Elsevier Butterworth-Heinemann, Oxford, UK, 268 pp.
- Perrine D. (2003) *Sea Turtles of the World*. Voyageur Press, MN.
- Sears J.A. (1977) Polymer pioneers. *Chemistry*, Vol. 50, No. 7, pp. 6–10.
- Spotila J.R. (2004) *Sea Turtles: A Complete Guide to Their Biology, Behaviour, and Conservation*. John Hopkins University Press, Baltimore, MD.
- Van der Vegt A.K. (2002) *From Polymers to Plastics*. Delft University Press, Delft, The Netherlands. Internet edition NUGI 831; <http://mail.vssd.nl/hlf/Polymers.pdf>.
- Voet D., Voet J.G., Pratt C.W. (2005) *Fundamentals of Biochemistry: Life at the Molecular Level*. John Wiley & Sons, Hoboken, NJ.
- Webster R. (1994) *Gems, Their Sources, Descriptions and Identification*, 5th ed. Rev. by P. G. Read, Butterworth-Heinemann, Oxford.
- White W.B. (1974) The carbonate minerals. In V. C. Farmer, Ed., *The Infrared Spectra of Minerals*, Mineralogical Society, London, p. 232.

Spring 1999

The Identification of Zachery-Treated Turquoise
Russian Hydrothermal Synthetic Rubies and Sapphires
The Separation of Natural from Synthetic Colorless Sapphire

Summer 1999

On the Identification of Emerald Filling Substances
Sapphire and Garnet from Kalalani, Tanzania
Russian Synthetic Ametrine

Fall 1999—Special Issue

Special Symposium Proceedings Issue, including:
Observations on GE-Processed Diamonds,
Abstracts of Featured Speakers, Panel
Sessions, War Rooms, and Poster Sessions

Winter 1999

Classifying Emerald Clarity Enhancement at the GIA
Gem Trade Laboratory

Clues to the Process Used by General Electric to Enhance
the GE POL Diamonds

Diopside Needles as Inclusions in Demantoid Garnet from Russia
Garnets from Madagascar with a Color Change of
Blue-Green to Purple

Spring 2000

Burmese Jade
Lapis Lazuli from Chile
Spectroscopic Evidence of GE POL Diamonds
Chromium-Bearing Taaffeites

Summer 2000

Characteristics of Nuclei in Chinese Freshwater Cultured Pearls
Afghan Ruby and Sapphire
Yellow to Green HPHT-Treated Diamonds
New Lasering Technique for Diamond
New Oved Filling Material for Diamonds

Fall 2000

GE POL Diamonds: Before and After
Sapphires from Northern Madagascar
Pre-Columbian Gems from Antigua
Gem-Quality Hatiyne from Germany

Winter 2000—Special Issue

Gem Localities of the 1990s
Enhancement and Detection in the 1990s
Synthetics in the 1990s
Technological Developments in the 1990s
Jewelry of the 1990s

Spring 2001

Ammolite from Southern Alberta, Canada
Discovery and Mining of the Argyle Diamond Deposit, Australia
Hydrothermal Synthetic Red Beryl

Summer 2001

The Current Status of Chinese Freshwater Cultured Pearls
Characteristics of Natural-Color and Heat-Treated
“Golden” South Sea Cultured Pearls
A New Method for Imitating Asterism

Fall 2001

Modeling the Appearance of the Round Brilliant
Cut Diamond: Fire
Pyrope from the Dora Maira Massif, Italy
Jeremejevitte: A Gemological Update

Winter 2001

An Update on “Paraíba” Tourmaline from Brazil
Spessartine Garnet from San Diego County, California
Pink to Pinkish Orange Malaya Garnets from
Bekily, Madagascar
“Voices of the Earth”: Transcending the Traditional in
Lapidary Arts

Spring 2002—Special Issue

The Ultimate Gemologist: Richard T. Liddicoat
Portable Instruments and Tips on Practical Gemology in the Field
Liddicoatite Tourmaline from Madagascar
Star of the South: A Historic 128 ct Diamond

Summer 2002

Characterization and Grading of Natural-Color Pink Diamonds
New Chromium- and Vanadium-Bearing Garnets from
Tranoroa, Madagascar
Update on the Identification of Treated “Golden” South
Sea Cultured Pearls

Fall 2002

Diamonds in Canada
“Diffusion Ruby” Proves to Be Synthetic Ruby Overgrowth
on Natural Corundum

Winter 2002

Chart of Commercially Available Gem Treatments
Gemesis Laboratory-Created Diamonds
Legal Protection for Proprietary Diamond Cuts
Rhodizite-Londonite from the Antsongombato Pegmatite,
Central Madagascar

Spring 2003

Photomicrography for Gemologists
Poudretteite: A Rare Gem from Mogok
Grandidierite from Sri Lanka

Summer 2003

Beryllium Diffusion of Ruby and Sapphire
Seven Rare Gem Diamonds

Fall 2003

G. Robert Crowningshield: A Legendary Gemologist
Cause of Color in Black Diamonds from Siberia
Obtaining U.S. Copyright Registration for the Elara Diamond

Winter 2003

Gem-Quality CVD Synthetic Diamonds
Pezzottaite from Madagascar: A New Gem
Red Beryl from Utah: Review and Update

Spring 2004

Identification of CVD-Grown Synthetic Diamonds
Cultured Pearls from Gulf of California, Mexico
X-Ray Fingerprinting Routine for Cut Diamonds

Summer 2004

Gem Treatment Disclosure and U.S. Law
Lab-Grown Colored Diamonds from Chatham
The 3543 cm⁻¹ Band in Amethyst Identification

Fall 2004

Grading Cut Quality of Round Brilliant Diamonds
Amethyst from Four Peaks, Arizona

Winter 2004

Creation of a Suite of Peridot Jewelry: From the Himalayas
to Fifth Avenue
An Updated Chart on HPHT-Grown Synthetic Diamonds
A New Method for Detecting Beryllium Diffusion—
Treated Sapphires (LIBS)

Spring 2005

Treated-Color Pink-to-Red Diamonds from Lucent Diamonds Inc.
A Gemological Study of a Collection of Chameleon Diamonds
Coated Pink Diamond: A Cautionary Tale

Summer 2005

Characterization and Grading of Natural-Color Yellow Diamonds
Emeralds from the Kafubu Area, Zambia
Mt. Mica: A Renaissance in Maine's Gem
Tourmaline Production

Fall 2005

A Review of the Political and Economic Forces Shaping
Today's Diamond Industry
Experimental CVD Synthetic Diamonds from LIMHP-
CNRS, France
Inclusions in Transparent Gem Rhodonite from
Broken Hill, New South Wales, Australia

Winter 2005

A Gemological Pioneer: Dr. Edward J. Gübelin
Characterization of the New Malossi Hydrothermal
Synthetic Emerald

70 PLUS Years of GEMS & GEMOLOGY

The Quarterly Journal
That Lasts A Lifetime



Fall 2003



Winter 2003



Fall 2005



Winter 2005



Spring 2003



Summer 2003



Spring 2005



Summer 2005



Fall 2002



Winter 2002



Fall 2004



Winter 2004



Spring 2002/Special Issue



Summer 2002



Spring 2004



Summer 2004

Order Your
**BACK
ISSUES**
Today!

E-Mail: gandg@gia.edu or visit www.gia.edu

Call Toll Free 800-421-7250 ext. 7142

or 760-603-4000 ext. 7142

Fax: 760-603-4595 or Write: G&G Subscriptions, P.O. Box 9022,

Carlsbad, CA 92018-9022 USA

	U.S.	Canada	International
Single Issues	\$ 12 ea.	\$ 15 ea.	\$ 18 ea.
Complete Volumes*			
1991–2005	\$ 40 ea.	\$ 48 ea.	\$ 60 ea.
Three-year set	\$ 115 ea.	\$ 135 ea.	\$ 170 ea.
Five-year set	\$ 190 ea.	\$ 220 ea.	\$ 280 ea.

*10% discount for GIA Alumni and active GIA students.

Some issues from 1981–1998 are also available. Please call or visit our website for details on these and the 2006 issues as they are published.

Limited Quantities Available.

EDITORS

Thomas M. Moses and
Shane F. McClure
GIA Laboratory

CONTRIBUTING EDITORS

G. Robert Crowningshield
GIA Laboratory, East Coast
Cheryl Y. Wentzell
GIA Laboratory, West Coast

Unusual Multicolored ASSEMBLED STONE

Although in some cases (such as backed opal) an assembled stone is created to increase the durability of a gem material, the more common purpose of manufacturing assembled stones is to deceive. Green synthetic spinel and synthetic quartz triplets have long imitated emeralds. Likewise, doublets consisting of natural green sapphire crowns and synthetic sapphire or synthetic ruby pavilions have fooled many buyers, as the natural inclusions in the crown mask the synthetic inclusions in the pavilion.

Rarely, however, do we see assembled stones created for other, more artistic purposes. It was therefore very surprising to receive for identification the nearly 6 mm transparent multicol-

ored square tablet in figure 1. This specimen was composed of six thin sections, each of a different color—red, orange, yellow, green, light blue, and light purple—joined with colorless cement. The client told us that he had purchased this “rainbow stone” with the intent to market it for use in commitment ceremonies for members of the Rainbow Coalition, a prominent civil rights organization.

The client wanted to verify the identification of each of the six sections. Due to the nature of the assemblage, the individual refractive indices were easy to obtain. The light purple, green, yellow, and orange sections had R.I.’s of 1.54. The red section had an R.I. of 1.76, and the light blue section had an R.I. of 1.72. A combination of standard and advanced gemological testing identified the red section as



Figure 1. This unusual specimen was assembled from slices of synthetic ruby, synthetic quartz, and synthetic spinel.

synthetic ruby, the light blue section as synthetic spinel, and the remaining four sections as synthetic quartz.

Wendi M. Mayerson

Figure 2. Fingerprint-like inclusions such as these have been reported in several colorless to near-colorless diamonds known to have been HPHT treated (from figure 10 in T. M. Moses et al., Fall 1999 *Gems & Gemology*, pp. 14–22). From left to right, magnified 32×, 18×, and 13×.



DIAMOND

With “Fingerprint” Inclusions

Fingerprint-like inclusions are common features in many colored stones, such as ruby and sapphire, but they are extremely rare in diamonds. In corundum, these “fingerprint” patterns are formed by fluid-assisted partial healing of pre-existing fractures. However, in the case of diamond, much higher pressures and temperatures are necessary to promote partial healing of fractures and, at these conditions, fluids are usually not present. A few instances of fingerprint-like patterns produced by groups of tiny inclusions in natural-color blue and colorless diamonds have been reported, but the interconnected channel-like structure that is common to sapphire “fingerprints” was not observed in these stones (see Lab Notes: Spring 1968, pp. 278–279; Spring 1993, pp. 47–48).

In recent years, fingerprint-like inclusions seen in colorless to near-colorless diamonds are most often associated with high pressure, high temperature (HPHT) treatment (figure 2; see also T. M. Moses et al., “Observations on GE-processed diamonds: A photographic record,” Fall 1999 *Gems & Gemology*, pp. 14–22). Similar to the HPHT-treated stones described in Moses et al., a small “fingerprint” extending from a graphitized inclusion was recently seen in an F-color, 4.79 ct, type IIa heart-shaped brilliant that was found to have been HPHT treated (figure 3).

Over the past few months, the West Coast laboratory has had the opportunity to examine three natural-color diamonds with a range of fingerprint-like inclusions. A pattern con-



Figure 3. This fingerprint-like inclusion extends from a graphitized crystal in a colorless diamond that was recently proved to have been HPHT treated. Magnified 45×.

sisting of several groups of tiny crystals, very similar to those described in the 1968 and 1993 Lab Notes referenced above, was observed in a Light blue, 0.64 ct, type IIb marquise brilliant (figure 4). However, the most intriguing discoveries were two colorless type IIa diamonds (a 2.28 ct D-color round brilliant and a 1.00 ct F-color pear shape) that contained inclusions with an appearance remarkably similar to the “fingerprints” seen in rubies and sapphires (figure 5). The diamonds were tested very carefully and determined to be of natural color. The channel-like patterns (not composed of tiny crystals) very strongly suggested that these were partially



Figure 4. A fingerprint-like inclusion seen recently in this 0.64 ct natural-color Light blue diamond actually consists of groups of many tiny crystals. Magnified 45×.

healed fractures in natural, untreated diamonds.

The geologic environment in which these two diamonds may have been heated to the temperatures necessary to cause partial healing of fractures remains a mystery. The heating must have occurred very deep in the earth (i.e., at high pressures), in that the clarity of these relatively large gem-quality diamonds did not show any evidence of the intense graphitization that occurs in diamonds heated at lower pressures. These samples also serve as a caution to gemologists that fingerprint-like features in colorless or near-colorless diamonds do not always mean the stones have been HPHT treated.

Christopher M. Breeding

Figure 5. These fingerprint-like inclusions seen in two natural-color type IIa colorless diamonds show a channel structure that is remarkably similar to the “fingerprints” commonly found in ruby and sapphire. Magnified 45× (left), 30× (right).



Editor's note: The initials at the end of each item identify the editor(s) or contributing editor(s) who provided that item. Full names are given for other GIA Laboratory contributors.

GEMS & GEMOLOGY, Vol. 42, No. 1, pp. 54–61
© 2006 Gemological Institute of America

Pink Diamond with Etch Channels at the Intersections of Glide Planes

Pink graining and pink glide planes are the main causes of a pink-to-red body-color in natural diamond. In contrast to pink graining, which is usually rather irregular in morphology, the glide planes typically occur as a set of well-defined, parallel, and highly color-concentrated planes that extend through the entire stone or a large part of it. In our experience, only a few percent of pink diamonds are colored by glide planes, and pink stones of this type usually have only one set. However, the East Coast laboratory recently examined a pink diamond that had *two* sets of glide planes (figure 6), as well as etch channels that occurred at the intersections of the planes. This feature is not only rare among pink diamonds, but it also supplied an opportunity to examine the mechanism by which etch channels form in diamond.

The 0.77 ct round brilliant cut ($5.87 \times 5.76 \times 3.61$ mm) was color graded Light pink. Two large fractures were present at the girdle. The diamond displayed a weak blue fluorescence to long-wave ultraviolet (UV) radiation and was inert to short-wave UV, with no phosphorescence. Consistent with other diamonds with sim-

Figure 6. In this 0.77 ct Light pink diamond, the pink color is clearly concentrated in two sets of glide planes, which are nearly perpendicular to each other. Magnified 38 \times .

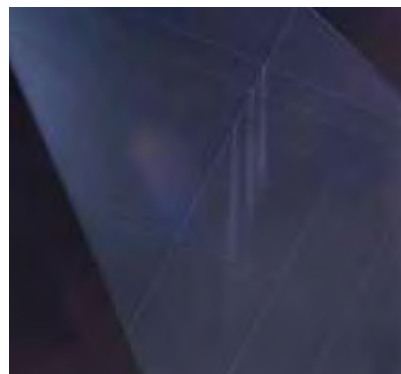


ilar pink glide planes, it contained a high concentration of nitrogen, mostly in the A-form aggregation, and a relatively weak platelet peak around 1365 cm^{-1} in the infrared absorption spectrum. As expected, the UV-visible absorption spectrum displayed moderately strong and sharp absorptions at 316, 330, and 415 nm (N3), and a broad band centered at ~ 550 nm.

The distance between individual planes varied from about 0.2 to 1.0 mm. The two sets of planes were nearly perpendicular to each other (again, see figure 6), and etch channels were observed where the two sets intersected. All the channels were likewise straight and parallel. Depending on the development of the glide planes, the dissolution channels varied from less than 1 mm to over 2 mm deep. The shape and diameter of the channels were too small to be determined with a regular gemological microscope, but the diameter appeared to be less than $50 \mu\text{m}$. Nevertheless, the channels were readily seen with proper lighting (figure 7).

The physics of the crystalline defect that generates the ~ 550 nm broad absorption band is not well understood. However, it is widely believed to be related to plastic defor-

Figure 7. As can be seen here, etch channels developed at the intersections of the two sets of glide planes in the 0.77 ct Light pink diamond. With reflected light, the planes appear as distinct lines on the polished faces. Magnified 98 \times .



mation of the diamond lattice (see, e.g., A. T. Collins, "The colour of diamond and how it may be changed," *Journal of Gemmology*, Vol. 27, 2000, pp. 341–359). A glide plane is a distortion of the crystal lattice, with the carbon atoms shifted away from their normal, stable positions. This distortion would be significantly intensified where the two sets of glide planes intersect, since it is occurring in two separate directions. The carbon atoms in these strongly distorted regions would not have a normal diamond structure, and thus they would not be chemically as stable. As a result, dissolution or etching could selectively occur in these regions.

Etch channels are a common sight in natural diamonds, though their formation mechanisms are not fully understood (see, e.g., T. Lu et al., "Observation of etch channels in several natural diamonds," *Diamond and Related Materials*, Vol. 10, 2001, pp. 68–75). This unusual pink stone revealed that intersections of plastic deformation planes are chemically less stable, so they are one of the localities where etching can selectively occur.

Wuyi Wang, Vinny Cracco,
and TMM

Two Diamonds from the Same Octahedron

Typically a diamond cutter will fashion at least two stones from a single octahedral crystal; however, these stones rarely remain together for long. One is commonly larger than the other, so the diamonds tend to get distributed in different lots. Certain spectroscopic methods can sometimes be used to detect similarities in once-contiguous stones, but natural zoning of impurities and lattice defects in colored diamond crystals often makes it difficult to match spectroscopic data from different parts of the crystal. Other techniques such as X-ray topography may have more potential (see I. Sunagawa et al., "Fingerprinting of two diamonds cut from the same rough," *Winter 1998 Gems &*

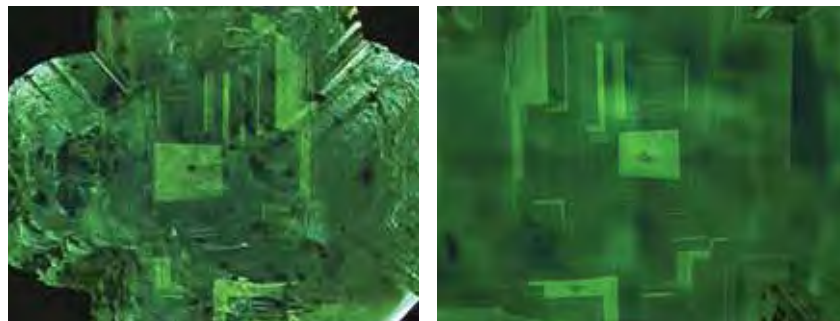


Figure 8. High-energy DiamondView UV fluorescence patterns from these two diamonds (left, 0.38 ct; right, 2.39 ct) are nearly perfect mirror images of each other, strongly suggesting that they were at one time part of the same crystal.

Gemology, pp. 270–280; R. Diehl and N. Herres, “X-ray fingerprinting routine for cut diamonds,” Spring 2004 *Gems & Gemology*, pp. 40–57).

The West Coast laboratory recently examined two partially polished colored diamonds that appeared to have been cut from the same piece of rough. The stones had been submitted at the same time, but for separate origin-of-color reports. One (0.38 ct) consisted of the rough top of a brownish yellow octahedron with only the cut base polished. The other was much larger (2.39 ct) and had been blocked into a yellow cut-cornered rectangular modified brilliant. Unpolished surfaces on both diamonds showed abundant brown radiation stains. The diamonds exhibited similar strain patterns with cross-polarized light, and both showed greenish yellow fluorescence to long- and short-wave UV lamps. Infrared spectroscopy revealed that both stones were type Ia with abundant nitrogen impurities; the spectra were almost identical. These similarities suggested that at one time these two diamonds might have been part of the same crystal.

In an effort to confirm this speculation, the diamonds were examined with a Diamond Trading Company (DTC) DiamondView, which uses a high-energy UV source to reveal differences in the fluorescence of diamond growth zonations. Distinctive fluorescence patterns were present in both

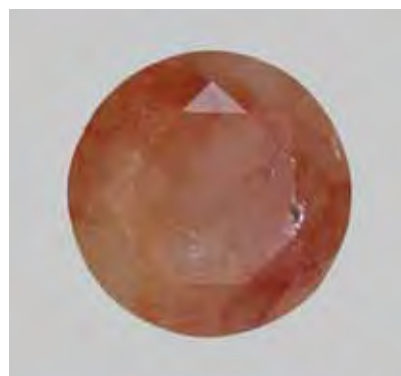
stones (figure 8). Furthermore, the high-energy fluorescence pattern from the base of the smaller diamond was almost a mirror image of that seen in the larger, blocked stone. The correlation of their DiamondView images, gemological observations, and spectroscopic data indicates that these two diamonds were indeed cut from the same octahedron.

Christopher M. Breeding

Unusual Translucent Brown-Orange Diamond

Micro-inclusions in diamond, such as water and carbonates, are useful in

Figure 9. This translucent 1.58 ct brown-orange diamond (7.20 × 7.09 × 4.76 mm) appears to owe its unusual hue to large amounts of carbonate micro-inclusions.



studying the formation and evolution of the fluids/melts that are essential for diamond formation in the upper mantle. These inclusions usually occur in the fibrous coatings on some octahedral diamond crystals. Although such coated diamonds from the DRC/Zaire and Botswana have been described previously (O. Navon et al., “Mantle-derived fluids in diamond micro-inclusions,” *Nature*, Vol. 335, 1988, pp. 784–789), and we have recently reported on a colorless diamond and a Fancy Dark brown-greenish yellow diamond with carbonate micro-inclusions (Lab Notes: Winter 2004, pp. 325–326; Summer 2005, pp. 165–167), it is still extremely rare to see a faceted gem diamond with these inclusions throughout the entire crystal.

The 1.58 ct translucent brown-orange round brilliant in figure 9 was submitted to the East Coast laboratory for identification and origin-of-color determination. Upon examination, we saw fractures that appeared to have orange color concentrations. With the microscope, we also observed extensive surface graining (figure 10), as well as micro-inclusions throughout the stone.

Since this diamond was translucent, we used diffuse reflectance infrared spectroscopy to study the inclusions. As seen in figure 11, absorption bands at

Figure 10. With reflected light (here, on the table facet), surface graining was observed over most of the diamond in figure 9. Magnified 40×.



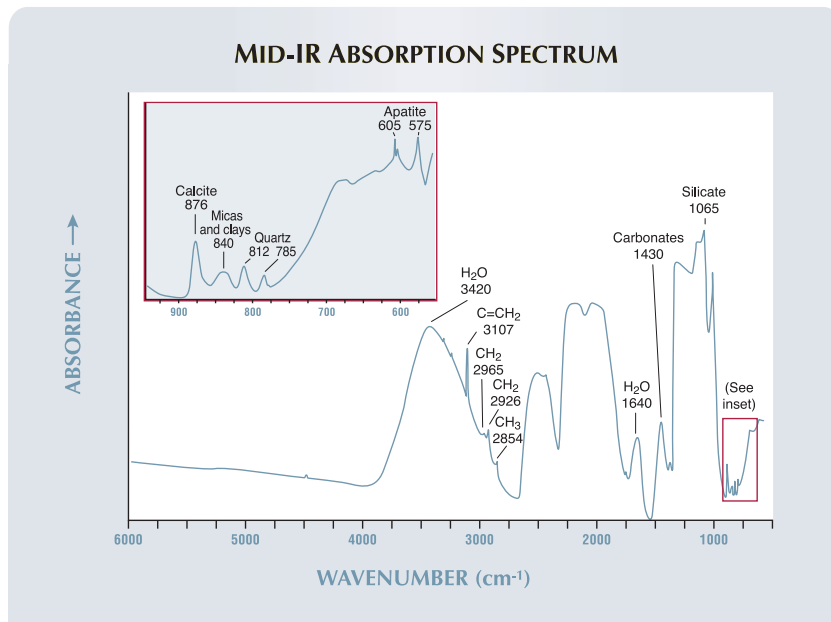


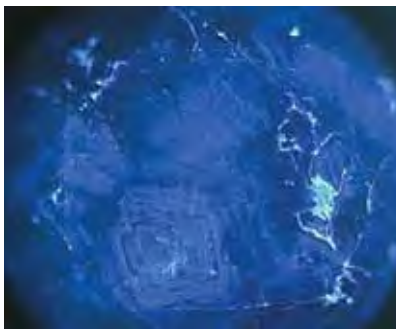
Figure 11. Diffuse reflectance IR absorption spectroscopy showed that this diamond is type Ia with carbonate and water micro-inclusions. By subtracting the spectrum of a pure type Ia diamond, the absorption bands of other micro-inclusions such as apatite and micas can be seen in detail (inset).

3420 and 1640 cm^{-1} suggested the presence of water molecules. A silicate absorption band was also seen at 1065 cm^{-1} . The two bands at 605 and 575 cm^{-1} are due to apatite (M. Schrauder and O. Navon, "Hydrous and carbonatic mantle fluids in fibrous diamonds from Jwaneng, Botswana," *Geochimica et Cosmochimica Acta*, Vol. 58, No. 2, 1994, pp. 761–771). The bands at 812 and 785 cm^{-1} are due to quartz. They are shifted from their normal positions at 798 and 779 cm^{-1} as a result of the high internal pressure within the micro-inclusions. The band at 840 cm^{-1} is characteristic of micas and clay minerals. The bands for carbonates (CO_3^{2-}) were also observed at 1430 and 876 cm^{-1} ; these are the main carbonate band and the characteristic band for calcite, respectively (again, see Navon et al., 1988).

The bands at 2965 and 2926 cm^{-1} are caused by the CH_2 group, the one at 2854 cm^{-1} by the CH_3 group, and the sharp peak at 3107 cm^{-1} is assigned to the $\text{C}=\text{CH}_2$ group (J. Lindblom et al.,

"Luminescence study of defects in synthetic as-grown and HPHT diamonds compared to natural diamonds," *American Mineralogist*, Vol.

Figure 12. High-energy Diamond-View fluorescence imaging shows that the diamond in figure 9 grew from a cube to an octahedron with multiple growth centers. This was further confirmed by a distinctive cubic growth center seen when the diamond was viewed through the pavilion.



90, No. 2–3, 2005, pp. 428–440). These peaks are observed in natural diamonds and may also be attributed to artifacts from contamination within the fractures of this diamond, so their presence is probably unrelated to inclusions.

Our examination of this unusual diamond allows us to infer some geologic conditions of its formation. The shift in the peak positions of quartz in the IR spectrum corresponds to a pressure of 1.5 GPa at room temperature (see Schrauder and Navon, 1994). Extrapolating to a typical mantle temperature of 1,000°C would correspond to a pressure of 4.5 GPa, which falls within the diamond stability field. Therefore, the micro-inclusions in this diamond appear to have crystallized from fluids that were trapped during its growth in the upper mantle. As the mantle-derived fluids in the diamond cooled during its travel to the surface, they developed into a secondary-phase assemblage that formed the micro-inclusions (i.e., water, carbonates, silicates, apatites, micas, and clays). This assemblage, with an absence of molecular CO_2 , suggests that the diamond formed under conditions that were fluid-rich and gas-poor. The inclusions correspond to both carbonatic fluids (carbonates) and hydrous fluids (water, SiO_2), which may coexist at upper-mantle temperatures and pressures.

Because this diamond was polished, there was no obvious evidence of its crystal habit. However, when it was examined with the DTC DiamondView, the fluorescence image showed that the internal morphology evolved from cube to octahedron with multiple growth centers (figure 12). It also indicated that the brown-orange color followed the growth zoning. This could be important evidence that the color was caused by micro-inclusions that were captured by different growth zones rather than along the fractures as it initially appeared. Another DiamondView image through the pavilion showed a distinctive cubic growth center, confirming that this diamond grew from multiple growth centers.



Figure 13. This emerald-in-matrix specimen was known to be assembled prior to being submitted to the laboratory, but it proved to have another, very unusual, characteristic.

This brown-orange diamond is the first we have analyzed with this variety of micro-inclusions. Advanced spectroscopic testing not only confirmed that its color was of natural origin but also provided keys to its geologic formation. An orange hue is not common in naturally colored diamonds; it is mainly due to the presence of point and/or extended defects. This diamond demonstrated that micro-inclusions may also contribute to an orange coloration.

Kyaw Soe Moe and Paul Johnson

Inscriptions Inside EMERALD Crystals

Occasionally the laboratory receives mineral specimens for identification, usually for the purpose of determining whether or not they are natural or have been assembled (see, e.g., Spring 2003 Lab Notes, p. 42). The emerald-in-matrix specimen shown in figure 13 was submitted to the West Coast laboratory, but this time the owner knew in advance that it had been assembled from Colombian material.



Figure 14. The extent of the glue used to affix the emerald crystals in the matrix became very apparent when the specimen was exposed to long-wave UV radiation. Notice how visible the writing in one of the crystals is.

The purpose of the examination was to make sure the emerald crystals were natural, as well as to document something very unusual that had been done to them.

Spectroscopic testing and microscopic examination confirmed that the crystals were natural emeralds. Close observation of the specimen at the base of the crystals revealed an adhesive that had been mixed with crushed matrix to give it a more natural appearance—a practice that is very common in the construction or reconstruction of mineral specimens. The glue was easily visible when exposed to long-wave UV radiation, as it fluoresced a strong blue (figure 14).

This was not, however, the most interesting aspect of the specimen. The two largest crystals (26.75 × 25.50 × 20.50 mm and 17.00 × 20.80 × 19.90 mm) had what appeared to be some sort of internal inscription. With a loupe, it could be seen that the writing was in Arabic and was not on the surface of the crystals. With the microscope, the answer to this mystery became clear. While out of the matrix,



Figure 15. This view through the termination of one of the emerald crystals in figure 13 reveals that a hole had been drilled down the center from the bottom without breaking the surface of the termination. Magnified 10 \times .

the crystals apparently had been core drilled from the bottom, with care being taken not to cut through the termination or any of the prism faces. What appeared to be a rolled up piece of paper or some other writing material was then inserted into each of the crystals, conforming to the cylindrical shape of the drilled holes. The holes were then filled with a resin or similar compound (figure 15), and the specimen was reassembled. We surmise that once the paper was saturated by the resin, it became transparent, leaving only the wording, in black, visible from the outside of the crystal (figure 16). Although this is not the only possible scenario, it seems the most likely.

One of our staff members at the time, Maha Calderon, was able to read most of the two inscriptions, the first of which she translated as, "To the people, guidance, and wisdom to the believers." Only part of the second inscription was legible because of inclusions in the emerald.

SFM



Figure 16. It appears that some sort of material with Arabic writing was inserted into the holes made in the two largest emerald crystals. Magnified 10 \times .

Color-Coated Star QUARTZ

Recently, the East Coast laboratory received for identification a grayish blue oval cabochon displaying asterism. The stone measured approximately 12.35 \times 10.25 \times 6.45 mm and was set in a white metal ring (figure 17). Standard gemological testing revealed a spot refractive index of 1.54 and a bull's-eye optic figure, which identified the stone as quartz.

The lab has reported on star quartz many times over the years, discussing the typical colors, cause of asterism, and sources of the material (see, e.g., Lab Notes: Winter 1981, p. 230; Spring 1985, pp. 45–46; Spring 1987, pp.

Figure 17. Although the asterism in this rock crystal quartz cabochon is natural, the color is caused by a blue coating on the back, probably to help it imitate star sapphire.



47–48). This stone contained numerous oriented needles, which caused the star, so we concluded that the asterism was natural. What was unnatural, however, was the apparent color. When the bottom of the cabochon was viewed with magnification and a combination of overhead and darkfield lighting, a slightly uneven blue coating was clearly visible. In fact, two small chips near the stone's edge revealed colorless quartz underneath (figure 18).

Coating is one of the simplest ways to change a stone's color and is frequently used on a variety of materials, including diamond, beryl, topaz, cubic zirconia, and, of course, quartz. What made this particular ring interesting was that the color of the coating on the natural star quartz cabochon created an extremely convincing imitation of a star sapphire. As noted above, this is hardly a new material. GIA reported on a nearly identical stone—a star quartz with blue backing added to imitate star sapphire—in the Summer 1938 *GeG* (p. 168), which shows that no matter how many new treatments come on the market, gemologists must still be on guard for simple ones such as this. [Editor's note: *The Summer 1938 issue is available in PDF format on the Gems & Gemology website at www.gia.edu/gemsandgemology.*]

Wendi M. Mayerson

Figure 18. A chip on the bottom of the cabochon in figure 17 reveals colorless quartz underneath the blue coating. Magnified 30 \times .



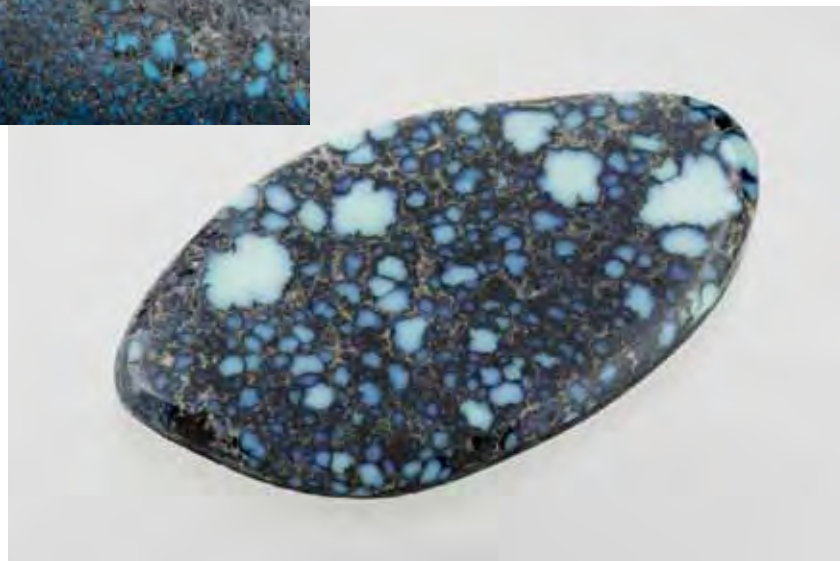


Figure 19. This 25.35 × 17.70 × 5.75 mm cabochon was one of several samples submitted to the laboratory that at first appeared to be spiderweb turquoise, but proved to be variscite. Its resemblance to true spiderweb turquoise from the Lander Blue turquoise mine in Nevada (inset) is quite striking.

VARISCITE, Resembling Turquoise

Several cabochons of a mottled green-blue material in black matrix (figure 19), represented as turquoise from Lander, Nevada, were recently submitted to the West Coast laboratory for identification. The now-inactive Lander Blue turquoise mine was noted for small pockets of nodular turquoise with black matrix (figure 19, inset) that was called “spiderweb” turquoise. The deposit has been referred to as a “hat mine” because the pockets were small enough to be covered by a hat. The deposit was discovered in 1973, and during its relatively short lifespan only 104 lbs. (47 kg) of spiderweb turquoise was mined (A. Ahmed et al., “Türkis: der

Edelstein mit der Farbe des Himmels” [Turquoise: The Jewel of the Sky], *extraLapis* No. 16, Christian Weise, Munich, 1999, pp. 34–41).

The submitted material strongly resembled this unusually textured turquoise, but the color was less saturated than we would expect from this locality. Microscopic examination revealed a structure and texture that were not typical of turquoise, but could not rule it out given the many deposits and treatments possible for this gem material. The refractive indices of the 20.16 ct piece we tested were 1.570–1.590, which are lower than the published values for turquoise. Again, however, many impreg-

nated turquoises have lower refractive indices that may fall within this range. The samples were all backed with a black material, so a meaningful specific gravity could not be obtained.

Our standard laboratory procedure is to test all turquoise for polymer impregnation using infrared spectroscopy. The IR spectrum of this material, however, did not resemble that of turquoise at all. This effectively eliminated turquoise as a possible identification, so the next step was to obtain a Raman spectrum. The results showed a very close, but not exact, match to variscite ($\text{AlPO}_4 \cdot 2\text{H}_2\text{O}$). Variscite is a mineral in the variscite group that forms a complete solid solution with strengite ($\text{Fe}_3\text{PO}_4 \cdot 2\text{H}_2\text{O}$).

The final test was X-ray diffraction (XRD) analysis. After comparing the sample to known patterns, we determined that the material was in fact variscite. Minor variations in the Raman spectrum and the XRD pattern were probably due to variations within the variscite series. This was the first time that a sample of variscite with an appearance this close to turquoise was seen in our lab. Even our most experienced gemologists would not have suspected this material to be variscite at first glance.

Eric Fritz and Kimberly Rockwell

PHOTO CREDITS

Elizabeth Schrader—1; Shane F. McClure—2 (left), 15 and 16; Shane Elen—2 (center and right); Maha Calderon—3, 5, 13, and 14; Christopher M. Breeding—4 and 8; Wuyi Wang—6 and 7; Jessica Arditi—9 and 17; Kyaw Soe Moe—10 and 12; Wendi Mayerson—18; Don Mengason—19 and 19 (inset).

For regular updates from the world of **GEMS & GEMOLOGY**, visit our website at:

www.gia.edu/gemsandgemology



EDITOR

Brendan M. Laurs (blaurs@gia.edu)

CONTRIBUTING EDITORS

Emmanuel Fritsch, *IMN, University of Nantes, France* (fritsch@cnrs-immn.fr)

Henry A. Hänni, *SSEF, Basel, Switzerland* (gemlab@ssef.ch)

Franck Notari, *GIA GemTechLab, Geneva, Switzerland* (franck.notari@gia.edu)

Kenneth V. G. Scarratt, *GIA Research, Bangkok, Thailand* (ken.scarratt@gia.edu)

Tucson 2006

Although fewer new gem finds debuted in 2006 than in previous Tucson shows, there were nevertheless a variety of items that appealed to those with an eye for the unusual. These materials originated from many parts of the world, rather than the strong emphasis on African countries seen in recent years. Nevertheless, Africa was the source of some spectacular gem discoveries over the past year, such as copper-bearing tourmalines from Mozambique (see

Winter 2005 Gem News International, pp. 360–361, and the article by A. Abduriyim et al. on copper-bearing tourmaline in this issue). There was a strong showing of this tourmaline in Tucson, including some large stones (see, e.g., figure 1). Another notable African gem seen at the shows was a 62.81 ct tsavorite from Merelani, Tanzania (figure 2). Although large tsavorites from Merelani have

Figure 1. Mozambique is the source of this 48.23 ct tourmaline, which has a bright blue color that is typical of the fine-quality copper-bearing elbaite mined from the Alto Ligonha region since mid-2005. Courtesy of Evan Caplan and Omi Gems, Los Angeles; photo © Harold & Erica Van Pelt.



Figure 2. This 62.81 ct tsavorite was cut from rough that was reportedly recovered in late 2005 from the “Karo” area, which lies just east of Block D at Merelani, Tanzania. The tsavorite was found at about 180 m depth, in an area that also produced some fine tanzanite and bright green-yellow diopside. Courtesy of New Era Gems; photo © Jeff Scovil.



been faceted previously (see, e.g., Spring 2004 Gem News International, pp. 72–73), this stone showed a particularly saturated green color. Additional Tucson items are described below, with more to be included in the Summer 2006 GNI section. *G&G* thanks our many friends who shared material with us this year.

COLORED STONES AND ORGANIC MATERIALS

Aquamarine from a new primary deposit in Sri Lanka. Except for moonstones that are mined from a weathered pegmatite in Meetiyaogoda and *in situ* chrysoberyl from Pattara, no other commercially viable primary gem deposit has been known from Sri Lanka. This changed in mid-2005, with the accidental discovery of gem-quality aquamarine at the Akkerella estate (owned by Kahawatta Plantations Ltd.), about 25 km southeast of Ratnapura. The aquamarine was found during mining of vein quartz for industrial silica, and the discovery led to a sudden gem rush, followed by clashes between police and gem miners (see J. Henricus-Prematilleke, “New aquamarine find sparks gem rush in Sri Lanka,” *Jewellery News Asia*, No. 254, 2005, pp. 56, 58). Previously, aquamarine from Sri Lanka was known from Ratnapura and Nawalapitiya, but only as water-worn pebbles.

The new aquamarine crystals range up to 10+ cm long, and vary from pale blue to a saturated dark blue resembling “Santa Maria” aquamarine from Minas Gerais, Brazil. They are embedded in quartz (figure 3), in association with mica and black tourmaline. The quartz-vein field at Akkerella measures about 2 km long. The nearby estate of Hunuwala, which is about 6 km northwest of Akkerella, shows evidence for the continuation of vein mineralization. Sri Lanka’s National Gem and Jewellery Authority recently auctioned mining claims on both estates, and they are being mined currently. The Hunuwala estate has produced large crystals of gem-quality colorless topaz, some weighing 2–10 kg. The total production of aquamarine since mining began is estimated by one of us (EGZ) to exceed 100 kg of rough, of which 20%–30% is facetable; at least



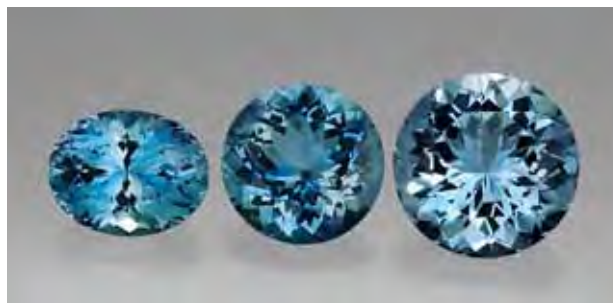
Figure 3. Aquamarine from a new primary deposit on the Akkerella estate in Sri Lanka is found embedded within quartz veins. Courtesy of E. G. Zoysa.

5,000 carats of the aquamarine have been faceted so far.

At the 2006 AGTA show in Tucson, Dudley Blauwet (Dudley Blauwet Gems, Louisville, Colorado) had a selection of faceted aquamarine from the new Sri Lankan deposit. The stones, which were reportedly unheated, showed a range of color from light blue to a saturated blue with little or no greenish overtones (figure 4). Most of the stones weighed 2–3 ct, and were cut from a parcel that he obtained in Sri Lanka in November 2005 that consisted of 29 clean pieces weighing a total of 68.88 carats.

Mr. Blauwet loaned three samples of the aquamarine (4.37, 5.28, 8.19 ct; again, see figure 4) to GIA for examination, and the following gemological properties were determined by one of us (EPQ): pleochroism—strong blue and near colorless; R.I.— $n_o = 1.584\text{--}1.587$ and $n_e = 1.577\text{--}1.580$; birefringence—0.007; S.G.—2.71; and fluorescence—inert to both long- and short-wave UV radiation. Vis-NIR spectroscopy displayed a 427 nm absorption peak typical of aquamarine. Microscopic examination revealed “finger-

Figure 4. These aquamarines (4.37–8.19 ct) are reportedly unheated and demonstrate the range of color seen in fine material from the new Sri Lankan deposit. Courtesy of Dudley Blauwet Gems; photo © Robert Weldon and GIA.



Editor's note: The initials at the end of each item identify the editor or contributing editor who provided it. Full names and affiliations are given for other contributors. Dr. Mary L. Johnson of the GIA Laboratory in Carlsbad is thanked for her internal review of the Gem News International section.

Interested contributors should send information and illustrations to Brendan Laurs at blaur@gia.edu (e-mail), 760-603-4595 (fax), or GIA, The Robert Mouawad Campus, 5345 Armada Drive, Carlsbad, CA 92008. Original photos will be returned after consideration or publication.

GEMS & GEMOLOGY, Vol. 42, No. 1, pp. 62–80
© 2006 Gemological Institute of America



Figure 5. This attractive blue, 14.71 ct cabochon (sample no. FN-7692), reportedly from Mogok, appears to be a combination of massive haiüyne and sodalite. Note the strong zoned orange fluorescence to long-wave UV (right); the chalky blue spots correspond to the white areas seen in normal lighting. Photos by C. Grobon (left) and T. Hainschwang (right).

prints," doubly refractive crystals with reflective halos, minute crystals, stringers of particles, needles, and near-parallel reflective dendrites surrounded by clouds.

The recent discovery of *in situ* aquamarine in Sri Lanka has generated a renewed interest in the geology of gem deposits in that country. More discoveries are anticipated with further exploration in the region.

BML

E. Gamini Zoysa (mincraft@slt.lk)
Mount Lavinia, Sri Lanka

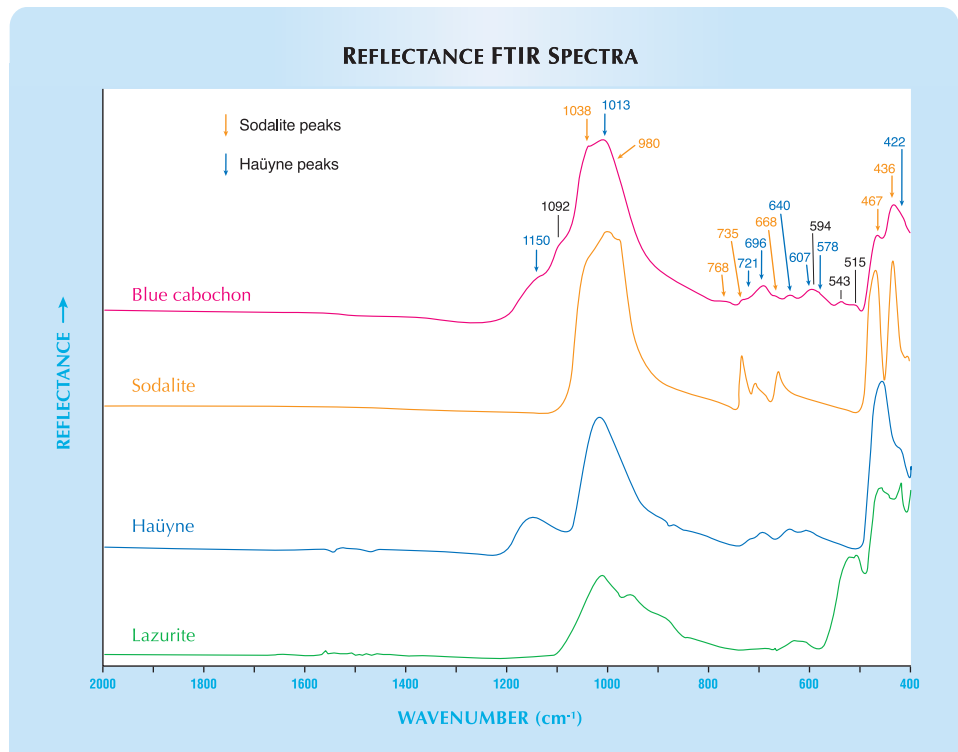
Elizabeth P. Quinn
GIA GemTechLab, Geneva, Switzerland

Massive haiüyne-sodalite from Myanmar. These contributors recently examined a 14.71 ct translucent blue cabochon (figure 5, left) acquired at the 2006 Tucson gem

shows, where it was represented as a mixture of haiüyne and sodalite. The seller, Mark Smith of Thai Lanka Trading Ltd., Bangkok, indicated that he had initially purchased such material several years ago. This sample was reportedly found in the Dattaw mining area, a few kilometers northeast of the center of Mogok. According to Mr. Smith, the material occurs as massive blue veins within a host rock of white calcite marble.

The color was a relatively homogeneous intense blue, with some thin white veins and some irregular white patches. The hydrostatic S.G. was 2.51, and the spot R.I. was around 1.50. The material showed strongly zoned orange fluorescence, with some chalky blue spots to long-wave UV radiation (figure 5, right) and a very weak red glow to short-wave UV. Microscopic observation revealed tiny inclusions with the appearance of pyrite. For the most part, these properties are consistent with haiüyne.

Figure 6. The specular reflectance FTIR spectrum of the 14.71 ct blue cabochon mainly indicated the presence of haiüyne, with some sodalite and a third unidentified mineral phase.



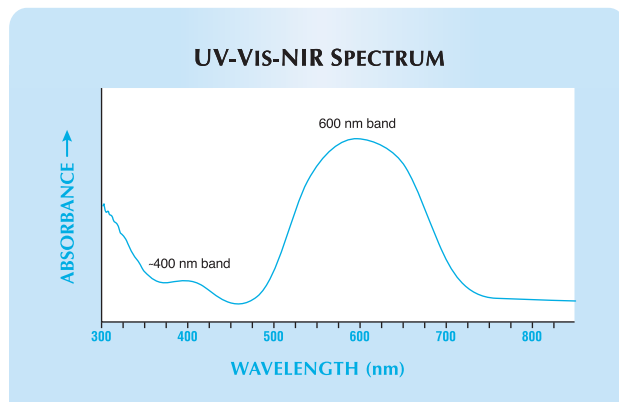


Figure 7. The UV-Vis-NIR spectrum of the *häüyne-sodalite cabochon* is characterized by a very strong and broad band centered at 600 nm and a weaker band at ~400 nm. This is quite similar to published spectra for *häüyne*. The spectrum was acquired by reflectance and converted to an absorption spectrum.

Häüyne is a cubic silicate with the general formula $(\text{Na}_6\text{Ca}_2\text{Al}_6\text{Si}_6\text{O}_{24})(\text{SO}_4)_2$ that is related to *sodalite*—which has the general formula $\text{Na}_8\text{Al}_6\text{Si}_6\text{O}_{24}\text{Cl}_2$ —along with the species *lazurite* and *nosean*. To identify the mineral(s) present in this cabochon, we recorded a specular reflectance FTIR spectrum. The spectrum showed features for both *häüyne* and *sodalite*, plus some additional unidentified peaks, although *häüyne* appeared to be the dominant mineral (figure 6). Unfortunately, our reflectance database lacks *nosean*, so we could not determine whether it was responsible for the additional peaks.

The UV-Vis-NIR spectrum revealed absorption bands very similar to those described by L. Kiefert and H. A. Hänni (“Gem-quality *häüyne* from the Eifel District, Germany,” Fall 2000 *Gems & Gemology*, pp. 246–253), with the main feature being a very broad band centered at 600 nm and a second weaker band at ~400 nm (figure 7).

EDXRF chemical analysis detected major amounts of Si, Al, K, and Sr, and minor Ca, Na, Cl, and S. These are all part of the chemical formula of *häüyne* (and also *sodalite*), with the exception of K and Sr. Minor amounts of K are known to occur in *häüyne*. The origin of the relatively high Sr content may be due to the material’s formation within a *calcite* host rock, which often contains Sr impurities.

Our analyses indicate that this attractive blue material is mainly massive *häüyne* mixed with other related mineral phases, one of which is most likely *sodalite*. The materials appear to be intimately mixed with one another and no particular distribution could be observed, even according to color. Although these minerals are closely related, these contributors are not aware of substantial solid solution between them, and therefore assume that the individual mineral phases are present. The white spots were deter-

mined to be the same material as the blue host, but this is not surprising since *häüyne* and *sodalite* are both known in colorless (or white) forms. In some of these white spots, accumulations of inclusions could be seen. These are most likely *calcite*, which explains the chalky blue luminescence of these spots to long-wave UV radiation.

Candice Grobon (candice.grobon@gia.edu)
and Thomas Hainschwang
GIA GemTechLab, Geneva, Switzerland

Gem-quality massive pink muscovite from Brazil.

Minerals of the mica group are only rarely used as gem materials. *Lepidolite*, a lithium-bearing mica, is known mainly as lavender fine-grained aggregates containing opaque pink *tourmaline* crystals from the Stewart mine in Pala, California. These aggregates have been fashioned as cabochons and carvings, as has similar material from a *lepidolite* pegmatite at Rožná, Czech Republic. A cabochon of reddish purple mica (*lepidolite* or *muscovite*) from northern New Mexico was described in the Fall 1993 *Gem News* (pp. 210–211). *Lepidolite* also forms platy purple crystals from several pegmatites in Minas Gerais, Brazil, and elsewhere, but these are not cuttable due to the micaceous cleavage of the single-crystal material. While in Brazil in 2004, one of these contributors (JH) encountered an unusual mica (figure 8) that was sold as *rose quartz* and reportedly came from an undisclosed pegmatite in Minas Gerais State. In light of its attractive color and translucency, several stones were faceted (see, e.g., figure 9) and offered by this contributor at the Arizona Mineral & Fossil Show (Clarion Hotel) in Tucson.

Gemological properties were measured on five cut stones weighing 0.76–23.19 ct. The R.I. was very difficult to read because of the poor polish (as expected for a mica

Figure 8. This aggregate of fine-grained *muscovite* (about 7 cm wide) was represented as *rose quartz* in Minas Gerais, Brazil. Photo by J. Hyršl.





Figure 9. A few faceted stones (here, 23.19 ct) have been produced from the massive Brazilian muscovite. Photo by J. Hyršl.

aggregate due to the low hardness and perfect cleavage); only a weak shadow in the 1.53–1.58 region was visible. Specific gravity (measured hydrostatically) was 2.83–2.85, and the Mohs hardness was about 2.5 (determined by scratch testing with halite and calcite). The

TABLE 1. Chemical composition of a pink muscovite from Brazil.^a

Oxide (wt.%)		Ions per 12 anions	
SiO ₂	45.32	Si ⁴⁺	3.055
TiO ₂	bdl	Ti ⁴⁺	bdl
Al ₂ O ₃	36.93	Al ³⁺	2.934
FeO	bdl	Fe ²⁺	bdl
MnO	0.12	Mn ²⁺	0.007
ZnO	bdl	Zn ²⁺	bdl
MgO	bdl	Mg ²⁺	bdl
K ₂ O	10.41	K ⁺	0.895
Na ₂ O	0.40	Na ⁺	0.052
Rb ₂ O	0.37	Rb ⁺	0.016
Cs ₂ O	0.13	Cs ⁺	0.004
F	0.33	F ⁻	0.070
Cl	bdl	Cl ⁻	bdl
H ₂ O	4.29	H ⁺	1.930
-O=F	-0.14	O ²⁻	11.930
-O=Cl	0.00		
Total	98.16		

^a Average values for eight analyses of one sample, obtained with a Cameca SX 100 electron microprobe at Masaryk University. Abbreviation: bdl=below detection limit. Detection limits (wt.% oxide) at 2 σ : Ti=0.02, Fe = 0.05, Zn=0.06, Mg=0.02, and Cl=0.02. Also analyzed but not detected in any of the analyses were Cr, Ni, Ca, and Ba. The ions per formula unit and H₂O were calculated on the basis of 12 anions and F+OH = 2.

samples were inert to UV radiation and showed no features in the desk-model spectroscope. In the polariscope, they stayed bright during rotation, as would be expected for an anisotropic aggregate. These properties are consistent with both muscovite and lepidolite, except for the rather low R.I. values (which are probably due to the low quality of the readings).

A powder X-ray diffraction analysis also suggested muscovite or lepidolite, and muscovite was confirmed by electron-microprobe analysis (see table 1). The chemical composition was very close to the ideal formula of KAl₂AlSi₃O₁₀(OH)₂, with traces of Mn, Na, Rb, Cs, and F. Observation with a scanning electron microscope in backscattered electron (BSE) mode revealed that the muscovite formed very fine-grained monomineralic aggregates of individual flakes about 100 μ m in size, with random orientation; no other minerals were observed in BSE mode. The very small grain size and compact nature of the aggregate accounts for its distinctive translucent appearance.

The presence of significant F, Rb, and Cs suggests that this muscovite formed as a late-stage mineral in the pegmatite, possibly by replacement of another mineral or from hydrothermal fluids within a mineralized cavity (see, e.g., M. Novák and P. Černý, "Abundance and compositional trends of Rb and Cs in micas from lepidolite- and elbaite-subtype pegmatites in the Moldanubicum, Czech Republic," *Acta Universitatis Carolinae Geologica*, Vol. 42, 1998, pp. 86–90). The slightly elevated Mn contents, a high Mn/Fe ratio, and the general absence of Ti and Fe are likely responsible for its deep "rose" pink color.

Jaroslav Hyršl (hyrsl@kuryr.cz)
Prague, Czech Republic

Milan Novák and Radek Škoda
Institute of Geological Sciences, Masaryk University
Brno, Czech Republic

Pyrope-spessartine from Tanzania. At the 2006 Pueblo Gem & Mineral show in Tucson, Steve Ulatowski (New Era Gems, Grass Valley, California) showed one of these contributors (BML) some new garnets from Tanzania. Marketed as "Imperial" garnets, they have been produced since late 2005 from Lindi Province, near the Mowemkulu River in the Namtamba village area of southeastern Madagascar. Similar stones have been mined from southern Madagascar for several years (see K. Schmetzer et al., "Pink to pinkish orange Malaya garnets from Bekily, Madagascar," *Winter 2001 Gems & Gemology*, pp. 296–308).

Mr. Ulatowski indicated that there is a fair production of small rough (weighing <0.1 g), averaging about 40 kg/month. Stones over 0.5 g are rare, with clean rough limited to only about 500 g/month. He reported that faceted material over 1 ct is quite rare, and the largest stone with good clarity he has seen weighed about 3 ct.



Figure 10. This 2.29 ct pyrope-spessartine is from a new deposit in the Lindi Province of southeastern Tanzania. Courtesy of New Era Gems; photo by Axel Respinger.

Mr. Ulatowski loaned a rough and cut sample of the garnet to GIA for examination, and the following gemological properties were determined by one of us (EPQ) on the cut stone (2.29 ct; figure 10): color—pink in both incandescent and daylight, but brownish pinkish orange in fluorescent (5,500 K) light; R.I.—1.756; S.G.—3.85; and fluorescence—inert to both long- and short-wave UV radiation. Microscopic examination revealed iridescent needles (possibly rutile), subhedral transparent birefringent crystals, and dust-like particles. The physical properties identified the garnet as pyrope-spessartine. This is consistent with an absorption spectrum taken with a handheld spectroscope, and also with EDXRF chemical analysis.

The properties of this garnet are quite similar to the

Madagascar garnets described by Schmetzer et al. (2001), and it is quite possible that the deposits share similar geologic conditions in light of their close proximity before Madagascar separated from Tanzania.

BML

Elizabeth P. Quinn

Transparent faceted sillimanite from India. At the AGTA show, Anil B. Dholakia Inc. (Franklin, North Carolina) had a large quantity of transparent sillimanite, reportedly from a new locality in the Vishakhapatnam region of Andhra Pradesh, India. Several colors were available (figure 11), but most notable were the large greenish yellow to yellow-green stones, which Mr. Dholakia first brought to GIA's attention in November 2005. He indicated that he had faceted about 20,000 carats of the sillimanite, all in checkerboard cuts, with most pieces weighing 1.5–10 ct (70% in calibrated sizes); a few larger stones ranged up to 25 ct (rarely, 50 ct). In addition to greenish yellow, the hues included near colorless, grayish green, green-brown, brownish orange-yellow, and violetish gray. Mr. Dholakia characterized the production as sporadic.

Similar material was obtained in mid-2004 during a buying trip to Jaipur, India, by Scott Davies of American-Thai Trading, Bangkok. In addition to the colors mentioned above, Mr. Davies noted very light to dark grays and grayish browns. In his experience, the best greenish yellow sillimanites have an appearance resembling fine chrysoberyls from India. Most of the 3,000+ carats of sillimanite that he obtained were loupe-clean, or contained only thin parallel needles. The largest clean stones he purchased weighed more than 80 ct. About half had been cut with normal "Portuguese" patterns, and the other half had checkerboard crowns. Some of the stones needed

Figure 11. Transparent sillimanite has been recovered in a variety of colors from a new deposit that is reportedly located in the Vishakhapatnam region of Andhra Pradesh, India. The sillimanites shown here range from 4.43 ct (brownish orange-yellow) to 10.77 ct (grayish green). Courtesy of Anil B. Dholakia Inc.; photo © Robert Weldon and GIA.





Figure 12. At 49.29, 25.05, and 21.12 ct, these greenish yellow to yellow-green sillimanites from India are impressive for their size and color. Courtesy of Anil B. Dholakia Inc.; photo by Axel Respinger.

recutting, and caution was required to avoid breaking the stones when the cleavage direction was oriented nearly parallel to the table facet.

Mr. Dholakia loaned several of the sillimanites to GIA for examination, and the three largest stones (49.29, 25.05, and 21.12 ct; see figure 12) were characterized by one of us (EPQ): color—yellow-green, greenish yellow, and yellow-green, respectively; pleochroism—moderate, in yellow and grayish green; diaphaneity—transparent; R.I.— $n_o = 1.584\text{--}1.587$ and $n_e = 1.577\text{--}1.580$; birefringence— $0.017\text{--}0.018$; S.G.—3.26; no Chelsea filter reaction; and inert to both long- and short-wave UV radiation. A strong absorption band at 460 nm was observed with a desk-model spectroscope. Microscopic examination revealed that the two yellow-green stones contained parallel iridescent needles and the greenish yellow stone contained groups of fine whitish parallel needles. The properties of these stones are generally consistent with those listed for sillimanite (fibrolite) by R. Webster (*Gems*, 5th

ed., revised by P. Read, Butterworth-Heinemann, Oxford, England, 1994, p. 337). The colors of these three stones are unusual for sillimanite. We found no indication of treatment, but additional research would be necessary to determine the origin of their color.

Although this greenish yellow to yellow-green sillimanite may resemble chrysoberyl, the two gem materials can be easily separated with standard gemological techniques.

BML

Elizabeth P. Quinn

Sphene from Pakistan. At the AGTA show, Dudley Blauwet had an impressive selection of sphene from Pakistan. The stones were notable for their range of color, strong dispersion, and availability in matched pairs and calibrated suites. Mr. Blauwet first obtained this material in mid-2004, and reported that it comes from a mining area that the locals refer to as Mullah Ghani Baba (after an Islamic saint, who was buried in the area), in the Mohmand Agency of Pakistan's Federally Administered Tribal Areas, within the North West Frontier Province. It takes about 5–6 hours to reach the deposits from Peshawar (or 2 hours from Warsak); they are located fairly close to Sapari village at an elevation of about 7,000 feet (2,130 m). The mines are worked by hand tools and explosives.

The sphene is typically a saturated "golden" orange color with intense dispersion, especially "red flash." The material ranges from yellow to orange-brown, with greenish brown and greenish yellow seen less commonly. Much of the sphene is sold in Peshawar as broken crystal fragments, although some fine crystals are also encountered (see, e.g., figure 13). The rough is sometimes recovered in large pieces (up to several centimeters), but only small areas of such crystals are suitable for faceting. For example, Mr. Blauwet mentioned that a 40 kg parcel



Figure 13. Sphene from Pakistan has been faceted into a variety of shapes and shows a range of color. The cut examples (1.47–6.21 ct) are shown together with a crystal (2.8 cm wide). Courtesy of Dudley Blauwet Gems; photo © Jeff Scovil.



Figure 14. These samples of yellow to yellowish orange-brown sphenes from Pakistan were studied for this report (0.16–1.16 ct). Gift of Dudley Blauwet; GIA Collection no. 32497. Photo by Maha Calderon.

mined in June 2005 contained only a limited amount of clean material with a small cutting yield. Nevertheless, stones as large as 18 ct have been faceted, according to Scott Davies. He indicated that the strong red component of the brown material makes the stones quite salable, even without the green coloration that is so highly prized in gem sphenes.

Mr. Blauwet loaned and donated several samples of this sphenes to GIA for examination, and gemological properties were collected on five faceted samples (0.16–1.16 ct; figure 14) by one of us (EPQ): color—yellow, brownish yellowish orange, and yellowish orange-brown; pleochroism—strong yellow and red-orange for the orange and brown sphenes, moderate yellow and brownish orange for the two yellow sphenes; diaphaneity—transparent; dispersion—strong; R.I.—above the limits of a standard refractometer; S.G.—3.51–3.54; and fluorescence—inert to both long- and short-wave UV radiation. A 580 nm doublet was visible with the desk-model spectroscopy for the orange and brown stones, but no features were observed for the two yellow stones. These properties are comparable to those reported for sphenes by R. Webster (*Gems*, 5th ed., revised by P. Read, Butterworth Heinemann, Oxford, UK, 1994, pp. 375–376). Microscopic examination of the five samples revealed strong doubling, “fingerprint” inclusions, two-phase inclusions, straight and angular transparent growth lines, twinning, and (in one of the brown stones) yellow and brownish orange-yellow color zoning.

EDXRF spectroscopy of three samples indicated Si, Ca, and Ti as expected, along with varying amounts of Fe, Nb, Y, Zr, and Sr. In addition, Vis-NIR spectroscopy of the three sphenes showed a typical rare-earth spectrum. No rare-earth elements (REEs) besides Y were detected by EDXRF spectroscopy, even though the Vis-NIR spectra indicated the presence of other REE(s). The other(s) may not have been detected by EDXRF due to overlapping peaks from the other elements in the samples.

Unfortunately, Mr. Blauwet reports, the supply of sphenes from this locality has tightened in recent months due to disputes over the ownership of the mining area, which have resulted in instability and occasional gun battles. Meanwhile, demand for the sphenes remains strong, particularly from lapidaries in Bangkok and Hong Kong.

BML

Elizabeth P. Quinn

New spinel from Mahenge, Tanzania. At the GJX show, Advanced Quality A.C.C. Ltd. (Ramat Gan, Israel) had some faceted spinels in a variety of colors that were from new mining locations in the Mahenge area, near the villages of Kibangili and Ipanko, according to company president Menahem Sevdermish. The spinels, which have been produced since mid-2005, ranged from blue to violet and violetish purple to purple (figure 15), in low saturation and light to very dark tones. Typical colors were described by Mr. Sevdermish as medium dark grayish violetish purple to very dark slightly grayish bluish violet, corresponding to Gemwizard colors vP(26)7/2 and bV(24)8/2, respectively (see the Spring 2003 GNI section, pp. 57–58, for an introduction to Gemwizard software).

Mr. Sevdermish reported that the spinels are recovered as waterworn pebbles from alluvial deposits. In general, only 1–2 kg/month of good-quality facetable rough is recovered. The clean rough typically weighs up to 3–4 g. The faceted stones range from melee to 2–3 ct, but the larger sizes are rare and tend to appear very dark.

The color appearance of these spinels is significantly different from the pink and more saturated blue-to-purple colors that are more typical of the material from elsewhere in the Mahenge area, or from Umba. Mr. Sevdermish noted that strong sales of this material, as well as other gems displaying nontraditional colors, reflect a greater openness to alternative colors in the gem trade.

BML

Figure 15. These spinels (0.40–0.70 ct) are from mining areas in the Mahenge area of Tanzania. Courtesy of Advanced Quality A.C.C. Ltd.; photo by Kobi Sevdermish.

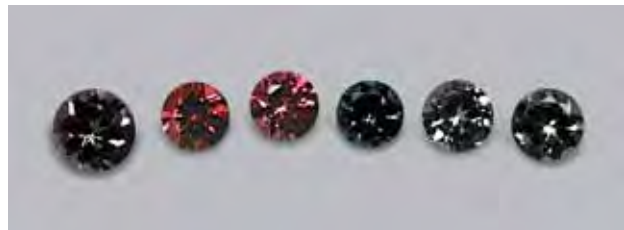




Figure 16. Framed by a thin ovoid tension fracture, this unusually large 2.1 mm skeletal ilmenite dendrite looks like a rather curious form of ancient cuneiform writing. Photomicrograph by J. I. Koivula for *microWorld of Gems*.

INCLUSIONS IN GEMS

Cuneiform aquamarine inclusion. One of the microscopically interesting gems this contributor saw during the February Tucson gem shows was a relatively large (19.27 ct) faceted greenish blue aquamarine from India that looked like it had been sprinkled internally with black pepper. Gemologists Kiran and Kusam Malhotra of K&K International, Falls Church, Virginia, subsequently loaned this gem for a more detailed examination of the inclusions.

As with all such examinations, the first step was to confirm the identification as a natural aquamarine; this was accomplished through standard gemological testing. Microscopic examination of the inclusions showed them to be relatively typical, skeletal-looking opaque black to deep translucent red dendrites. Previous experience with aquamarines containing similar inclusions has shown that the opaque black dendrites are usually ilmenite, while the red ones are hematite.

Because the inclusions in this stone were all oriented in the basal plane of the host aquamarine, they produced a silvery gray reflective aventurescence when examined with oblique fiber-optic illumination. One inclusion was particularly noteworthy because of its size, position in the host, and a general appearance of some type of ancient cuneiform-like writing (figure 16). While most inclusions of this type are microscopic, this one was eye-visible and measured more than 2 mm in longest dimension. It was also framed by an iridescent oval fracture, which is very unusual for such dendritic inclusions. And, as can be seen in figure 16, its position in the aquamarine made it very photogenic.

Regardless of their appearance, such inclusions offer a message from nature if one is schooled in their interpretation: They indicate that the color of the host is natural and has not been altered by heat treatment.

John I. Koivula (johnkoivula@hotmail.com)
AGTA Gemological Testing Center, Carlsbad

“Blood trail” in copal. In the Spring 2000 Gem News section (pp. 67–68), this contributor reported on a polished specimen of light yellow copal from Madagascar that contained brownish red fluid inclusions. The unusual appearance of this fluid and its visible absorption spectrum led to speculation that the inclusions might contain blood. However, because of the unusual nature of the inclusions and the rarity of the sample itself, no further testing was performed to identify them, since a more complete analysis would have required destructive opening of the voids.

At the 2006 Tucson gem shows, this contributor discovered a second specimen of copal containing red-brown liquid, but from an entirely different locality—Colombia—which is also known to produce copal with interesting inclusions (see, e.g., Spring 2004 Lab Notes, pp. 58–59).

Even to the unaided eye, this Colombian sample exhibited numerous tiny bright brownish red bubbles. Microscopic examination revealed that the red drops were contained within spherical to somewhat distorted cavities in their copal host. Most of these inclusions appeared to be randomly scattered in the fossil resin, but in one instance (figure 17), they were arranged in a linear “blood trail.” Some of these inclusions also contained free-floating gas bubbles, confirming that the red substance was indeed a liquid.

Although no analytical equipment was available to identify the fluid, this Colombian specimen was also examined with a small diffraction grating spectroscope. The absorption spectrum was similar to that obtained from a human finger when illuminated by a strong fiber-optic light source. As with the first sample from Madagascar, this spectrum suggested that iron was present, at least as a coloring agent, in fluid inclusions from the Colombian copal.

John I. Koivula

Figure 17. Strongly resembling a trail of blood, this row of brownish red fluid droplets was discovered in a polished specimen of copal resin from Colombia. Similar fluid inclusions in the sample contained movable gas bubbles. Photomicrograph by J. I. Koivula for *microWorld of Gems*; magnified 15 \times .





Figure 18. The unusual two-phase orange fluid inclusions in this quartz from Bahia, Brazil, are situated in two different growth zones, suggesting that they are primary inclusions and not the result of healed fractures. Photomicrograph by J. I. Koivula for *microWorld of Gems*; magnified 10 \times .

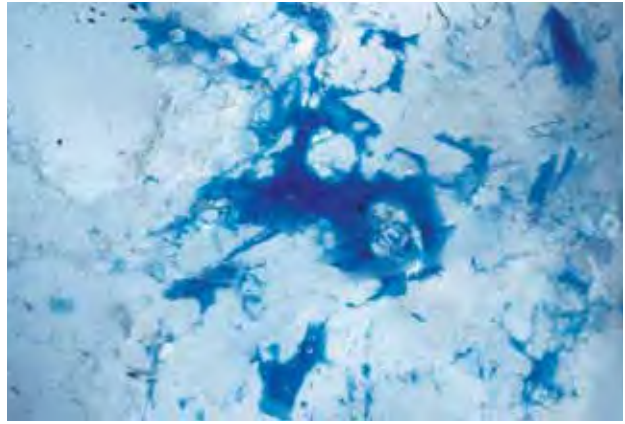


Figure 19. This relatively large, bright blue fluid inclusion in quartz from Bahia, Brazil, has a color reminiscent of a saturated copper sulfate solution. Photomicrograph by J. I. Koivula for *microWorld of Gems*; magnified 2 \times .

Colored fluid inclusions in quartz. Luciana Barbosa of the Gemological Center, Belo Horizonte, Brazil, always has a number of interesting inclusion specimens on display in Tucson, as both cut gems and as rough and polished crystals. This year, at the GJX show, she had some samples of rock crystal quartz with unusual fluid inclusions.

One of these was a small faceted step-cut rectangular gem containing numerous two-phase fluid inclusions, with a liquid phase having a distinctive slightly pinkish orange color. According to Ms. Barbosa, this sample was from Bahia, Brazil. As seen in figure 18, the color of this fluid was somewhat different from what would be expected from a solution stained with iron oxide or hydroxide. These fluid inclusions were inert to UV radiation, and were situated in two growth zones at different depths in the quartz. Their general appearance along growth planes, and their widely differing size, suggested that they were primary fluid inclusions and not the result of fracture repair or regrowth. No daughter crystals were observed, and none of the gas bubbles moved when the specimen was tilted and examined with the microscope. Completing the picture were a number of very fine fibrous inclusions.

Ms. Barbosa also had a selection of interesting faceted colorless quartzes that hosted bright blue fluid inclusions, the largest of which is shown in figure 19. The color of the fluid was reminiscent of a saturated copper sulfate solution. The source of this quartz was also reported as Bahia.

Because of the bright blue color of the fluid, even very small inclusions were visible to the unaided eye. With magnification, it was noted that most of the fluid inclusions were two-phase, each containing a single gas bubble. Some of them, however, also appeared to have

minute solid phases along the inner walls of the inclusion chambers. The blue fluid fluoresced a weak to moderate chalky bluish white (light blue) to long-wave UV radiation.

These inclusions seemed to be randomly arranged and of widely varying sizes. Most of the largest ones possessed ragged-to-rough-looking outlines, but some of the smaller ones had a well-developed negative crystal form (figure 20), and a few had movable gas bubbles. Also present were occasional micaceous crystals (figure 21) and numerous jumbled ultra-thin fibrous inclusions, which were very similar in appearance to those observed in the specimen with the pinkish orange fluid.

John I. Koivula

Figure 20. A few of the smaller blue fluid inclusions in the Brazilian quartz had a well-developed negative crystal form. Photomicrograph by J. I. Koivula for *microWorld of Gems*; magnified 30 \times .





Figure 21. An occasional light brown micaceous crystal and numerous fibrous inclusions were also present in the quartz containing the blue fluid inclusions. Photomicrograph by J. I. Koivula for *microWorld of Gems*; magnified 15 \times .

“Platinum quartz” with star. In the Winter 2003 GNI section (pp. 334–335), this contributor reported on a material from Brazil sold as “platinum quartz.” Initial examination proved that it was formed by a combination of two titanium oxide minerals, rutile and brookite, included in rock crystal and light brown smoky quartz from Curvelo in Minas Gerais State.

Over the past few years, this researcher has studied several hundred “platinum quartz” samples, as both fashioned gems and crystals. Through micro-observation,

it appears that the silvery fibers of rutile grew epigenetically in relation to the elongated blades of brookite (i.e., as epitaxial overgrowths). Both the rutile and brookite are protogenetic to (i.e., grew before) the quartz containing them.

At the recent Tucson gem shows, Kevin Lane Smith, a lapidary and jewelry designer based in Tucson, displayed a most remarkable example of “platinum quartz” in his show room. This 94.75 ct shield-shaped colorless plate was polished on all sides. Unlike other “platinum quartz” examples this contributor has seen, this particular gem contained a superb, silvery, six-rayed star (figure 22) formed by the growth of numerous rutile fibers on a substrate that appeared to be three individual brookite blades arranged at angles of approximately 60° to one other. While four-rayed stars have been seen previously in this type of Brazilian quartz, this is the first six-rayed rutile star that this contributor has observed in this type of quartz.

As an added optical bonus, the star was positioned so that the central brookite blades were parallel to the optic axis of the quartz host. And, since this particular quartz was twinned on the Brazil law, when observed between crossed polarizers the background of the rutile star was quite colorful (again, see figure 22). One always hesitates to apply the word *unique* to anything, since that implies it is the only one to exist. However, if this stone is not unique, then the circumstances that created it have at least resulted in a most unusual gem.

John I. Koivula



Figure 22. This polished “platinum quartz” from Curvelo, Minas Gerais, Brazil, displays a most unusual six-rayed star (approximately 2.5 cm across) of silvery rutile needles. The colorful appearance of the background is created by Brazil-law twinning of the host quartz, as viewed between crossed polarizers. Photomicrograph by J. I. Koivula for *microWorld of Gems*.

CONFERENCE REPORTS

New Madagascar mining laws. Madagascar has adopted a series of new laws to reduce restrictions on the trade and export of gems mined in that country. Under the new regulations, which went into effect in December 2005, foreign dealers and companies no longer need to go through a local business to buy and export rough and cut gems. Details of the new system were presented at a press conference during the AGTA show by Tom Cushman, a gem dealer who is also a consultant to the country's government, and Pamphile Rakotoarimanana, director of Mines and Geology at the Ministry of Energy and Mines in Antananarivo.

Interested dealers need to secure a business visa that will permit buyers to obtain a license from the Department of Mines and Geology for the purchase of gems. Buyers must keep a detailed record of their purchases, both rough and polished, which must be taken to the mines department for sealing before export. There, the buyer must pay an export duty of 2% on the stated value of gem rough; there is no duty for polished stones. The government maintains a reference guide listing wholesale price ranges for gems found in the country, and values stated in an invoice must be consistent with those in the guide.

Under the former system, foreign traders were not allowed to export gems at all, which resulted in widespread smuggling and cost the government millions of dollars in lost revenues. The country's new presidential administration has embarked on a campaign to reform and liberalize the country's economy in partnership with the World Bank. In addition, the government, in cooperation with various industry organizations including GIA, has established the Institute of Gemmology of Madagascar to train locals in identifying, evaluating, and polishing gemstones.

Also announced at the press conference was the availability of organized gem buying trips to Madagascar that are guided by Jim Fiebig of Fiebig Jewelers, Sturgis, Michigan. Mr. Fiebig conducts trips lasting from 7 to 13 days that include visits to local markets, excursions to the country's main gem-producing areas, and meetings with gem producers and miners (see www.gemstonetrips.com).

Madagascar produces significant quantities of corundum, aquamarine, tourmaline, spinel, and spessartine and rhodolite garnets.

*Russell Shor (rshor@gia.edu)
GIA, Carlsbad*

GNI Regular Features

DIAMONDS

Black diamond with unusual growth structures. The Dubai Gemstone Laboratory received a large black round brilliant mounted in a ring for identification (figure 23, left). As measured in the mounting, the stone was approximately 20 mm in diameter and 12 mm deep. It was identified as diamond with standard gemological testing and the presence of the 1332 cm^{-1} diamond Raman peak. It was inert to both long- and short-wave UV radiation. With very strong fiber-optic illumination, the stone appeared dark

brown (figure 23, right). Due to the size of the stone and the nature of the mounting, it was not possible to perform a detailed investigation of the color origin using FTIR spectroscopy. Nevertheless, there was no indication that the color was the result of treatment.

Closer examination with fiber-optic illumination revealed some unusual growth features in this diamond (figure 24). Near the center of the table were dark bands that defined a roughly four-sided curvilinear structure. The shape of this feature is fairly typical of cuboid growth in

Figure 23. This large (20 mm) apparently black diamond (left) had a dark brown bodycolor with intense fiber-optic illumination (right). Photos by S. Singbamroong, © Dubai Gemstone Laboratory.



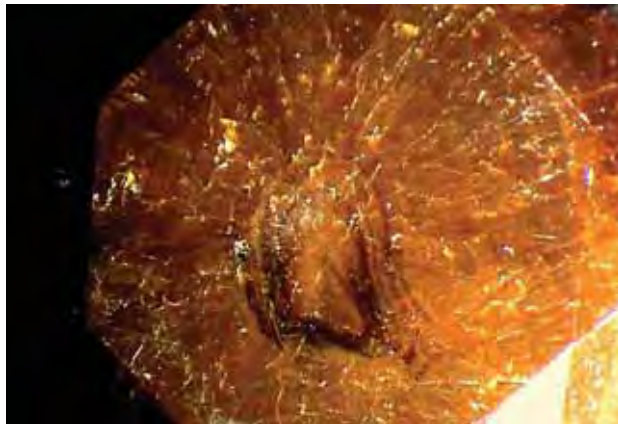


Figure 24. Curvilinear growth layers, which are fairly typical of cuboid growth, are visible near the center of the “black” diamond’s table facet. A more puzzling, aggregate growth structure appears to radiate from the curvilinear core. Photomicrograph by S. Singbamroong, © Dubai Gemstone Laboratory; magnified 16x.

diamond. Surrounding these dark bands were faint concentric bands and a radiating structure, which are suggestive of fibrous growth.

Both of these growth types can be found in brown diamond. Cuboid growth is always curvilinear, never straight, with a mean orientation corresponding to cube faces (hence the name). Moreover, because the table apparently intersected this growth pattern in a random orientation, the near-cubic orientation of the growth in the core was not immediately evident. Although the structure observed in the outer portion was strongly suggestive of fibrous growth, such diamond is typically opaque (relative to cuboid growth), and when it is brown, it is usually not as saturated as seen in the present stone. Therefore, the fibrous structure seen in this dark brown diamond was rather puzzling. An alternate explanation for this diamond’s growth would be that the entire stone formed via spherulitic (fibrous) growth; however, a diamond spherulite of this size would be quite unusual. Only X-ray topography could unambiguously confirm the growth sequence, but this technique was not available to study this sample.

If our interpretation is correct, this growth succession of a cuboid core followed by a fibrous overgrowth is quite unusual. Theoretically, there is no reason why there could not be a progression of cuboid to fibrous growth; the sequence from octahedral to fibrous growth in “coated” diamonds is well-known. It is therefore surprising that a cuboid-fibrous growth combination has not yet been previously noted. The reason for the apparent rarity of this sequence of growth conditions is unknown at this time.

Sutas Singbamroong (SSSUTAS@dm.gov.ae)
Dubai Gemstone Laboratory
Dubai, United Arab Emirates

EF

COLORED STONES AND ORGANIC MATERIALS

Sapphire with unusual color zoning. Recently, the Gem Testing Laboratory, Jaipur, India, encountered an 11.29 ct blue oval stone with unusual color zoning. The refractive index was measured at 1.760–1.770 and the hydrostatic specific gravity at 3.98, which identified the sample as corundum.

The stone had been faceted with a large flat area on the pavilion, and the reasons for this were quickly apparent. When the sapphire was viewed table up, it appeared uniformly blue (figure 25). From the side, however, it appeared almost colorless, with a strong blue color zone concentrated on the large pavilion surface (figure 26). Although the stone was inert to long-wave UV radiation, with short-wave UV the blue area displayed strong chalky greenish blue fluorescence. A visible spectrum taken with a desk-model spectroscope showed a moderate absorption band at 450 nm and a weak band at 470 nm. The optic axis of the stone was oriented parallel to the color plane.

With magnification, clouds of minute globular inclusions were observed around a sugary crystal, along with some cloudy whitish healed “fingerprints.” Such inclusions are typically associated with high-temperature heat treatment of corundum. In addition, when the stone was immersed in methylene iodide and observed using diffuse illumination, straight parallel color zones were seen across the blue color plane (figure 27). There were additional blue zones present in the pavilion, though weaker in intensity, also parallel to the color plane.

Although strong color zoning evoked suspicions of diffusion treatment, the absence of color concentrations along facet or girdle edges, the thickness and pattern of the color zones, and their location along only one side of the

Figure 25. Although this 11.29 ct sapphire appears an attractive, uniform blue when viewed face up, its color is actually restricted to a narrow zone on the pavilion. Photo by G. Choudhary.





Figure 26. When viewed from the side, the colorless body and strong blue color plane of the sapphire in figure 25 are apparent. Photo by G. Choudhary.

sample eliminated this possibility. Therefore, we concluded that the stone had been cut from a piece of strongly color-zoned sapphire rough in which the blue color was restricted to narrow zones parallel to the prism faces. Strong blue/colorless zoning has been noted previously in sapphires from Songea, Tanzania, and Sri Lanka (as cited in the Winter 2004 GNI, pp. 354–355), as well as in some greenish blue sapphires from India.

Gagan Choudhary (gtljpr_jpr@sancharnet.in)
Gem Testing Laboratory, Jaipur, India

Väyrynenite from Pakistan. For years, gem dealer Dudley Blauwet has sourced unusual gems and minerals from northern Pakistan, including an unusually transparent and brightly colored example of triplite, $Mn_2(PO_4)F$ (see GNI: Winter 2004, pp. 346–347, and Fall 2005, p. 277). Recently, Mr. Blauwet obtained another gem-quality phosphate mineral from this region, called väyrynenite (vuh-REN-i-nite), $MnBe(PO_4)(OH,F)$. He obtained a few gem-quality crystals and fragments in June 2005, while on a buying trip to the Shigar and Braldu valleys of Pakistan. The stones reportedly came from a granitic pegmatite near the village of Apaligun (Apo Ali Gun), in the Braldu Valley. This locality is only about 10 km upriver (east) of Dasso, which was the source of the triplite. Mr. Blauwet first encountered väyrynenite from the Braldu Valley in 2004, and the identity of the material was confirmed by a mineralogical laboratory.

Mr. Blauwet loaned one rough and one cut (2.02 ct) sample of the väyrynenite to GIA for examination (figure 28), and the following gemological properties were determined by one of us (EAF) on the faceted gem: color—orange-pink, with orange and pink pleochroism; R.I.—1.640–1.663; birefringence—0.023; S.G.—3.22; and fluorescence—inert to both long- and short-wave UV radiation. Vis-NIR spectroscopy showed a line at 413 nm and weak bands at approximately 435, 465, and 545 nm. Microscopic examination revealed numerous fractures and interconnected growth tubes; some of the smaller tubes contained



Figure 27. With immersion in methylene iodide and diffuse illumination, straight and parallel blue color zones are clearly visible across the color plane in the sapphire. Photomicrograph by G. Choudhary; magnified 35x.

two-phase inclusions. The properties of this sample are comparable to those published in a Summer 1994 Lab Note on another faceted väyrynenite (p. 121). According to *Minerals and Their Localities* (J. H. Bernard and J. Hyršl, Granit, Prague, Czech Republic, 2004, p. 640), väyrynenite has a Mohs hardness of 5 and has also been found in gem quality from a locality near Sassu (actually Sassi), about 40 km east of Gilgit in northern Pakistan.

It is remarkable that two unusual gem-quality phosphate minerals showing similar colors have come from northern Pakistan's pegmatites. In Mr. Blauwet's experience, the crystals and fragments of both minerals are commonly stained with a black material (probably manganese oxides; again, see figure 28). He noted that the Pakistani triplite is commonly reddish orange to orange brown in comparison to the pinkish orange väyrynenite, which typically has a flatter and more prismatic crystal morphology than the triplite.

BML

Eric A. Fritz
GIA Laboratory, Carlsbad

Figure 28. Northern Pakistan is the source of this crystal and 2.02 ct step-cut väyrynenite. Courtesy of Dudley Blauwet Gems; photo by C. D. Mengason.



SYNTHETICS AND SIMULANTS

A convincing moonstone doublet. The GIA GemTechLab recently encountered a 19.40 ct transparent slightly brownish gray cabochon that appeared to show intense blue adularescence (figure 29). It was represented as natural moonstone, but microscopic observation immediately revealed a very distinct separation plane (figure 30), indicating that the specimen was assembled. The intense blue sheen was restricted to the approximately 0.5-mm-thick bottom portion of the assemblage (figure 31); this section also contained inclusions and apparent cleavage cracks in two directions that clearly suggested it was natural feldspar. The top portion, representing more than 95% of the sample volume, appeared to be glass, since gas bubbles were quite evident (again, see figure 30). These identifications were confirmed by specular reflectance FTIR spectroscopy.

The base was apparently cut from gray labradorite exhibiting a blue sheen; the black needles and particles were identical to the inclusions typically seen in such material. The convex form of the glass top acted to focus and magnify the blue iridescence from the flat base. This gave rise to a very convincing blue-sheen effect, and gave the sample the appearance of an unusually transparent moonstone of very high quality.

*Thomas Hainschwang (thomas.hainschwang@gia.edu)
GIA GemTechLab, Geneva, Switzerland*

A rutilated quartz doublet. Rutilated quartz has grown in popularity in recent years and occupies a distinct niche of the gem market. This, combined with its limited avail-

Figure 30. The separation plane between the two halves of the doublet (feldspar base; glass top) is clearly apparent when viewed with magnification. A large gas bubble is visible in the upper part of the glass portion. Photomicrograph by T. Hainschwang; magnified 7×.

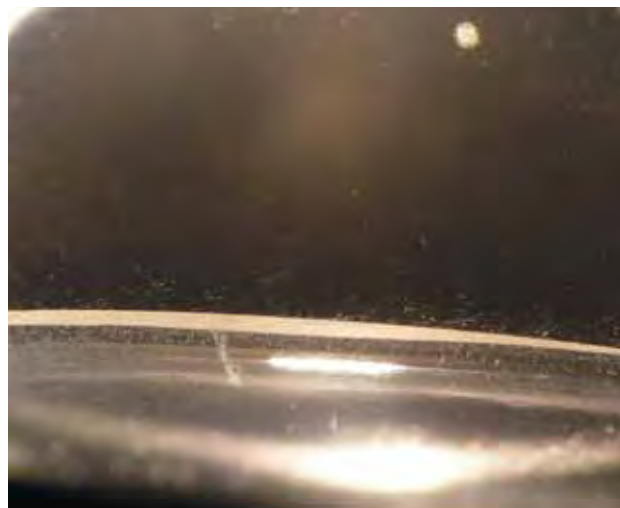
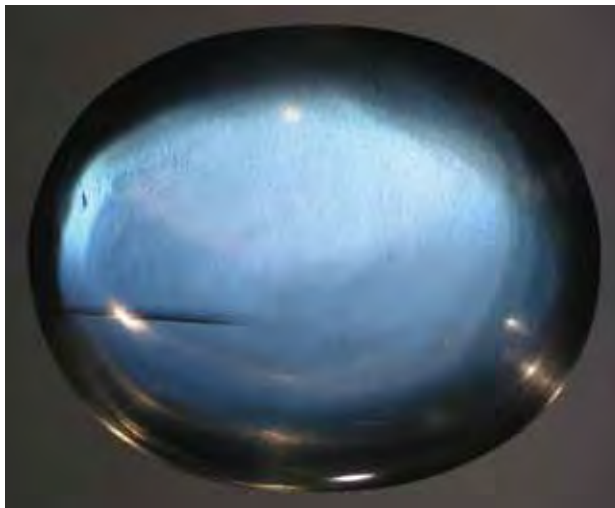


Figure 29. This 19.40 ct cabochon appears to show strong adularescence, but it proved to be a doublet imitating a high-quality moonstone. Photo by T. Hainschwang.

ability (nearly all material is found only in Bahia, Brazil), has led to a significant increase in price during the last two years. However, as with other gem materials, the elevated value has encouraged experimentation by enterprising entrepreneurs.

During a September 2005 trip to Teófilo Otoni, Minas Gerais, these contributors were offered the seven-stone parcel shown in figure 32. The low price and a preliminary visual inspection raised questions about the authenticity of the stones, prompting us to perform a more detailed examination. The refractive indices were 1.544–1.553, typical for quartz. However, when viewed from the side, it

Figure 31. The feldspar base of the doublet exhibited a strong blue iridescence, which created the illusion of adularescence when viewed through the glass top. Photo by T. Hainschwang.



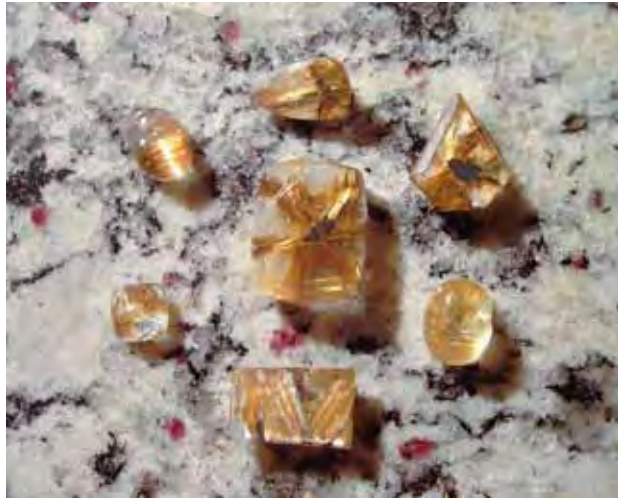


Figure 32. The rutilated quartz cabochons (12–20 mm in longest dimension) in this parcel proved to be doublets. Photo by M. Macri.

was evident that they were doublets, with a thin layer of semitransparent rutilated quartz joined by a transparent adhesive to a backing of transparent quartz that contained little or no rutile. The assembled nature of the samples was even more obvious when the samples were immersed in water, as shown in figure 33.

Although a trained observer would easily detect this falsification in a loose stone, the same observer might fail to identify the doublets after they were mounted, since there were no gas bubbles or other evidence of the glue layer when they were viewed face-up with a loupe.

Michele Macri (michele@minerali.it)
and Simone Macri
Laboratorio di Gemmologia Geo-Land
Rome, Italy

An unusual triplet. For decades, a wide variety of assembled gems have been seen in the trade, incorporating both natural and synthetic materials. Occasionally some rather inventive and unusual combinations are used to create



Figure 33. When this cabochon (20 mm in diameter) was viewed from the side in immersion, its assembled nature was readily apparent. This doublet consists of a layer of rutilated quartz with a backing of transparent quartz that contains little or no rutile. Photo by M. Macri.

the desired optical effect. Such was the case with a triplet that was designed to simulate cat's-eye chrysoberyl.

The 8.85 ct oval triplet (figure 34) formed part of a collection of rough and cut gems that was recently donated to GIA by H. Obodda, Short Hills, New Jersey. According to Herb Obodda, the triplet was manufactured in about 1960 by C. Stastny, a New York City lapidary. He indicated that Mr. Stastny enclosed a piece of ulexite within a dome and base consisting of yellow synthetic corundum. The dome and base were confirmed as corundum in the GIA Laboratory, but a natural or synthetic origin was not determined due to the nature of the sample. The dome had been carefully hollowed out to accommodate the core that was responsible for the chatoyancy. Although the identity

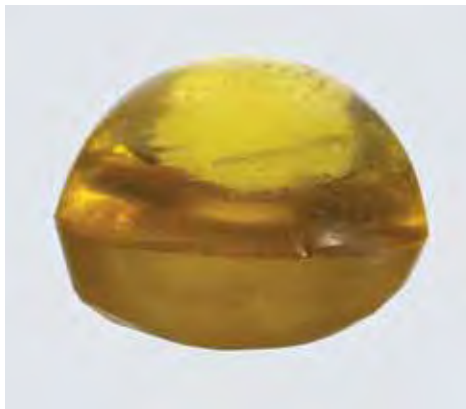


Figure 34. In this 8.85 ct triplet, gas bubbles can be seen in the glue layer between the ulexite core and the synthetic sapphire dome (left). The profile view on the right shows the boundary between the dome and base of synthetic corundum. Gift of Herb & Monika Obodda; GIA Collection no. 32391. Photos by C. D. Mengason.

of the chatoyant core could not be confirmed, its visual appearance was consistent with ulexite. The bright yellow color of the synthetic corundum is quite unlike that seen in typical cat's-eye chrysoberyl. Nevertheless, the well-executed assembly of the triplet resulted in an attractive, even if artificial, appearance.

BML

MISCELLANEOUS

New CRJP Code of Practices released. The Council for Responsible Jewellery Practices (CRJP) has produced a draft of its Code of Practices, which seeks to establish a worldwide standard of corporate conduct for the gem and jewelry industry. The CRJP is a foundation formed by a number of large mining and retailing firms and industry organizations to harmonize various corporate governance codes. Currently, the London-based organization is only seeking new members in the gold and diamond sectors.

Released on February 10, 2006, the proposed code sets forth a series of guides that cover three basic areas:

- *Business ethics:* Forbids member companies from engaging in bribery and corruption, requires full and accurate disclosure of all of the products sold by members, and stipulates full adherence to all laws regarding money laundering and Kimberley Process participation.
- *Social:* Requires adherence to all fair labor standards, to workplace health and safety regulations, and to nondiscriminatory hiring and pay; also forbids the use of child labor with the exceptions noted by the International Labor Organization.
- *Environmental:* Requires conducting business in an environmentally responsible manner and assessment of possible adverse effects arising from business activities.

The code also provides for appointment of independent monitors to review member firms' compliance with its provisions.

The full proposal can be found at the Council's website, www.responsiblejewellery.com.

Russell Shor

Update on the use of biological remains in gem materials. The Spring 2003 GNI section (p. 62) reported on LifeGem synthetic diamonds, which the company claims are produced from carbon recovered from cremated human or animal remains. At the time, the process was described as "patent pending," though no other information was available. Since then, a number of patent applications covering this and similar processes have been published, and these applications are summarized here.

The founders of LifeGem have submitted two patent applications for the methods LifeGem uses to recover and purify carbon from the cremation process for diamond synthesis (R. P. VandenBiesen et al., *Method for Making*

Synthetic Gems Comprising Elements Recovered from Complete or Partial Human or Animal Remains and the Product Thereof, U.S. patent application publication 2003/0017932 A1, filed March 18, 2002, published January 23, 2003; and R. P. VandenBiesen et al., *Method of Making Synthetic Gems Comprising Elements Recovered from Remains of a Species of the Kingdom Animalia*, U.S. patent application publication 2004/0031434 A1, filed August 19, 2003, published Feb. 19, 2004). These patent applications do not cover the method of synthesizing diamond using high-pressure and high-temperature growth conditions, since such processes were patented long ago by other parties (see, e.g., H. M. Strong, *Novel Diamond Products and the Manufacture Thereof*, U.S. patent 4,042,673, issued August 16, 1977).

A more recent Japanese patent application expands on the methods described by VandenBiesen et al. to include additional techniques for preparing the remains for cremation (E. Fukasawa, *Artificial Gem and Its Producing Method*, International [PCT] patent application WO 2004/105540 A1, filed May 29, 2003, published December 9, 2004). This application also covers the process of adding carbon when insufficient amounts have been recovered from cremation to produce a synthetic diamond of the desired size (with conventional cremation, most of the carbon in the human body is lost when it is converted to carbon dioxide).

A similar but more extensive process is covered by a patent application submitted by R. E. Page of Streamwood, Illinois (*Method for Making Synthetic Gems Comprising Elements Recovered from Humans or Animals and the Product Thereof*, U.S. patent application publication 2004/0154528 A1, filed Feb. 11, 2003, published Aug. 12, 2004). This method covers not just diamonds but many other gem materials that are composed of elements found in the human body. These elements can be recovered and used for the growth of gem materials such as synthetic garnet, spinel, quartz, and moissanite. Interestingly, the application also mentions a number of gems (such as tourmaline, pearls, and ivory) that are not currently synthesized; this was probably done to ensure that the patent covers these materials should synthetic varieties come on the market at a later date.

Another team of inventors, from Edmonton, Alberta, Canada, has developed a method of incorporating human or animal remains into a glass filling material for diamonds (M. Weisbrot and V. Galon, *Method of Encapsulating Material from Humans or Animals in a Natural Gemstone and Its Product*, International (PCT) patent application WO 2004/076058 A1, filed Feb. 25, 2004, published Sept. 10, 2004). The patent application describes a method of creating a high-refractive index glass from a mixture of calcium phosphate recovered from cremated remains, lead oxide, a chloride compound (such as NaCl or KCl), and a bromide or bismuth compound. The resulting glass is then injected in molten form into laser drill holes in natural

diamonds. This glass filling process is currently being employed by Memorial Gem Inc. of Edmonton; the diamonds are sold through associated funeral homes.

It should be emphasized that these patents are still in the examination stage, and none have been issued yet.

This contributor thanks Dr. Karl Schmetzer, Petershausen, Germany, for bringing these patents to our attention, and Dr. Taijin Lu of GIA Research for translating the Japanese patent application.

*Thomas W. Overton (toverton@gia.edu)
GIA, Carlsbad*

ANNOUNCEMENTS

AGTA Spectrum Awards competition. The 2007 AGTA Spectrum Awards will recognize outstanding colored gemstone and cultured pearl jewelry designs from North America, as well as achievements in the lapidary arts. Winning entries will be displayed and award recipients honored at the 2007 AGTA GemFairs in Tucson and Las Vegas. The entry deadline is September 22; the competition will be held in New York City during October. For entry forms and more information, visit www.agta.org or call 800-972-1162.

Conferences

SEG 2006. The annual meeting of the Society of Economic Geologists will take place May 14–16 in Keystone, Colorado. The program will include two sessions on Canadian diamonds. Visit www.seg2006.org, call 720-981-7882, or e-mail seg2006@segweb.org.

GAC-MAC 2006. The 2006 joint meeting of the Geological Association of Canada and the Mineralogical Association of Canada will take place May 14–17, in Montreal. Diamonds will be covered in some of the sessions. Visit www.er.uqam.ca/nobel/gacmac/welcome.html.

ICNDST-11. The 11th International Conference of New Diamond Science and Technology will be held in Raleigh-Durham, North Carolina, May 15–18, 2006. Among the topics covered will be HPHT synthesis and processing and the growth of CVD synthetic diamond. Visit <http://lucy.mrs.org/meetings/workshops/2006/icndst>.

Bead Expo. The 2006 International Bead Expo will be held in Charleston, South Carolina, May 17–21. Over 60 workshops and educational lectures on bead jewelry design and manufacture are scheduled. E-mail info@beadexpo.com or visit www.beadexpo.com.

GAA-NSW conference. The 2006 conference of the New South Wales Division of the Gemmological Association of Australia will be held May 19–21 in Sydney. The event will also include a jewelry design competition and a post-

conference tour that will visit corundum and opal mines at Barrington Tops, Inverell–Glen Innes, and Lightning Ridge. Visit www.gem.org.au/conference.htm or e-mail nsw@gem.org.au.

2006 Joint Assembly. Several mineralogical and geological societies are sponsoring this conference, which will be held May 23–26 in Baltimore, Maryland. Diamonds will be covered in a session titled “Earth’s Carbon Cycle,” and granitic pegmatites will be included in a “Crustal Melts at Low Temperatures” session. Visit www.agu.org/meetings/ja06, call 202-777-7330, or e-mail ja-help@agu.org.

Maine Pegmatite Workshop. Taking place May 27–June 3, 2006, in Poland, Maine, this educational event will feature seminars and daily field trips to gem-bearing pegmatite quarries in Maine and New Hampshire. Visit <http://homepage.mac.com/rasprague/PegShop> or e-mail rasprague@mac.com.

JCK Show—Las Vegas 2006. Held at the Sands Expo and Convention Center and the Venetian Hotel on June 3–7, 2006, this gem and jewelry trade show will also host a comprehensive educational program beginning June 1. Scheduled seminars will cover industry trends, diamond cut, sales and marketing strategies, legal issues for retailers and manufacturers, and developments in gemology. The AGTA will also be offering seminars focusing on color and fashion on June 2 at the AGTA Pavilion. To register, call 203-840-5684 or visit jckvegas2006.expoplanner.com.

Diamonds at CIMTEC 2006. This large materials science convention will take place June 4–9, in Acireale, Sicily, Italy. Presentations on the growth and characterization of diamond will be included in “Diamond and Other New Carbon Materials,” which will form part of the 4th Forum on New Materials. Visit www.cimtec-congress.org.

Bangkok Gems & Jewelry Manufacturers Fair. Held June 14–18, 2006, this trade fair in Bangkok will include a silver-jewelry design contest and a colored gemstone cutting contest, in addition to educational seminars on developments in jewelry design technology. Visit www.jewelmgf.com.

18th European Workshop on Laser Ablation. Held July 19–21, 2006, in Zurich, Switzerland, this biennial event focuses on material analysis using laser ablation-based methods such as LA-ICP-MS and LIBS. Visit www.laser2006.evento.ethz.ch.

IMA 2006. The 19th General Meeting of the International Mineralogical Association will be held in Kobe, Japan, July 23–28. The conference will include special sessions on “Natural and Artificial Gem Materials” and “Kimberlites, Diamonds and Mineral Inclusions from the Mantle”; other sessions will cover crystal growth, fluid inclusions, and



Figure 35. This inlaid pectoral ornament is a rebus for the throne name of Tutankhamun-Nebkheprure—which can be translated as “Re is the lord of manifestations.” A carnelian sun disk, symbol of the sun god Re, is clasped between the scarab beetle’s front legs, while its wings are fashioned from carnelian, lapis, and turquoise. Photo © Andreas F. Voegelin; courtesy of the Field Museum, Chicago.

mineralogical museums. Post-conference field trips will include visits to Japanese jadeite deposits. Visit www.congre.co.jp/ima2006 or e-mail 2006ima@congre.co.jp.

JA New York Summer Show. Running July 30–August 2 at the Jacob K. Javits Convention Center in New York City, this show will also feature a range of educational programs and seminars. Topics to be covered include diamond cut, diamond treatments, store management, internet marketing, anti-money laundering compliance, and bench jewelry techniques. Visit www.ja-newyork.com or call 800-650-1591.

Goldschmidt 2006. The 16th Annual V.M. Goldschmidt Conference will take place August 27–September 1 in Melbourne, Australia. This important geochemistry confer-

ence will feature a session titled “The deepest lithosphere and beyond: Diamonds and related research, a session in honour of Jeff Harris.” Visit www.goldschmidt2006.org or e-mail goldschmidt2006@tourhosts.com.au.

Diamond 2006. The 17th European Conference on Diamond, Diamond-like Materials, Carbon Nanotubes, and Nitrides will be held September 3–8 in Estoril, Portugal. Presentations on the growth, processing, and characterization of diamond will be given at this meeting. Visit www.diamond-conference.elsevier.com or e-mail Nina Woods at n.woods@elsevier.com.

Santa Fe Symposium changes venue in 2006. The 20th annual Santa Fe Symposium on jewelry manufacturing technology will be held in Nashville, Tennessee, on September 10–13. Visit www.santafesymposium.org.

Exhibits

Arctic jewelry. “Arctic Transformations: The Jewelry of Denise and Samuel Wallace” is on exhibit at the George Gustav Heye Center in New York City through July 23, 2006. Visit www.nmai.si.edu/subpage.cfm?subpage=exhibitions&second=ny.

King Tut Returns. “Tutankhamun and the Golden Age of the Pharaohs,” an exhibition of more than 130 artifacts from the tomb of King Tut and other royal tombs in Egypt’s Valley of the Kings, will be on display until April 23, 2006, at the Museum of Art in Fort Lauderdale, Florida. Among the items included are a gem-studded gold diadem and a jeweled pectoral ornament (figure 35). Only a few of the artifacts in this exhibit were part of the famed 1977 exhibition, and many have never traveled outside Egypt. The exhibit will move to the Field Museum in Chicago May 26, 2006 through January 1, 2007. Visit www.kingtut.org.

Charles Loloma Retrospective. “Loloma: Beauty in Hopi Jewelry,” an exhibit of works by renowned Hopi jewelry artist Charles Loloma will be displayed through May 28, 2006, at the Heard Museum in Phoenix, Arizona. An array of pieces incorporating unusual materials such as gold-set lapis lazuli, fossilized ivory, and ironwood will be on exhibit. Visit www.heard.org/show-exhibit.php?id=35 or call 602-252-8848.

Take the
G&G
Challenge



The following 25 questions are based on information from the four 2005 issues of *Gems & Gemology*. Refer to the feature articles and “Notes and New Techniques” in those issues to find the **single best answer** for each question; then mark your choice on the response card provided in this issue. (Sorry, no photocopies or facsimiles will be accepted; contact the Subscriptions Department—dortiz@gia.edu—if you wish to purchase additional copies of this issue.) Mail the card so that we receive it no later than Tuesday, August 1, 2006. Please include your name and address. All entries will be acknowledged with a letter and an answer key **after the due date**.

Score 75% or better, and you will receive a GIA Continuing Education Certificate. If you are a member of the GIA Alumni Association, you will earn 10 Carat Points toward GIA’s Alumni Circle of Achievement. (Be sure to include your GIA Alumni membership number on your answer card and submit your Carat card for credit.) Earn a perfect score, and your name also will be listed in an upcoming issue of *Gems & Gemology*. Good luck!

- In Edward J. Gübelin’s classification system, mineral inclusions that formed after the host gem crystal completed its growth are called
 - genetic.
 - epigenetic.
 - protogenetic.
 - syngenetic.
- The only chromophore used in the growth of Malossi synthetic emeralds is
 - chromium.
 - iron.
 - magnesium.
 - vanadium.
- Useful identifying characteristics of treated-color pink-to-red natural diamonds observable through standard gemological testing include:
 - colored “graining” caused by plastic deformation.
 - moderate-to-strong chalky UV fluorescence.
 - the presence of unaltered natural mineral inclusions.
 - all of the above.
- The mechanism that the diamond industry devised to prevent conflict diamonds from entering the global diamond market is called the
 - World Diamond Council.
 - Kimberley Process.
 - PATRIOT Act.
 - Clean Diamonds Act.
- _____ imaging is useful in revealing the damage and wear to the coating of a coated diamond.
 - Magnetic resonance
 - Positron emission tomography (PET)
 - Scanning electron microscopy (SEM)
 - Thermal emission
- Most Zambian emeralds are cut and distributed in
 - China.
 - India.
 - Israel.
 - eastern Europe.
- The first major discovery of quantities of fancy-color yellow diamonds took place in the late 1860s in
 - Australia.
 - Brazil.
 - India.
 - South Africa.
- Chemical analysis has shown that most of the gem tourmaline mined recently from Mt. Mica, Maine, is
 - elbaite.
 - foitite.
 - rossmanite.
 - schorl.
- Chameleon diamonds exhibit a temporary change in color when
 - heated to approximately 150°C.
 - heated to approximately 80°C.
 - cooled to approximately 0°C.
 - cooled to approximately –100°C.
- Some of the CVD synthetic diamonds produced at the Laboratoire d’Ingénierie des Matériaux et des Hautes Pressions (LIMHP-CNRS) for research purposes were doped with nitrogen to improve their
 - color.
 - clarity.
 - cut.
 - weight.

- A. growth rates.
B. clarity.
C. thickness.
D. color.
11. _____ surveying is the main tool for emerald prospecting in Zambia's Kafubu region.
A. Ground-penetrating radar
B. Infrared-thermographic
C. Magnetic
D. Seismic
12. The presence of inclusions such as _____ may be characteristic of gem rhodonite from Broken Hill, Australia.
A. galena
B. sphalerite
C. rutile
D. both A and B
13. Using a microscope and his knowledge of mineralogy, Edward J. Gübelin was able to identify the inclusions of amphibole fibers that are characteristic of emeralds from _____, and thus determine the emerald's origin.
A. Brazil
B. Colombia
C. Nigeria
D. Sandawana, Zimbabwe
14. Long-lasting _____ is a characteristic of all chameleon diamonds.
A. fluorescence
B. phosphorescence
C. Raman effect
D. tenebrescence
15. Malossi hydrothermal synthetic emerald can be distinguished from its natural counterpart on the basis of
A. microscopic features.
B. chemical composition.
C. spectroscopic measurements.
D. a combination of all the above.
16. Anomalous birefringence is an important identification feature for CVD synthetic diamonds because
A. natural diamonds show distinctly different strain characteristics such as banded and "tatami" patterns.
B. HPHT synthetic diamonds commonly show no strain.
C. the strain patterns in CVD synthetic diamonds show clear traces of their growth on a substrate.
D. all of the above.
17. The South African government is requiring that greater amounts of rough diamonds be manufactured within its borders through a series of initiatives referred to as
A. Beneficiation.
B. Supplier of Choice.
C. Black Economic Empowerment.
D. Development Diamonds.
18. Emeralds from the Kafubu area of Zambia have refractive indices and specific gravities that are higher than those of most emeralds from _____, but comparable to emeralds from many other important localities.
A. Brazil
B. Colombia
C. Pakistan
D. Russia
19. The coloration of treated-color pink-to-red natural diamonds from Lucent Diamonds is likely a result of
A. HPHT treatment.
B. irradiation using a high-energy electron beam.
C. lower-temperature annealing in a vacuum.
D. a combination of the above methods.
20. The presence of which of the following internal features is evidence of synthetic origin in Malossi synthetic emeralds?
A. Irregular growth structures
B. Fingerprint-like inclusions
C. A seed plate
D. All of the above
21. The GIA Laboratory's studies have concluded that _____ diamonds consistently occur in larger sizes than other colored diamonds.
A. blue
B. red
C. pink
D. yellow
22. The discovery of abundant gem tourmaline in _____ in the early 1900s contributed to a decline in mining at Mt. Mica, Maine, during this period.
A. Arizona
B. California
C. New Hampshire
D. North Carolina
23. The fastest-growing consumer markets for diamond jewelry are
A. India and China.
B. the United States and Canada.
C. Thailand and China.
D. eastern Europe.
24. One of the instruments Edward J. Gübelin developed was the first desk-model _____ designed specifically for gemological use.
A. microscope
B. polariscope
C. refractometer
D. spectroscope
25. Which of the following is an identifying feature of CVD synthetic diamond?
A. An emission at 737 nm in the photoluminescence spectrum
B. Strong yellow fluorescence and phosphorescence
C. Colorless euhedral mineral inclusions
D. A weak, sharp absorption at 3107 cm^{-1} in the infrared absorption spectrum

EDITORS

Susan B. Johnson
Jana E. Miyahira-Smith
Stuart Overlin

Photoatlas of Inclusions in Gemstones, Volume 2

By E. J. Gübelin and J. I. Koivula, 829 pp., illus., hardcover, publ. by *Opinio Verlag, Basel, Switzerland*. US\$269.50*

This long-awaited second volume contains an abundance of new information collected by Edward J. Gübelin and John I. Koivula during the years since the publication of the original *Photoatlas* in 1986. Dr. Gübelin, a pioneer in the study of inclusions, supervised most of the preparatory work before he passed away in March 2005. Mr. Koivula, his friend of many years and an eminent gemologist and inclusion photographer in his own right, was able to complete the book.

With this middle volume—*Volume 3* is expected to appear later this year—the authors have produced a superlative work: 2,400 unsurpassable color photographs of inclusions in commercially significant gemstones, with clear captions and the necessary explanatory details. Its 829 pages are solidly bound, and a hard cover ensures that this classic work will withstand many years of consultation.

The book is divided into four major sections. The first contains a foreword, details on how to use this volume, historical background, and a discussion on the value of inclusions. This is followed by a section on the inclusions themselves, how they appear with the microscope, and how they are identified by scientific methods. (Most of the inclusions in the book were identified using analytical techniques such as X-ray diffraction, micro-X-ray spectrometry, or Raman spectrometry.) Once the inclusions

have been identified, they are often sufficient to identify the host gem material. This is where the book proves its value, for it contains a wealth of reference images that allow the observer to identify the inclusions—and the host gems—visually. The relevant topic is indicated at the top of every page, thus making the book much easier to use.

In the third section, on inclusion characteristics, chapters such as Diagnostic Colors, Diagnostic Morphology, Fluid Inclusions, and Geological Correlation lead to the core of the book. This fourth section—Inclusions in Gems of Commercial Importance—is arranged alphabetically according to the host material, from amber to zoisite. For quartz alone, there are more than 120 pages of inclusion photos. Pictures of synthetic crystals and imitations are also included.

The principal value of this volume is the vast number of different features depicted, bringing home to the reader the difference, for example, between natural oolitic opal and treated opal that has been stained black. The first volume contained only 24 photos of inclusions in tourmaline; the new one has 70, including recent arrivals (most notably copper-bearing “Paraíba” tourmaline). Again and again, the reader is surprised by the rare materials unknown to most gemologists that have been identified as inclusions (e.g., tangeite, ajoite, and papagoite), and thus are highly valuable from both diagnostic and aesthetic viewpoints. The book ends with a summary, a glossary, and an index.

It is quite clear that this beautifully produced and comprehensive second volume, like the first, will be an

essential reference work for gemologists, a source book for graphic designers, and edification for those who love beautiful pictures.

HENRY A. HÄNNI
*SSEF Swiss Gemmological Institute
Basel, Switzerland*

Schmuck Jewellery 1840–1940: Highlights Schmuckmuseum Pforzheim

By Fritz Falk, 176 pp., 206 illus., hardcover, publ. by *Arnoldsche Art Publishers, Stuttgart, 2004*. US\$60.00*

The Schmuckmuseum Pforzheim in southwest Germany was founded in 1961, making it a newcomer to the circle of the world’s great jewelry and art museums. From 1971 to 2003, under the ambitious directorship of art historian and master goldsmith Fritz Falk, the museum expanded its far-reaching collections of unique pieces. Here, Falk the author presents a selection of the museum’s most significant and beautiful pieces from the years 1840 to 1940, which aptly demonstrate a museum collection that has arrived.

The content is bilingual, presented in original German with sometimes clumsy English translations.

**This book is available for purchase through the GIA Bookstore, 5345 Armada Drive, Carlsbad, CA 92008. Telephone: 800-421-8161; outside the U.S. 760-603-4200. Fax: 760-603-4262. E-mail: myorder@gia.edu*

One hundred years of artistic and industrial jewelry making are blocked into three sections: the revival period (1840–1895), art nouveau (1898–1917), and the 1920s and 1930s (1918–1940). Introductory notes to each period provide historical background, with special emphasis given to German contributions, particularly with regard to Pforzheim. Known for centuries-old jewelry- and watch-making traditions and for its School for Applied Arts, Pforzheim evolved into a jewelry-manufacturing center during the industrial age. The town and its artists-manufacturers were especially adept at translating complex designs, such as art nouveau masterworks, into simplified and affordable mass-produced jewelry, a radical departure for its time in jewelry making and marketing.

Outstanding examples of each period abound, accurately rendered by clean photography, occasional full-page close-ups, and succinct captions. Masterworks by Lalique, Falize, Giuliano, Fouquet, and other all-stars are joined by lesser-known pieces from Elisabeth Treskow, who is credited with recreating ancient granulation techniques in the late 1920s, and Berliner Wilhelm Lucas von Cranach, whose 1900 octopus-and-butterfly brooch adorns the book's cover. The talents of Pforzheim's artists are evident in Theodor Wende's three-dimensional goldwork, while pieces by other German artists-manufacturers display the creative execution of jewelry inspired by masters, though rendered by a reductionist aesthetic often with the use of less costly, though lovely, materials.

Pendants and brooches are some of the most spectacular pieces in the collection, accompanied by ornaments of various types, as well as rings and necklaces, many of which presage the industrial styling identified with German and Scandinavian designers to this day. The book's bibliography and annotated register of 100 artists and workshops are useful reference tools.

While most (190) of the book's illustrations are well produced in color, text pages are accompanied by black-and-white period photographs and movie stills that readers should enjoy. A still of Brigitte Helm from 1927's "Metropolis" shows the actress striking a pose identified today with the look of pop star Madonna, reminding readers of the cyclical nature of art and fashion, as does an 1884 Pforzheim pendant in a style revived once more as modern chandelier earrings.

Whether art historians and others will consider Schmuckmuseum on par with Europe's other major jewelry collections remains to be seen. What is clear to date is that Falk has presented us with a remarkable collection—artfully rendered on these pages—that designers, art historians, and jewelry lovers will find worth seeking out.

MATILDE PARENTE
Libertine
Indian Wells, California

Working with Gemstones: A Bench Jeweler's Guide

*By Arthur Anton Skuratowicz and Julie Nash, 128 pp., illus., publ. by MJSA/AJM Press, Providence, RI, 2005. US\$34.95**

One of the most common—and most expensive—mistakes any jeweler can make is damaging a gemstone while manufacturing or repairing jewelry. I have heard the same story all too often, from beginners and experienced bench jewelers alike. The story goes like this: After doing a simple ring sizing, the jeweler examines the finished product, only to discover that the stone is now chipped, abraded, or discolored. The jeweler has no idea whether the damage occurred during soldering, pickling, polishing, or ultrasonic cleaning, but the end result is the same: A small profit on a \$30 sizing job has now turned into a loss of \$300 to replace the stone, not to mention a very upset customer.

Working with Gemstones: A Bench Jeweler's Guide offers very clear and practical recommendations on how to handle gemstones at the bench and avoid such unfortunate situations. Based on Skuratowicz and Nash's *AJM* column, this book provides a comprehensive understanding of the characteristics of gemstones and how those traits affect the bench jeweler.

A handy glossary is appropriately placed at the beginning of the book. The terms described in the glossary are integral to understanding the appearance of the stones as well as types of possible damage. These terms may be common knowledge for an experienced gemologist, but not necessarily for a beginning bench jeweler.

Information on each individual stone is presented clearly, starting with a visual guide that shows the likelihood of damage during the most common bench procedures. Each procedure's level of sensitivity is rated on a scale of one to four. Following this basic information is a much more in-depth description of each stone's characteristics. The discussion includes specific situations to be avoided, as well as common treatments that may dictate special handling.

There are many photographs illustrating stones that have been damaged by different operations, including chipping, abrasions, acid etching, and gem treatments, among others. Having good photos of these damaged stones might not save a gem that has already been damaged in your shop, but it will aid you in deciding which operation caused the damage, so that it can be avoided in the future.

Every major gemstone typically used in the jewelry industry is covered in this book, making it a fine resource for the beginning bench jeweler as well as anyone doing repair check-in at a retail store. In addition, some unusual, seldom-seen stones are included, making it a good reference for experienced jewelers as well.

MARK MAXWELL, CMBJ
Gemological Institute of America
Carlsbad, California

'06

gemological
ABSTRACTS

EDITORS

Brendan M. Laurs
Thomas W. Overton
 GIA, Carlsbad

REVIEW BOARD

Christopher M. Breeding
 GIA Laboratory, Carlsbad

Maha Calderon
 Carlsbad, California

Jo Ellen Cole
 Vista, California

Eric A. Fritz
 GIA Laboratory, Carlsbad

R. A. Howie
 Royal Holloway, University of London

Alethea Inns
 GIA Laboratory, Carlsbad

Paul Johnson
 GIA Laboratory, New York

David M. Kondo
 GIA Laboratory, New York

Taijin Lu
 GIA Research, Carlsbad

Wendi M. Mayerson
 GIA Laboratory, New York

Kyaw Soe Moe
 GIA Laboratory, New York

Keith A. Mychaluk
 Calgary, Alberta, Canada

James E. Shigley
 GIA Research, Carlsbad

Boris M. Shmakin
 Russian Academy of Sciences, Irkutsk, Russia

Russell Shor
 GIA, Carlsbad

Rolf Tatje
 Duisburg University, Germany

Sharon Wakefield
 Northwest Gem Lab, Boise, Idaho

COLORED STONES AND
ORGANIC MATERIALS

Determination and distribution characteristic [sic] of trace rare earth elements in pearls by ICP-MS. X. Wang, W. Ge, L. Jin, A. Li, S. Hu, and F. Huang, *Chinese Journal of Analysis Laboratory*, Vol. 24, No. 2, 2005, pp. 8–12 [in Chinese with English abstract].

The main trace elements in both saltwater and freshwater pearls (e.g., Na, K, Mg, Cr, Cu, Zn, Mn) have been extensively investigated by various researchers. However, these studies have typically omitted rare-earth elements (REEs) due to their extremely low concentrations. In this article, the authors analyzed REEs using inductively coupled plasma–mass spectrometry in powdered samples of both saltwater and freshwater cultured pearls from China. Four rare-earth standards were used, and two separate internal standards of ^{115}In – ^{103}Rh (indium–rhodium) were selected to compensate for the drift of analytical signals.

It was found that the “matrix” elements of Ca and Mg do not interfere with the signals for the REEs. The total concentration of REEs in the saltwater cultured pearls was about 0.6 mg/l and in the freshwater samples was 0.3 mg/l. The ratio of Eu/Eu^* (Eu^* is the standardized reference value for europium) in the two saltwater cultured pearls was less than 1, while in four freshwater samples this ratio was greater than 1. The concentration of REEs in the cultured pearls was related to their growth environment. TL

Granitic pegmatites: An assessment of current concepts and directions for the future. D. London [dlondon@ou.edu],

This section is designed to provide as complete a record as practical of the recent literature on gems and gemology. Articles are selected for abstracting solely at the discretion of the section editors and their reviewers, and space limitations may require that we include only those articles that we feel will be of greatest interest to our readership.

Requests for reprints of articles abstracted must be addressed to the author or publisher of the original material.

The reviewer of each article is identified by his or her initials at the end of each abstract. Guest reviewers are identified by their full names. Opinions expressed in an abstract belong to the abstracter and in no way reflect the position of Gems & Gemology or GIA.

© 2006 Gemological Institute of America

Lithos, Vol. 80, No. 1–4, 2005, pp. 281–303.

Granitic pegmatites are dike-like igneous bodies that are important sources of gem minerals such as tourmaline, beryl, and garnet, although in many cases they have a simple mineralogy consisting only of feldspar, quartz, and mica. Geologists have offered various theories to explain their patterns of mineral zoning, variety of rock textures (from giant crystals to fine-grained layering), and unusual geochemical features, which differ from those of ordinary granites. The author, a leading pegmatite researcher, presents an assessment of new thinking on the genesis of granitic pegmatites and describes several peculiarities that are still not fully understood.

Field studies of pegmatite occurrences and their mineral assemblages, and results of melt-crystallization experiments, suggest that some pegmatite dikes cooled over periods of weeks to months from temperatures of approximately 500°C to perhaps 300°C (a much more rapid cooling period at lower temperatures than previously believed). The presence of a water-rich vapor or other separate fluid phase, proposed earlier to aid in the formation of giant crystals as well as exotic minerals, may play a much less significant role than previously thought. The author compares this new thinking with traditional ideas on the formation of pegmatites, and suggests it provides a better explanation for their distinctive features. The genesis of pegmatite-forming melts, how these melts appear to have been extracted from larger magma bodies without bringing pre-existing crystals with them, and how the observed similarities in chemical and mineral zoning among multiple pegmatite bodies can be generated on a regional scale, are all questions that await further investigation.

JES

Guest editorial: How fast do minerals grow? A. Pring and J. Brugger, *Australian Journal of Mineralogy*, Vol. 11, No. 1, 2005, pp. 3–6.

Little is known about the growth rate of most crystals in nature. Geochronology is not of much use in mineral kinetics. The growth of crystals in rocks need not be a continuous process, but may occur in discrete episodes, sometimes resulting in zoned crystals. For some gem pegmatitic dikes in San Diego County, California, it is possible to calculate cooling rates using temperature estimates of the intruding magma and thermal conductivities of the host rocks. It has been deduced that cooling to <550°C at the center of these dikes occurred over approximately nine years for the 25-m-thick Stewart dike and in about five days for the <1-m-thick Himalaya dike. Growth rates for pegmatitic minerals such as the 10-cm-long black tourmaline crystals in the hanging wall of the Himalaya dike were at the remarkably high rate of 1 cm/day! For gypsum crystals growing in saline pools, growth rates of 0.5 mm per day have been recorded. Studies by the authors on the speed of replacement reactions and transformations of nickel sulfide minerals found that in the laboratory, the

transformation of pentlandite to violarite takes place over several weeks at 70°C and over several days at 120°C.

RAH

Pearls from the lion's paw scallop. K. Scarratt [ken.scarratt@gia.edu] and H. A. Hänni, *Journal of Gemmology*, Vol. 29, No. 4, 2004, pp. 193–203.

Lion's paw scallops produce some of the most attractive seashells in the world, and they can also host rare, beautiful, non-nacreous pearls. This article compares the characteristics of one perfectly round 5.91 ct "pearl" said to be derived from a Pacific lion's paw with data taken from the shells of several Atlantic and Pacific lion's paw scallops. Qualitative and quantitative chemical data, as well as infrared and UV-visible spectra, are presented for the 5.91 ct "pearl."

The composition and surface appearance of lion's paw "pearls" differ from those of other non-nacreous concretions (e.g., conch and melo "pearls"). The lion's paw "pearls" are composed mainly of calcite (versus aragonite in the case of the other non-nacreous pearls) and they have a peculiar surface sheen. This sheen results from "fibrous structures" composed of a patchwork of uniquely ordered cells.

WMM

DIAMONDS

Diamoniferous deposits in the Jequitá area (Minas Gerais, Brazil): A consequence of neotectonic processes. U. C. Penha [ulisses.penha@cvr.com.br], J. Karfunkel, and N. Angeli, *Neues Jahrbuch für Geologie und Paläontologie, Abhandlungen*, Vol. 236, No. 3, 2005, pp. 207–224.

Small-scale mining operations extract diamonds from Tertiary conglomerates and Quaternary gravels of the Rio Jequitá. The geology of northern Minas Gerais State, Brazil, has been of interest since *garimpeiros* began diamond mining in the early 20th century. Neotectonic processes reactivated Proterozoic crustal features, which divided the relatively flat area into several distinct mountain ranges. Diamond production comes from deposits on the slopes of Serra do Cabral and Serra da Água Fria. The uppermost areas of these mountains are covered by Early Cretaceous conglomerates that are poorly diamoniferous. The faulting created the Rio Jequitá graben, providing a depression for fluvial processes. The resulting erosion and transport by the river reworked and consolidated the diamond-poor conglomerates into the relatively diamond-rich (0.04–0.16 ct/m³) Tertiary conglomerates and Quaternary gravels. To date, no primary diamond-bearing deposits or minerals indicative of kimberlites/lamproites have been found in the region.

EAF

Geochemical diversity of Yakutian kimberlites: Origin and diamond potential (ICP-MS data and Sr, Nd,

and Pb isotope). V. A. Kononova, Yu. Yu. Golubeva, O. A. Bogatikov, A. A. Nosova, L. K. Levsky, and G. V. Ovchinnikova, *Petrology*, Vol. 13, No. 3, 2005, pp. 227–252.

The diamond-bearing kimberlites of the Nakyn field differ significantly from other Yakutian kimberlites in their chemical composition. Chemical and isotopic variations of kimberlites of the Yakutian diamond province were determined using new samples and the modern analytical techniques of ICP-MS and Sr, Nd, and Pb isotopic analysis. The data were used to help constrain kimberlite formation and emplacement conditions, as well as predict economic diamond potential.

Three chemically distinct groups of kimberlites were established, corresponding to different lithospheric and lower-crustal compositions. The first group, located in the Nakyn field, consists of low-Ti (<1 wt.%) kimberlites with ages from 1.4–0.9 billion years. The crustal components in this region are dominantly biotite-amphibole-garnet plagiogneisses that underwent consolidation roughly 3.2–2.7 billion years ago. The second chemical grouping consists of medium-Ti (1.1–2.7 wt.%) kimberlites, which are located among the southern group of pipes. They were emplaced 0.7–0.6 billion years ago. The lithosphere in this area is granulite-gneiss and includes a significant proportion of harzburgites. Consolidation took place 3.1–2.6 billion years ago. The high-Ti (>2.7 wt.%) kimberlites make up the third group and are located in the northern portion of the Siberian craton. This group was emplaced 0.8–0.5 billion years ago. The crust in this area consolidated 2.4–2.2 billion years ago and consists of pyroxene-plagioclase schists, enderbites, and charnockites. Pyrope from kimberlites is normally used as an indicator mineral for diamond prospecting, but pyrope is rare in the low-Ti kimberlites. An alternative method for predicting diamond potential was developed that uses rare-earth element concentrations and isotopic ratios.

EAf

Typomorphic peculiarities of giant Yakutian diamonds.

S. P. Bokalo, K. K. Kurbatov, and V. V. Bescrovanov [dsc@alrosa.mir.ru], *Mineralogical Museums Symposium*, St. Petersburg, Russia, 2005, pp. 333–334 [in Russian].

Numerous very large diamond crystals have been found in the Yakutian diamond province in Siberia since 1959. So far, 343 crystals weighing >50 ct have been documented from the following Yakutian deposits: Mir pipe (112), Udachnaya pipe (108), Yubileynaya (Jubileynaya) pipe (65), additional unspecified pipes (41), and placers (17). The crystals, which are stored in special facilities in Moscow and Yakutsk, are available for scientific study. Morphological and some physical properties were analyzed for 23 representative large crystals from five pipes.

Diamonds from the Mir pipe are always octahedral with smooth faces and sharp edges; they sometimes have

raised trigons on their faces. The largest stones from the Udachnaya pipe (>200 ct) have a characteristic irregular shape, but some form distorted octahedrons. The most distinctive feature of Udachnaya diamonds is their yellowish color, frequently with brown hues (i.e., the so-called tobacco tints). Diamonds from the Yubileynaya pipe are also octahedral but always have some development of rhombic dodecahedral faces. Diamonds from this pipe always display sheaf-like splintery striations on their faces, resulting in crystals with a dull appearance. Some of them have a yellowish green hue.

The authors conclude that large Yakutian diamonds have specific features that enable their kimberlite source to be determined. BMS

GEM LOCALITIES

Aquamarine aus neuen Vorkommen in Brasilien. C. C. Milisenda [info@gemcertificate.com] and H. Bank, *Gemologie: Zeitschrift der Deutschen Gemmologischen Gesellschaft*, Vol. 54, No. 1, 2005, pp. 47–51 [in German with English abstract].

Three sources of high-quality aquamarine from Minas Gerais, Brazil, are described: Padre Paraíso, Tatú, and Jacutinga. These deposits have recently started producing fine color and/or large aquamarines.

Padre Paraíso is approximately 80 km north of Teófilo Otoni in the eastern edge of the state. This location produces aquamarine of a pastel-colored greenish blue, with rough weighing up to 70 kg; faceted specimens as large as 100 ct have been produced. Properties are $n_o=1.571-1.752$, $n_e=1.565-1.566$ (birefringence 0.006), and S.G.=2.66–2.67.

Tatú is near the famous Santa Maria de Itabira deposit, in the central part of the state. Aquamarine from this area is intense blue, with faceted stones typically between 1 and 10 ct. Properties are $n_o=1.583-1.585$, $n_e=1.577-1.579$ (birefringence 0.006–0.008), and S.G.=2.72–2.74.

The third locality is Jacutinga, 60 km south of Pocos de Caldas. This locality is now producing some stones of exceptional color. Although typically less than 3 ct, the faceted goods are of an unusually intense blue. Properties are $n_o=1.588-1.590$, $n_e=1.580-1.590$ (birefringence 0.008), and S.G.=2.74–2.75. DMK

Chemical composition analysis of nephrites from different localities in China. R. Liao and Q. Zhu, *Journal of Gems and Gemmology*, Vol. 7, No. 1, 2005, pp. 25–30 [in Chinese with English abstract].

Nephrite, the more common and less costly type of jade, is a polycrystalline aggregate of amphibole of varying composition. Unlike jadeite jade, which is restricted to certain types of metamorphic rocks in a few areas, nephrite jade is much more widespread. China is the major source for nephrite, with two new deposits recently discovered. In this article, the authors compare the chemical composi-

tions of nephrite from several localities in China: Hetian and Manashi in Xinjiang, Germu in Qinghai, Wenchuan in Sichuan, Xiuyan in Liaoning, Hualian in Taiwan, and a deposit discovered in the 1990s at Xiaomeiling (near Suyang in Jiangsu). Detailed chemical analysis revealed that the average chemical compositions came very close to the theoretical value of tremolite ($\text{Ca}_2\text{Mg}_5\text{Si}_8\text{O}_{22}[\text{OH}]_2$). However, there were some differences in composition among the different localities. Variations in FeO and (FeO+MgO) appear to be an important indicator of geographic origin. For example, nephrite from Hetian showed a rather tightly constrained iron content of about 0.75 wt.% FeO, with (FeO+MgO) in a range of 24.2–26.7 wt.%. Samples from Xiuyan contained about 0.5 wt.% FeO and (FeO+MgO) of about 24 wt.%. Nephrite from Suyang had low contents of both FeO and (FeO+MgO). TL

Mechanical mining vs. traditional mining in Sri Lanka: A note on gem mining in Kumbukkana-Okkampitiya gem fields. M. Vithanage and M. Rupasinghe, *Canadian Gemmologist*, Vol. 25, No. 3, 2004, pp. 96–103.

Gem mining in Sri Lanka dates back more than 2,000 years and relies mostly on small-scale operations using traditional methods. Recently, large-scale mechanized mining has commenced in two gem-producing areas (Kumbukkana and Okkampitiya) in the southeastern part of the country, which is underlain by rocks of the Vijayan Complex. Most of the deposits are secondary (e.g., eluvial), with the gem-bearing gravel layers found near, or a few meters below, the surface. Traditional mining is relatively environmentally friendly, in that almost all pits are shallow. However, large-scale mechanized mining, using bulldozers and tractors, is having a major negative impact on the area, both environmentally and socially, in part because of the lack of enforcement of existing legislation and the requirements of the mining licenses.

Mechanized mining of riverbanks has caused large hardwood trees to fall, resulting in damage to the riverine ecosystem. Erosion of unconsolidated sediments from soil heaps created by the mechanized mining has fouled waterways. Abandoned craters (up to 25 m²) filled with water are breeding grounds for mosquitoes. The article concludes with a plea for the use of environmentally friendly mining methods, because the economy and the environment are interdependent, and damaging this balance may result in serious problems in the future. KSM

INSTRUMENTS AND TECHNIQUES

Application and development of digital image processing techniques in gemmology. Z. Qu, *Journal of Gems and Gemmology*, Vol. 7, No. 2, 2005, pp. 31–33, 41 [in Chinese with English abstract].

In recent years, many software applications for digital

image processing in gemology (such as for diamond cut evaluation) have been developed to gather image-related quantitative information. In this article, the author reports on a digital image processing system developed by China University of Geosciences, Wuhan, to assist in diamond cut grading and building three-dimensional images of gem materials.

The system consists of a light source with adjustable brightness and background illumination, a CCD (charged coupling device) camera, and a desktop computer with image-processing software. By measuring key spots (usually facet junctions) on a faceted diamond, the system can calculate proportion data in less than 10 seconds. The cut data and a three-dimensional model of the diamond are saved in a database, which can be placed on the Internet for searching and viewing by potential customers. For a rough diamond crystal, several potential cutting plans can be calculated and displayed.

The author claims that the system has reached a technological level equivalent to systems available elsewhere in the world for diamond cut measurement. These digital image processing techniques could also help study and identify inclusions and other characteristics in gem materials. TL

Cameras and computers: Photographing jewelry in the digital age. C. McCarthy, *Lapidary Journal*, Vol. 59, No. 3, 2005, pp. 16–22.

This article discusses the intricacies and difficulties inherent in jewelry and gemstone photography. Many of the challenges are related to the small size of the objects. Tips from top gem and jewelry photographers are offered on how to achieve the best results. Comparisons are made between film and digital photography, and today's experts tend to find they are spending more time using a computer to digitally manipulate images than using a regular film camera.

One major detriment to producing a good photograph is poor lighting. Opinions differ as to what is most effective, with strobe, tungsten, and combination lighting techniques discussed. Digital photography tends to be much more forgiving in this respect than film. Professional gem photography web sites are listed for reference to various lighting techniques by different photographers. For best color in a faceted stone, the goal is to light up as many of the back or pavilion facets as possible. Cabochons require more diffuse light and careful arrangements to avoid reflections of the photographer or the equipment. Opals require a limited focal range, and emeralds (due to their chromium component) tend to turn more blue or gray with film cameras. Digital photography seems to be gaining the upper hand in addressing this problem, as one can digitally manipulate and correct color results. Another factor is the proper use of backgrounds. If color accuracy is important, use a neutral background.

Also discussed are prices for cameras of different qualities. Printers are reviewed as well. JEC

Digital combination photography: A technique for producing improved images of microscopic minerals.

D. I. Green, *Australian Journal of Mineralogy*, Vol. 11, No. 1, 2005, pp. 13–24.

It is difficult to produce sharp photographs of three-dimensional micro-minerals using conventional single-shot film-based techniques. Software combining the sharply focused areas of different digital photographs offers considerable advantages at magnifications greater than life-size and is virtually indispensable at high magnifications. The depth of field and resolution of the microscope must be measured or calculated, and the size of the camera sensor (in megapixels) must be taken into account when deciding the most useful magnification. With a modern stereomicroscope and a high-resolution objective, it is possible to produce good-quality images for printing at a linear magnification of up to 100 \times ; for a more typical instrument, 30 \times –50 \times is the limit. The author's set-up for digital photography is shown, and 27 example photomicrographs are presented.

RAH

Growth zoning and strain patterns inside diamond crystals as revealed by Raman maps.

L. Nasdala [nasdala@uni-mainz.de], W. Hofmeister, J. W. Harris, and J. Glinnemann, *American Mineralogist*, Vol. 90, No. 4, 2005, pp. 745–748.

Recent advances in high-resolution luminescence spectroscopy have led to the widespread application of nondestructive Raman analysis to research on gem diamonds. Two-dimensional Raman maps were created for a suite of diamond crystals from Canada's Ekati mine (Panda pipe) to investigate the relationship between well-shaped, hexagonal plates of graphite and their octahedral diamond hosts. Analyses were done by the confocal Raman method, using 632.8 nm excitation from a He-Ne laser. Mapping was performed with a motorized X-Y stage and consisted of data sets containing 20,000–100,000 individual Raman spectra with lateral data resolution of 3–6 μm .

The focus of the data collection was the first-order diamond Raman band, which typically occurs at 1332 cm^{-1} with a width (full width at half maximum, FWHM) of $\sim 1.6 \text{ cm}^{-1}$. This band has been shown to become wider and shift toward higher wavenumbers in response to compressive strain. Immediately adjacent to the graphite inclusions, Raman shifts as high as 1336.7 cm^{-1} were measured, relative to the 1331.8 cm^{-1} value for the bulk diamond host. Additionally the inclusions were bounded by regions with FWHM values up to $\sim 3.7 \text{ cm}^{-1}$.

Contour plots of these data indicate that the origin of diamond growth texture was the graphite inclusions, and the surrounding patterns of diamond Raman peak variations represent internal strain. Thus, these Ekati diamonds must have overgrown preexisting graphite crystals in conditions relatively close to the graphite-diamond equilibrium boundary.

CMB

Observation of "centre cross" diamond: Distinction between natural and synthetic.

A. Abduriyim and H. Kitawaki, *Gemmology*, Vol. 36, No. 428, 2005, pp. 4–9.

It can be difficult to differentiate sector zoning in natural and HPHT-grown synthetic diamonds with a gemological microscope due to similarities in their appearance. The cross-shaped sector zoning that is typical for synthetic diamonds is rare in natural diamonds but has been observed in stones showing mixed-habit growth. However, differences in sector zoning between natural and synthetic diamonds can be seen clearly with cathodoluminescence (CL) or an X-ray analytical microscope. The authors examined a 0.105 ct purplish red diamond and a 0.21 ct orange-red Chatham synthetic diamond using these techniques. CL images of the natural diamond sample showed distinctive boundaries and a complicated zig-zag growth in {111} orientations and curved rough, linear growth on {100} directions interspersed with {111} growth. The synthetic sample showed smooth crystal surfaces, with no major variations in growth conditions. With the X-ray analytical microscope, the natural diamond sample showed distinctive boundaries as light/dark contrasts, but the synthetic sample showed only a homogenous light tone.

HyeJin Jang-Green

Oxygen isotope composition as a tracer for the origins of rubies and sapphires.

G. Giuliani, A. E. Fallick, V. Garnier, C. France-Lanord, D. Ohnenstetter, and D. Schwarz, *Geology*, Vol. 33, No. 4, 2005, pp. 249–252.

Oxygen isotope ($\delta^{18}\text{O}$) data are summarized for 249 natural rubies and sapphires (of various colors) from 106 primary and secondary (alluvial) deposits in 26 countries that represent many of the more important sources of these gem materials. These data were obtained by an analytical technique that involves heating approximately 1 mg of powdered sample with a laser, and reacting the heated powder with a fluorination agent (here, ClF_3) to release oxygen from the gem sample that is then converted to CO_2 for analysis.

The $\delta^{18}\text{O}$ data provide a good indication of the geologic environment and rock type of the corundum host. On the basis of the samples analyzed, the authors grouped the rubies into five categories, and the sapphires (excluding pinks) into six categories, each representing a different type of host rock. There is an overlap in the data for samples from some host rocks, so the analytical technique is not definitive in all cases. The authors found little variation in the oxygen isotope ratio among corundum samples collected from the same deposit. In addition, heat treatment of the corundum did not affect the isotope data. Although not definitive by itself, this minimally destructive analytical technique provides an additional means of distinguishing the geologic origin of gem corundum, with material from some localities displaying a unique oxygen isotope signature.

JES

JEWELRY HISTORY

Characters of gemstones from Liangzhuang King's tomb in Ming Dynasty in Zhongxiang, Hubei Province. M. Yang, J. Di, Y. Zhou, L. Fan, Z. Liang, L. Li, and H. Zhu, *Journal of Gems and Gemmology*, Vol. 6, No. 3, 2004, pp. 22–24 [in Chinese with English abstract].

More than 750 pieces of mounted gem materials (out of a total of more than 5,000 specimens of gems and jewelry) were found in the tomb of King Liangzhuang, who died in 1441. The tomb was discovered in 2001 in Zhongxiang, Hubei Province, China. The gem materials, which varied greatly in quality, were all well-polished cabochons. They were divided into 18 categories (the number of specimens identified in each category is shown in parentheses): ruby (173), sapphire (148), rock crystal (112), amber (93), agate (56), turquoise (54), emerald (50), nephrite (47), aventurine quartz (12), cat's-eye chrysoberyl (10), spinel (5), glass (4), garnet (2), pearl (2), wood (2), zircon (1), feldspar (1), and cinnabar (1). Most of the rubies and sapphires were large (the largest sapphire was nearly 200 ct), with good color and few inclusions. Whereas most of the other gems were in good condition, about half the turquoise samples displayed evidence of dissolution or corrosion, such as a porous texture and yellow or brown alteration colors. Drill holes in some of the necklace beads were noteworthy for their quality and uniformity of size. Based on inclusions and other gemological properties, the authors suggest that the pearls and turquoise came from China, while the other gem materials came from various parts of southeast Asia. TL

The Western lapidary tradition in early geological literature: Medicinal and magical minerals. C. J. Duffin, *Geology Today*, Vol. 21, No. 2, 2005, pp. 58–63.

This article explores ancient lapidary literature, with examples of folklore, mythology, and medicinal or other non-ornamental uses. One of the earliest lapidary works is by Theophrastus, a successor to Aristotle, who classified gems into male and female species. The text, written about 315 BC, led to speculation about whether gems were able to breed within the earth. A century later, Damigeron described the uses of 50 stones, such as hematite to stem bleeding, diamond as a talisman rendering the wearer undefeatable (both in battle and in lawsuits), and sapphire to reduce envy. The article describes more familiar texts by Pliny and then traces similar works through medieval times, many of which drew on ancient Greek lore. Finally, it reviews a number of early printed books and concludes with a notation on the recent rebirth of this literature in works on "crystal healing." RS

PRECIOUS METALS

Pt alloy materials for jewelry and ornaments. Y. Ning, *Precious Metals*, Vol. 25, No. 4, 2004, pp. 67–72 [in Chinese with English abstract].

This article briefly reviews the history of jewelry and ornaments made of platinum (Pt) and Pt alloys in China. It also summarizes selected basic properties (e.g., melting point, hardness, density, thermal properties) of Pt and its alloys as they apply to the manufacture of jewelry and ornaments, again, primarily in China.

Platinum jewelry was not popular in China before the early 1980s. But its popularity increased during the 1990s, and by 2002 about 46 tonnes of Pt (~ 52% of world production) were consumed by Pt jewelry manufactured in China (including Hong Kong). Platinum jewelry and ornaments made in China are marked on the basis of their Pt purity (1000 being 100% pure). In practice, most Pt jewelry is alloyed, and the most commonly encountered purities are 950Pt, 900Pt, and 850Pt; only a small percentage of Pt jewelry and ornaments are 800Pt. Unlike in the United States and European countries—which mainly use alloys of platinum-iridium (Pt-Ir), platinum-ruthenium (Pt-Ru), and a few other Pt alloys—in China platinum-palladium (Pt-Pd) alloys, often with copper, cobalt, or ruthenium added, are most widely used for jewelry. The most common Pt alloys are Pt-5Pd, Pt-10Pd, and Pt-15Pd, all of which have excellent chemical properties (e.g., high resistance to corrosion and oxidation) and thermal properties that enable easy casting and manufacturing. The author suggests that new Pt-Pd based alloys, particularly with the addition of Cu and Co, should be developed in China because of their favorable physical properties and price advantages. TL

SYNTHETICS AND SIMULANTS

Gem show beads. S. Frazier and A. Frazier, *Lapidary Journal*, Vol. 58, No. 7, 2004, pp. 54–59.

This article describes six bead materials that were misrepresented but were interesting nonetheless. These materials were: glass purported to be moss agate (mossy glass); iridescent synthetic quartz sold as "quartz crystal"; "sea bamboo," a fine-grained limestone with coral fossils that had been dyed red; green and yellow synthetic quartz sold as "real quartz"; pink glass with bubbles labeled as "strawberry quartz"; and dark pink glass described as "cherry quartz." JEC

Gemmological characteristics and identification of a kind of dyed red coral imitation. Q. Wei and Z. Qiu, *Journal of Gems and Gemmology*, Vol. 6, No. 1, 2004, pp. 24–26 [in Chinese with English abstract].

Red coral is one of the most valued organic gem materials due to its rarity and beauty, and the Chinese market is flooded with various red coral simulants. In this article the authors describe a new type of dyed red coral that is very difficult to distinguish from natural-color red coral.

The new red coral simulant is made from the *Isis reticulate* reef coral that naturally is gray-white or gray-

brown. Mineralogically, it is a high-magnesium calcite (determined by X-ray diffraction analysis). After the dyeing process, it displays various shades of red that are darker along fractures and grain boundaries. The thickness of the dyed red layer is usually ~0.5–2.0 mm. The infrared spectrum of the dyed material is similar to that of natural red coral. Chemical analyses (including mass spectrometry) indicate that the dyes used to create the red color are complicated, and those used in early imitations are different from those identified in the latest red coral simulants. The early dyes had a molecular weight of about 728 g/mol, whereas the latest dyes are composed of a mixture of three organic components with molecular weights of 312.8, 326.9, and 340.9 g/mol; these are very similar to the molecular weights of the organic components found in natural red corals. TL

Luminescence study of defects in synthetic as-grown and HPHT diamonds compared to natural diamonds. J. Lindblom [joachim.lindblom@utu.fi], J. Hölsä, H. Papunen, and H. Häkkänen, *American Mineralogist*, Vol. 90, No. 2-3, 2005, pp. 428–440.

Synthetic diamonds are becoming readily available in the marketplace, making it important that the optically active defects associated with different synthetic processes and post-growth treatments are well understood. Luminescence and absorption features were analyzed at room temperature and under cryogenic conditions (10–77 K) for six natural diamonds (colorless, yellow, brownish, and black), three nitrogen-rich synthetics (yellow to brown), two HPHT-annealed synthetics (yellow), two boron-doped synthetics (blue), and two synthetics grown with a “nitrogen getter” (near colorless). The authors collected cathodoluminescence (CL), photoluminescence (PL), and time-resolved luminescence spectra (TRL), as well as UV-Vis-NIR and FTIR absorption spectra.

Absorption spectra indicated that the as-grown N-rich and B-doped synthetic diamonds were types Ib and IIb, respectively. After HPHT treatment, the N-rich samples changed to type IaA. The samples grown with a nitrogen getter were nominally type IIa; however, both those and the boron-doped samples showed evidence of minor N-related defects, indicating a synthetic growth environment. The natural diamonds showed a weak hydrogen-related feature at 3107 cm^{-1} that was not present in the synthetics.

When exposed to UV and CL excitation, the as-grown N-rich samples showed a green star-shaped pattern that was blurred in the HPHT-treated samples. The blue and colorless samples showed no distinct patterns. Some of the natural diamonds showed octahedral growth patterns. The PL spectra of all the synthetic diamonds revealed sharp Ni-related features from the catalyst used during growth. The natural diamonds showed broad PL bands without sharp superimposed lines. CL

and TRL spectra of the synthetic diamonds contained Ni-related and nitrogen-vacancy-related bands, as well as features that were attributed to possible chromium impurities inherited from the growth chamber. In both CL and UV-excited spectra, the natural samples showed complex N-related defects and a 491 nm band related to slip traces and plastic deformation. Interestingly, the CL band in natural diamonds also shifted from blue to green with increasing exposure time in the instrument. The most reliable features for distinguishing natural from synthetic diamonds are distinct luminescence patterns and the N3 defects that are present only in natural diamonds. However, because these features are not always present, luminescence spectroscopy is important for the separation. CMB

Polymerization recycling of wasted [sic] turquoise. Y. Zhang and Q. Chen, *Journal of Gems and Gemmology*, Vol. 7, No. 1, 2005, pp. 31–35 [in Chinese with English abstract].

With the growth of the Chinese economy and jewelry industry, demand for various turquoise products is increasing rapidly. At the same time, waste materials from turquoise processing have become more common due to inefficient mining and manufacturing methods. It is estimated that several tons of turquoise waste materials are produced in China each year. In this article, the authors report on an attempt to recycle these waste materials by a variety of thermochemical polymerization processes.

Turquoise waste materials from Bijishan, Maanshan city, Anhui Province, China, were used for the experiments. After removal of iron oxides, the material was powdered to less than 200 mesh. The polymerization processes were mainly carried out by reaction with a solution of hydrogen aluminum phosphoric acid ($\text{AlH}_2\text{P}_3\text{O}_{10}$), followed by compression at 25–30 MPa for about 30–50 minutes, and heating and hardening at different temperature ranges (80, 120, 160, and 180°C). Various auxiliary materials for adjusting the solidification speed, reducing the water content, removing gas bubbles, and affecting color were added.

The resulting products were investigated by powder X-ray diffraction, SEM, FTIR, and other advanced analytical techniques. Gemological properties were also compared to natural turquoise. Some weak XRD peaks were found, corresponding to d-spacings of 4.144, 3.890, 1.4820, and 1.4543 Å, possibly as a result of the added chemicals. The concentrations of P_2O_5 and MgO were higher than those of natural turquoise, also probably related to the added materials.

Thermochemical polymerization facilitates bonding of turquoise crystals to form a lumpy structure. Mechanical properties, such as density, strength, etc., were also improved. TL

TREATMENTS

Glass-filled rubies: Clarity-enhanced rubies with glass-forming additives. T. Themelis [ted@themelis.com], *Australian Gemmologist*, Vol. 22, No. 4, 2005, pp. 360–365.

The filling of fractured rubies with glass containing Pb, Bi, Ta, and other oxides as additives, including chromophores, is described. Combinations of certain metal oxides in glass can effectively fill surface-reaching cavities in rubies at the relatively low temperature range of 900–1300°C. The structure of most of these fillers is amorphous glass (not necessarily SiO₂), and the treated stones are referred to as *glass-filled rubies*. In Thailand, these rubies are known as *ruby star* or by their alternative name *pao-mai*, meaning “new burn” in Thai. This treatment is easily identified with a gemological microscope; its disclosure is mandatory, and the selling price is relatively low.

RAH

Identification of treated chicken-blood stones and imitations. L. Tian, Y. Cheng, H. Liu, and Z. Zhang, *Journal of Gems and Gemmology*, Vol. 6, No. 3, 2004, pp. 18–21 [in Chinese with English abstract].

“Chicken-blood” stone, a fine-grained mixture of dickite/kaolinite and quartz with varying amounts of red cinnabar as the coloring agent, is among the most expensive ornamental materials in China. True chicken-blood stones come from only two localities: Changhua, in Zhejiang Province, and Balin, in Inner Mongolia. In this article, the authors compare natural chicken-blood stones from Changhua with various enhanced specimens and imitations using standard gemological techniques and several advanced techniques (e.g., X-ray diffraction, gas chromatography) to determine the characteristics of each material.

Four main types of enhancements were recognized: agglutination, repairing with glue, coating with cinnabar powder and/or red pigments, and reconstruction. Agglutination can be detected by microscopic observation, which reveals the presence of glues (usually concentrated in fractures or shallow depressions), gas bubbles, and variations in grain size and cleavage orientation between the natural cinnabar and the added material. Repairing with glue involves applying either a colorless artificial resin or a mixture of resin and dickite powder to broken surfaces. Stones artificially coated with cinnabar and/or red pigments are easily identified because the coloring materials are concentrated in surface regions. Reconstructed stones contain Pb₃O₄+PbO added to the cinnabar and/or red pigments. Imitations of chicken-blood stone usually have a base of kaolinite, chlorite, or talc. The specific gravities and other gemological properties of the imitations are sufficiently different from those of natural chicken-blood stone to enable easy identification.

TL

Spectroscopic studies on irradiated enhanced fancy color diamonds. J. C. C. Yuan, M.-S. Peng, and Y.-F. Meng, *Journal of Mineralogy and Petrology*, Vol. 25, No. 3, 2005, pp. 47–51 [in Chinese with English abstract].

FTIR, UV-Vis-NIR, photoluminescence, and Raman spectroscopy were used to study 10 natural diamonds with colors induced by radiation. Their visible absorption and low-temperature photoluminescence spectra showed a number of color-center peaks attributable to point defects. In addition to the N3 absorption feature, peaks at 595 and 637 nm were also observed. The authors suggest that peaks at 575, 595, and 637 nm in the low-temperature photoluminescence spectra, in combination with the H1b color center at 4929 cm⁻¹ and the H1c color center at 5156 cm⁻¹ in the near-infrared spectra, provide an indication of irradiation in green diamonds, and are also important characteristics of other colors that are produced in diamond by irradiation.

RAH

Three dimensional fluorescence spectra representation of natural and treated amber. L. Qi, X. Yuan, G. Peng, and Y. Wang, *Journal of Gems and Gemmology*, Vol. 7, No. 1, 2005, pp. 10–16 [in Chinese with English abstract].

Amber is often treated by various laboratory processes such as heating, filling, and/or pressing. To determine characteristics for distinguishing natural from treated amber, the authors have investigated differences in various types of spectra, mainly analyzing features related to carbon and hydrogen, which are the major chemical components of amber. Forty-six samples of natural amber (mainly from Huxuan, Liaoning Province, China) and 39 samples of amber treated by various enhancement processes (collected mainly from an amber manufacturing factory in Shenzhen) were studied by a three-dimensional fluorescence spectrophotometer and a UV-Vis spectrophotometer. All the samples were sliced and both sides were polished.

Amber treated by heating and filling processes showed a cut-off (general absorption) in the UV region at about 395 nm, due to unsaturated organic materials (unsaturated ester copolymer and aromatic compounds from foreign sources) added during the treatment processes. The cut-off position varied depending on the materials added. Other spectral differences were noted. For example, 346/437 nm (excitation/emission wavelength) was the characteristic peak for natural amber, while 354/415 nm was seen in heat-treated amber. Many luminescence centers were also found.

The spectral differences between natural and treated ambers can be explained by changes in the molecular bond structure of the carbon-hydrogen compounds during treatment. These differences could possibly be used for identification.

TL

MISCELLANEOUS

A valuation model for cut diamonds. M. G. M. S. Cardoso [margarida.cardoso@iscte.pt] and L. Chambel, *International Transactions in Operational Research*, Vol. 12, No. 4, 2005, pp. 417–425.

The authors examined two theoretical approaches to predicting diamond prices: decision trees and neural networks. A decision-tree model operates by splitting (“branching”) a large data set into smaller groupings until all the data in each final group (or “leaf”) are statistically similar to one another. A neural-network model connects input nodes (one for each value of “nominal attributes” such as diamond shape or source of grading report, and one for each “ordinal attribute”—color, clarity, or weight) to outputs (the predicted price of test diamonds) by way of an intermediate “hidden layer” of connecting functions that are determined recursively, using a computer program.

Pricing data for 2,778 diamonds sold in 2002 were obtained on the Internet and categorized according to diamond weight, color (coded in 27 classes, including brown hues), clarity (11 classes), shape (9 choices), and grading report (7 choices, including no report). Data from 65% of the diamonds were used to calculate parameters for the two types of models; the remaining diamonds were chosen to be statistically similar to the set as a whole, and were reserved to test the models’ prediction of their prices.

Each type of model had its own advantages. The neural-network model had better predictive capacity, in that it accounted for about 96% of diamond price variation. However, because of the “hidden layer” necessary to calculate prices, it did not provide good insights into the rationale for diamond pricing.

Although the decision-tree models (two in this paper) only accounted for 85% of price variation, they had two advantages: reasons for price variations could be prioritized, and the error of the price in each diamond group could be separately calculated. In this case, the most important variable was the type of diamond grading report (GIA, AGS, or HRD versus EGL, IGI, GGL, or none), followed by carat weight. For example, price predictions were much riskier for larger (>0.9 ct) diamonds with low clarity and no grading report than for H-or-lower-color diamonds between 0.98 and 1.5 ct with a grading report from GIA, HRD, or AGS.

Nevertheless, the authors found that the *Rapaport Diamond Report* price list was better still at prediction (98% of price variation accounted for) and these models could not reliably extrapolate prices for diamonds that were not in the data set (e.g., 1 ct D-IF). However, both the neural-network and decision-tree methods showed considerable promise, and the authors plan to extend their analysis to include such factors as cut quality grades and fluorescence, as well as a time-related dimension.

Mary L. Johnson

Conflict diamonds: A new dataset. E. Gilmore, N. P. Gleditsch [nilspg@prio.no], P. Lujala, and J. K. Rød, *Conflict Management and Peace Science*, Vol. 22, No. 3, 2005, pp. 257–272.

While studies have pointed to natural resources, diamonds in particular, as a cause of civil conflict, there has been no systematic means of evaluating such conclusions. Using diamonds as a model, the authors have constructed a dataset of various criteria to analyze whether, or to what extent, commodities are involved in fueling civil conflicts (available at www.prio.no/page///9649/47115.html). These factors include conflicts in producing countries; accessibility of rebel groups to the production sites; and the ability to extract, export, and market the commodities.

The authors hypothesize that primary diamond deposits in kimberlite pipes have a low probability of being the object of conflict because they require costly mining operations to exploit. Nations with secondary diamond deposits may show a greater incidence of civil strife than those without such a resource because these shallow deposits are easily exploited. The degree to which these factors incite and prolong conflict remains to be established; this dataset is intended to facilitate such research.

RS

Study on disease status of gem worker’s silicosis. C. Chen, D. Zhang, C. Qiu, W. Li, and L. Hwang, *China Journal of Public Health*, Vol. 21, No. 3, 2005, pp. 317–318 [in Chinese with English abstract].

Guangdong Province hosts one of the largest gem manufacturing centers in China. This article reports on the prevalence of dust-related diseases, primarily silicosis, in workers at two Guangdong factories that produce jewelry and ornamental objects containing mainly colorless quartz, amethyst, and citrine. Workers are involved in stone selection, cutting and polishing, hole drilling, and assembling the final products. The study involved 1,078 male and 485 female workers with an average age of 23.75 years, who had been working at the factories for an average of 1.23 and 4.72 years, respectively. In addition to examining the workers for lung functionality, the study evaluated hygienic conditions in the factories (particularly air quality).

The average concentration of dust in the air within the factories was 2.4 mg/m³, of which 92.8% was silica. About 72% of the work sites sampled exceeded the national health standard of 1 mg/m³ for particulates in air. About 4% of the workers were diagnosed with silicosis. These workers were relatively young (average 27.12 years old) and had been subjected to excessive dust exposure for an average of 4.74 years. Improving environmental conditions in the gem factories is clearly the key to preventing lung-related diseases among their workers.

TL

One Hundred Issues at Your Fingertips: The *G&G* Twenty-Five Year Index



Suppose you need to find everything *G&G* has published on the subject of tanzanite since 1981. Or you want to consult an article by a certain author but can't remember which issue it appeared in. Rather than searching through all 100 issues, more than 7,300 pages in all, simply go online and let the free *Gems & Gemology* Twenty-Five Year Index (1981–2005) do the work for you.

To use this powerful tool, visit www.gia.edu/gemsandgemology and click on "G&G Indexes." There you will see links to a **Subject Index** of articles, Lab Notes, Gem News entries, editorials, and book reviews, as well as a separate **Author Index**. (Both indexes are PDF files, so to open them you will need Adobe Acrobat Reader installed on your computer; a link to this free software can be found on the "G&G Indexes" home page.) Locating information in either index is simple with Acrobat's built-in search feature. On the toolbar that pops up with the specific index file, just click on the Search button (represented by a binoculars icon) and type in the word or phrase you want to search for. Every match for your search term will be listed in the order it appears in the index.

The online index is cumulative and will be updated at the end of each volume year. For those who prefer a hard copy, the

print version of the Twenty-Five Year Index will be released this summer, at a cost of \$9.95 in the U.S. and \$14.00 elsewhere.

Still other useful features continue to be added to the *Gems & Gemology* website. The previous Last Page announced free, unlimited access to the entire set of 1934–1980 back issues, available now. Beginning in mid-2006, *G&G* readers will also be able to subscribe to the new electronic version of the journal and purchase online issues from 1981 to the present—immediately. Even the rare out-of-print issues will now be readily available. A sample digital issue will be posted on our website to help you decide if you'd rather have the journal delivered to your desktop or, for a small additional charge, have both online access *and* the beautiful (and color controlled) print version. Letters will go out to all subscribers when this service goes live.

The Twenty-Five Year Index and online issues are there to help *G&G* users find the gemological information they need, when they need it. As always, comments and suggestions are welcome: e-mail us at gandg@gia.edu.

Stuart Overlin
Associate Editor